MECHANISTIC FUNCTIONS OF THE 9-1-1 COMPLEX SUBUNIT HUS1 IN THE MAINTENANCE OF GENOMIC INTEGRITY

A Dissertation

Presented to the Faculty of the Graduate School

of Cornell University

In Partial Fulfillment of the Requirements for the Degree of

Doctor of Philosophy

by

Pei Xin Lim

May 2015

MECHANISTIC FUNCTIONS OF THE 9-1-1 COMPLEX SUBUNIT HUS1 IN THE MAINTENANCE OF GENOMIC INTEGRITY

Pei Xin Lim, Ph. D.

Cornell University 2015

The mammalian RAD9A-HUS1-RAD1 (9-1-1) complex is a heterotrimeric clamp that promotes checkpoint signaling and DNA repair by functioning as a scaffold at DNA damage sites. While activation of the ATR checkpoint kinase via 9-1-1/TOPBP1 interactions is well established, less is known about checkpoint signaling-independent roles of 9-1-1. The 9-1-1 complex is thought to recruit DNA repair proteins from various repair pathways to damage sites via hydrophobic domains on the outer surface of the clamp. However, the molecular mechanisms and the physiological significance of these interactions remain mostly unknown. I hypothesize that 9-1-1 has a direct role in DNA repair that is coordinated with ATR checkpoint signaling to maintain genome integrity. This dissertation aims to elucidate the importance of checkpoint signaling-independent functions of HUS1 and the 9-1-1 complex using molecular and genetic approaches.

First, we conducted the first comprehensive structure/function study of HUS1 by testing the ability of HUS1 mutants with various targeted mutations to complement the genotoxin sensitivity of *Hus1*-deficient fibroblasts. In this study, we elucidated functional residues of HUS1 that drive clamp assembly, DNA interactions, and downstream effector functions. Importantly, we found two hydrophobic pockets on the HUS1 outer surface that may serve as HUS1-effector interaction domains that are separable from the checkpoint

activation function of 9-1-1. These results indicate that, once properly loaded onto damaged DNA, the 9-1-1 complex executes multiple, separable functions that promote genome maintenance.

We also investigated the functional relationship between 9-1-1 complex and the homologous recombination repair (HRR) pathway by analyzing genetic interactions between *Hus1* and *Rad54*. Previous studies suggested that *Hus1* may play an important role in double strand break (DSB) repair, and *Rad54*$^{-/-}$ mice are mildly perturbed for HRR. We found that simultaneous *Hus1* and *Rad54* defects in mice and cultured cells caused synergistic effect on spontaneous and genotoxin-induced genomic instability, as well as male subfertility. These findings reveal *Hus1* may directly participate in DSB repair pathways to respond to DNA damaging stresses.

Together, these studies provide insights into novel functions of HUS1 that underlie a successful DNA damage response, which potentially could be exploited for targeted anticancer therapy.

BIOGRAPHICAL SKETCH

Pei Xin Lim was born on December 22, 1986 in Johor, Malaysia. In 2003, he graduated from Batu Pahat High School and entered Anderson Junior College in Singapore under the ASEAN Pre-University scholarship. Six months later, he was awarded a scholarship from the Public Service Department of the Malaysian government for an opportunity to pursue a degree in the United States of America. Pei Xin enrolled at Purdue University, West Lafayette, Indiana in 2005, majoring in general biology and minoring in chemistry. In the course of four years, he worked in the lab of Dr. Donna Fekete on the roles of axon guidance molecules in the neuronal circuit development of the chick inner ear, and in the lab of Dr. Sergey Savinov screening libraries of selected small peptides for the inhibition of p53 interaction with its negative regulators. He was fortunate to learn basic research skills from many mentors in the two labs and was instilled with the importance of multidisciplinary research. After graduating with a B.S. degree in 2009, Pei Xin came to Cornell University for graduate studies under the field of Genetics and Development (now Genetics, Genomics and Development). He found interest in mechanisms of genome maintenance and joined the lab of Dr. Robert Weiss in 2010. There he laid the groundwork for the molecular and physiological requirements of checkpoint protein HUS1 in DNA damage response in cells and in mouse models. He was also involved in projects on HUS1 requirements in genotoxin-specific response, meiosis and tumorigenesis. Opportunities for TAing an undergraduate course, mentoring new lab members and presenting at conferences also enriched Pei Xin's experience as a graduate student. He plans to pursue a career in cancer research after graduation.

To *Cikgu* Saramma,

from whom I first learned the central dogma of molecular biology.

ACKNOWLEDGMENTS

First, I would like to thank Dr. Weiss for his support, care and guidance as my mentor and my role model. Under his tutelage I have learned to become a better researcher. Dr. Weiss has taught me many things, among which scientific skills and mindset inculcated in me are the most cherished. With Dr. Weiss' guidance, I have honed experimental techniques in mouse genetics and molecular biology; I have come to believe the importance of inquisitiveness and tenacity in research. I think this is a big step forward for me in preparation for the coming challenges.

I would also like to thank the past and present members of the Weiss lab for all their support and collaboration. Special thanks to Drs. Gabriel Balmus, Amy Lyndaker, Stephanie Yazinski, Minxing Li, Kelly Hume, Erin Daugherty and Jennifer Page for their guidance and help when I was struggling as the youngest member of the lab. Thank you for creating a collaborative and wonderful lab environment for me to work in. Also, thank you to labmates who joined the lab after me: Tim Pierpont, Dr. Joanna Mleckzo, Dr. Elizabeth Moore, Yashira Negron, Darshil Patel, and Dr. April Blong. It has been a pleasure working with you all.

Finally I would like to give thanks to the people who were directly involved in my projects: my committee members, Dr Eric Alani and Dr. John Schimenti, for their scientific input and suggestions regarding the direction of my projects; Dr. Marcus Smolka, Dr. Joseph Peters, Dr. Holger Sondermann, Dr. Alba Guarne, and Dr. Ivaylo Ivanov for their gracious offers of consultations and technical support; my senior graduate mentors Dr. Gabriel Balmus and Dr. Amy Lyndaker, as well as my mentees Lucy Duan, Kelsey Poisson, Siddharta Sinha, Manpreet Basuita, Darshil Patel, Cindy Luan, Charlton Tsai and Gabriel Mpilla for their efforts in experimental work. I would not have made it without them. Last but not least, I appreciate fundings from Cornell Presidential Life Sciences Foundation, Center for Vertebrate Genomics and Comparative Cancer Biology Program, as well as NIH grant CA108733 from Dr. Weiss.

TABLE OF CONTENTS

LIST OF FIGURES

LIST OF TABLES

CHAPTER 1

LITERATURE REVIEW

1.1 Mechanisms for DNA damage response in mammalian cells

In order to survive and propagate, living organisms need to maintain viable genetic composition and transmit genetic information from one generation to another with minimal error. Therefore, cells must protect the integrity of their genomic contents against myriads of insults from both exogenous and endogenous sources (Ciccia and Elledge, 2010, Jackson and Bartek, 2009) (Figure 1.1). Extrinsic DNA damaging agents include ionizing radiation, ultraviolet light and chemical genotoxins. Cells also undergo spontaneous DNA alterations due to the production of metabolic reactive oxygen species (ROS) and intrinsic DNA lesions arising from replication stress, oncogenic stress, erroneous DNA metabolism, meiotic recombination and telomere erosion. Failure to counteract and regulate these damaging events can cause genomic instability that subsequently leads to premature aging, heritable diseases and tumorigenesis.

[2]

To prevent these deleterious outcomes, mammalian cells have evolved methods for fastidious sensing of acute DNA lesions, careful regulation of cell cycle progression, and adept coordination of DNA repair before resuming transcriptional and replication activities (Hoeijmakers, 2001, Zhou and Elledge, 2000, Jackson and Bartek, 2009). These sophisticated surveillance networks and signaling mechanisms are collectively termed the DNA damage response (DDR). Molecularly, the DDR involves complex sets of regulatory mechanisms that impose transcriptional controls and post translational modifications in order to recruit factors and drive signaling cascades (Ciccia and Elledge, 2010, Polo and Jackson, 2011). These signaling

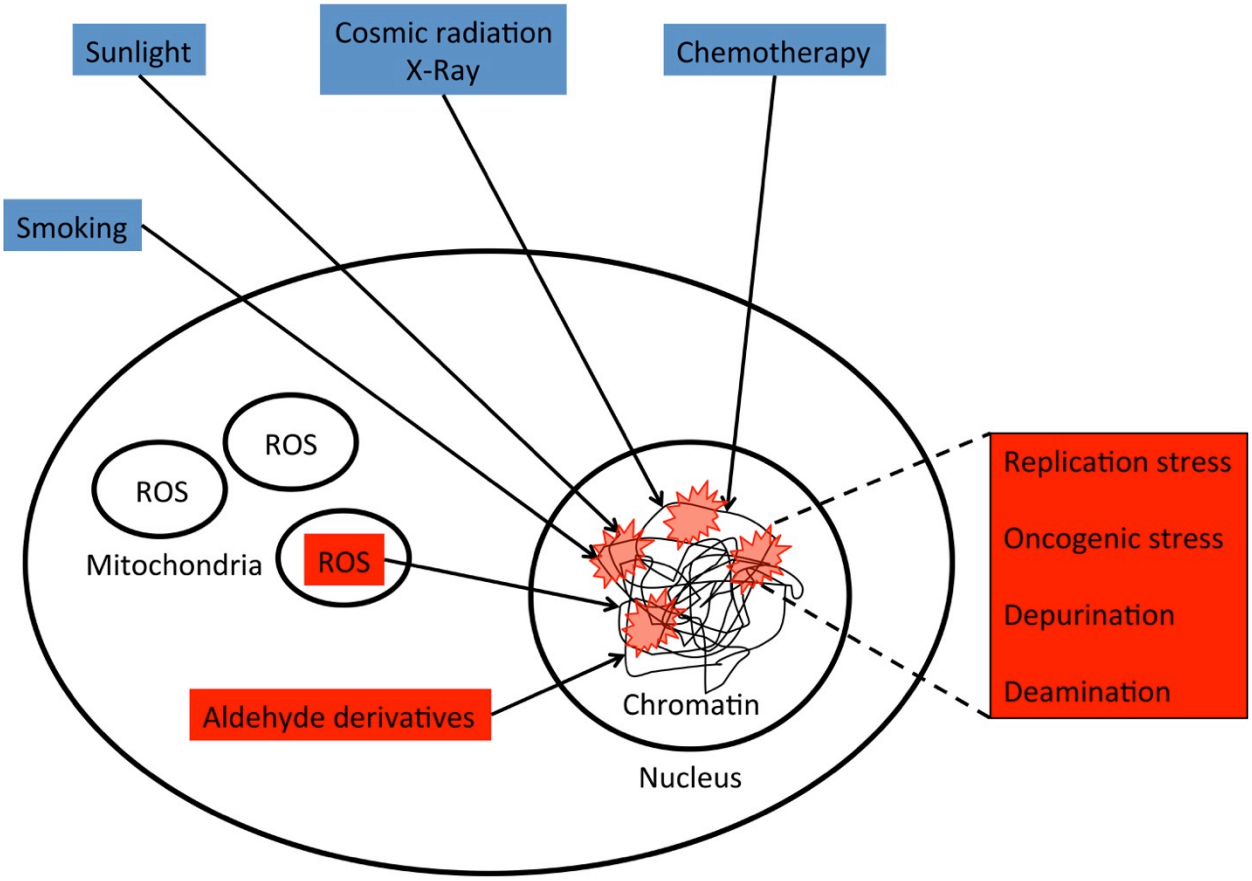

Figure 1.1. Sources of DNA damage in mammalian cells. Cells sustain DNA damages from exogenous (blue) and endogenous (red) agents. If left unchecked, these damages will jeopardize genome integrity and will lead to deleterious events such as premature aging, heritable diseases and tumorigenesis.

cascades activate DNA damage checkpoint signaling pathway to trigger cell cycle arrest, and modulate specific DNA repair pathway(s) for proper restoration of damaged DNA.

.

1.1.1 DNA damage checkpoint signaling

Mammalian cells have two major DNA damage checkpoint signaling pathways separately headed by two phosphatydylinositol-3-kinase-related kinases (PIKKs) – Ataxia Telangiectasia Mutated (ATM) and Ataxia Telangiectasia and Rad3-related (ATR) (Figure 1.2). The ATM pathway responds primarily to double strand breaks (DSBs). ATM kinase is recruited to DSBs by the Mre11-Rad50-Nbs1 (MRN) complex and upon autophosphorylation, ATM activates many substrates, including CHK2 and p53 which are involved in cell cycle arrest, senescence and apoptosis (Kurz and Lees-Miller, 2004). On the other hand, the ATR pathway mainly recognizes replication protein A-coated single-strand DNA (RPA-ssDNA), a common substrate that is generated at stalled DNA replication forks, processed DNA lesions and exposed telomeric ends (Cimprich and Cortez, 2008). It is also the basis of the versatility of the ATR pathway to respond to various genotoxins. Activation of the ATR pathway is a two-step mechanism involving recruitment of ATR kinase to RPA-ssDNA and stimulation of ATR kinase activity by DNA topoisomerase 2-binding protein 1 (TOPBP1), which is recruited by the phosphorylated C-terminal tail of RAD9A in the RAD9A-HUS1-RAD1 (9-1-1) heterotrimeric ring complex (Delacroix et al., 2007). The loading of the 9-1-1 clamp is dependent on RAD17-replication factor C (RFC) clamp loader complex (Bermudez et al., 2003). Activated ATR phosphorylates several substrates, including the effector kinase CHK1, which induce cell cycle arrest, stabilize stalled forks and inhibit origin firing, also through phosphorylation (Cimprich and Cortez, 2008). Although portrayed as two parallel pathways, there is considerable crosstalk

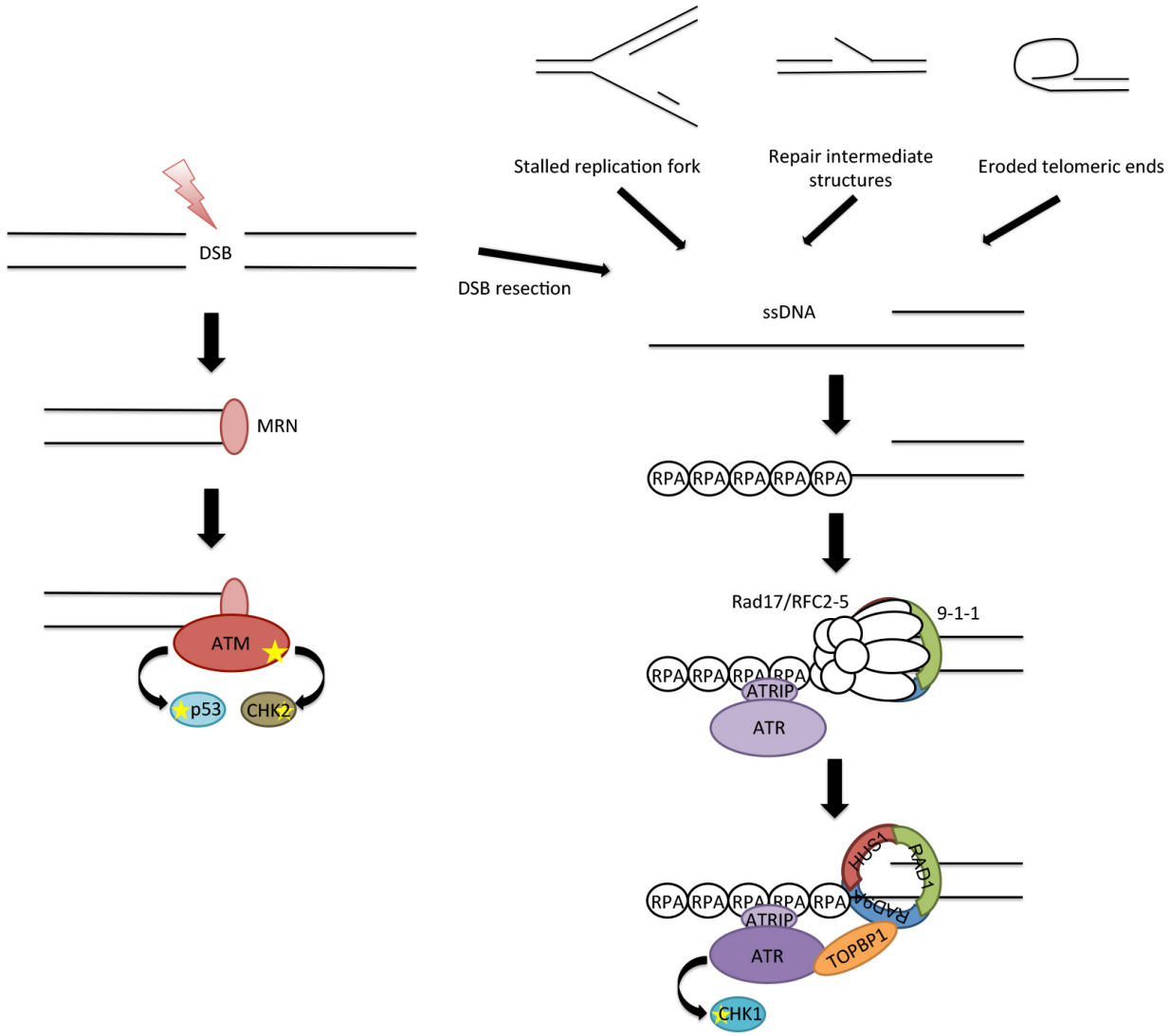

Figure 1.2. The ATM and ATR checkpoint signaling pathways. When DNA double-strand break (DSB) occurs, ATM pathway is activated. Various types of DNA damages lead to the exposure of single-strand DNA (ssDNA) which triggers ATR checkpoint activation. The two pathways are not mutually exclusive, as ATM and ATR kinases have many common substrates.

between the ATM and ATR pathways as they share many common substrates (Matsuoka et al., 2007) and deactivation of one pathway modulates signaling to the other (Balmus et al., 2012). In the most recent finding of ATM/ATR interplay, the MRN complex from the ATM pathway is found to interact with TOPBP1 in a RAD17-independent manner (Lee and Dunphy, 2013, Duursma et al., 2013) and this interaction may alternatively activate ATR on long exposed ssDNA unreachable by 9-1-1 complex (Shiotani et al., 2013). Ultimately, both pathways lead to cell cycle arrest (primarily due to downstream activities of checkpoint proteins CHK1 and CHK2), allowing cells to repair DNA or undergo senescence or apoptosis if the damage is too severe.

1.1.2 DNA repair

It is remarkable that mammalian cells have evolved many DNA repair pathways to cope with all kinds of DNA lesions (Hoeijmakers, 2001, Friedberg, 2008) (Figure 1.3). For the repair of DSBs, cells are equipped with two most prominent repair pathways, the homologous recombination repair (HRR) and non-homologous end joining (NHEJ), and two other minor pathways, single strand annealing (SSA) and alternative NHEJ (A-NHEJ), which is also known as microhomology-mediated end-joining (MMEJ). For the repair of uracil incorporation, 8-oxo-guanine, and single strand breaks (SSBs), base excision repair (BER) is used; whereas for bulky adducts, such as 6-4 photoproducts (6-4PP) and cyclobutane pyrimidine dimers (CPD), nucleotide excision repair (NER) is preferred. Furthermore, for nucleotide mismatch, insertion and deletion mutations, mismatch repair (MMR) pathway is utilized. Finally, the repair of DNA interstrand crosslink involves multiple repair pathways, including the Fanconi Anemia (FA) pathway, translesion synthesis (TLS), HRR, and NER. Each pathway utilizes unique enzymes

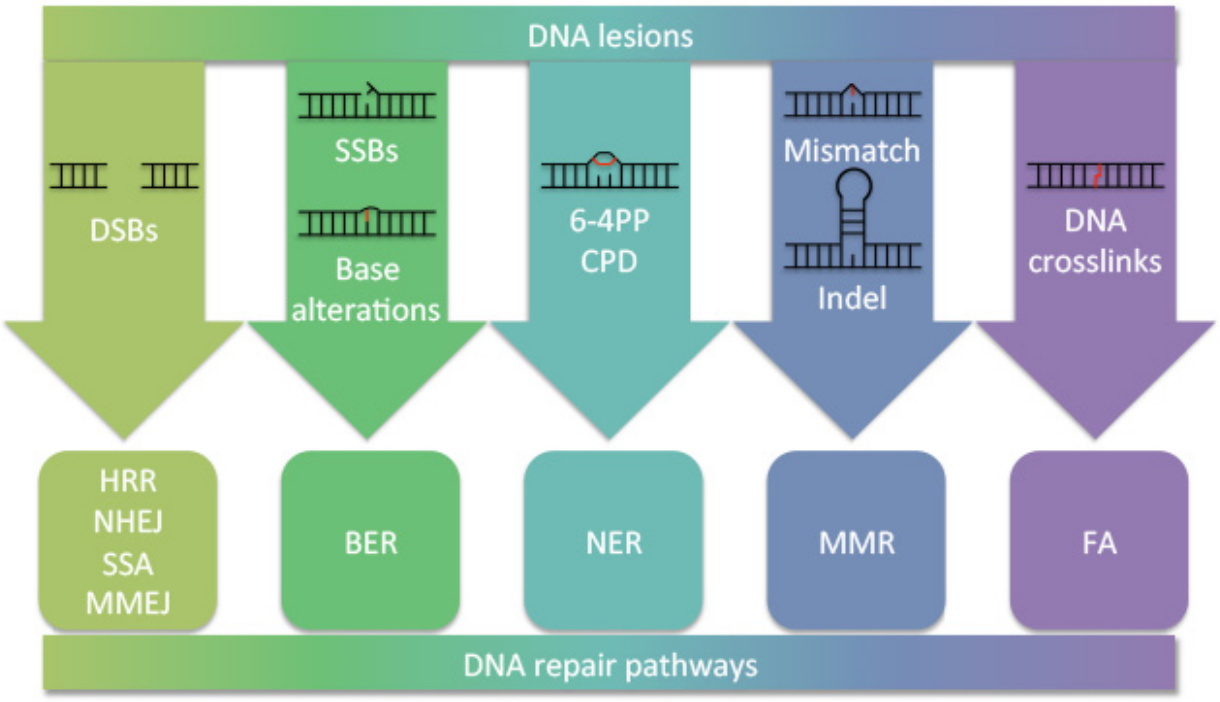

Figure 1.3. The types of DNA damages and the corresponding repair pathways needed for proper repair. DSBs, double-strand breaks; SSBs, single-strand breaks; 6-4PP, 6-4 photoproduct; CPD; cyclobutane pyrimidine dimer; Indel, insertion/deletion; HRR, homologous recombination repair; NHEJ, non-homologous end joining; SSA, single-strand annealing; MMEJ, microhomology-mediated end joining; BER, base excision repair; NER, nucleotide excision repair; MMR, mismatch repair; FA, Fanconi Anemia repair.

that excise or hydrolyze damaged DNA followed by enzymes that synthesize or join new nucleotide strands. The mechanisms of and the known enzymes involved in each major pathway are briefly described below:

1.1.2.1 HRR and NHEJ

DSBs arise from direct damage from ionizing radiation, unrepaired single-strand breaks (SSBs), replication fork collapse or programmed DSBs in meiotic cells. HRR is important for both mitotic repair and meiotic recombination in mammalian cells. HRR begins when the MRN complex, BRCA1, and CtBP-interacting protein (CtIP) are recruited to DSB ends (in meiosis, programmed DSBs are created by SPO11). The nuclease activity of MRE11 of the MRN complex initiates limited 5' to 3' DNA end resection (Buis et al., 2008). More extensive resection is taken over by exodeoxyribonuclease 1 (EXO1), with its activity stimulated by Bloom helicase (BLM) to produce long stretches of 3' ssDNA which are bound by RPA (Nimonkar et al., 2008). RAD51, with the help of accessory factors like RAD51 paralogs (XRCC2, XRCC3, RAD51B, RAD51C and RAD51D), RAD52, RAD54, PALB2 and BRCA2, displaces RPA from the ssDNA tails and invades sister chromatid strand to form a displacement loop (D-loop) and heteroduplex DNA (Sung et al., 2003). An additional factor, DMC1, is needed in meiosis for the strand invasion of homologous chromosome (Yoshida et al., 1998). From this step, repair can be completed by two ways: synthesis-dependent strand annealing (SDSA) or DSB repair (DSBR) (Moynahan and Jasin, 2010). In SDSA, the newly synthesized DNA is displaced from template and annealed back to the other resected DNA end, and a second DNA synthesis completes the repair. In DSBR, the other resected DNA end is captured by the D-loop, forming a double Holliday junction, which can be resolved by endonuclease cleavages. HRR is regarded as high

fidelity repair of DSBs because the error-free process suppresses DNA mutations.

On the other hand, NHEJ is an error-prone DSB repair mechanism that can introduce insertion/deletion mutations and can inappropriately join heterologous DNAs. NHEJ begins with DSB binding by Ku70/80, which in turn recruits DNA-PKcs, a PIKK kinase in the same family as ATM and ATR checkpoint kinases (Burma and Chen, 2004). DNA-PK phosphorylates many substrates, among which is Artemis that trims DNA ends to prepare for end joining. Finally, the XRCC4-LIG4-XLF complex is recruited to ligate the ends (Ahnesorg et al., 2006).

The choice between HRR and NHEJ for DSB repair is cell cycle regulated. HRR usage is restricted to S and G2 phases, since the sister chromatid template used in HRR is only replicated during S phase, whereas NHEJ is available throughout the whole cell cycle, and predominantly used during G1 phase (Rothkamm et al., 2003). An early determinant factor that favors NHEJ over HRR is DSB end protection by Ku70/80 (Doherty and Jackson, 2001), and inhibition of DNA resection by 53BP1 binding partners, RIF1 and PTIP (Di Virgilio et al., 2013). During S phase, phosphorylation of CtIP induces complex formation with MRN and BRCA1, and together, this complex displaces 53BP1, eventually leading to DNA end resection, removal of Ku70/80, and HRR initiation (Chen et al., 2008). Perturbation of either 53BP1 or BRCA1 disrupts the molecular regulation of HRR and NHEJ, revealing the interdependency and ease of modulation of repair choice (Escribano-Diaz et al., 2013).

1.1.2.2 BER

As the name suggests, BER repairs single damaged nucleotide by removing the base, creating nicked DNA and repairing it with DNA synthesis and ligation (Dianov and Hubscher, 2013). Altered nucleotides due to deamination, depurination, alkylation and oxidation are

recognized by specialized DNA glycosylases and excised by N-glycosylic bond cleavage, creating apurinic/apyrimidic (AP) sites. These AP sites are nicked by AP endonuclease 1 (APE1) at the 5' phosphodiester bond to create single strand breaks (SSBs). SSBs are repaired through either the short-patch or the long-patch method (Fortini, 1996). In short-patch BER, DNA polymerase β removes the nick and adds one nucleotide, which is then properly ligated by XRCC1-LIG3 complex (Cappelli et al., 1997). In the long-patch BER, actions of DNA polymerases β and δ synthesizes a new strand of DNA far beyond the nicked site, creating a flap that is removed by flap endonuclease 1 (FEN1) before proper ligation by DNA ligase I (Klungland and Lindahl, 1997). This concerted event seems to involve the proliferating cell nuclear antigen (PCNA), as DNA POL β, POL δ, FEN1 and DNA ligase I have been reported to interact with the processivity clamp (Kedar et al., 2002, Montecucco et al., 1998, Warbrick et al., 1997, Ducoux et al., 2001).

The importance of BER manifests in its ability to not only recognize and repair many different types of DNA lesions, but also in doing so prevent these lesions from deteriorating into DSBs. However, when the number of lesions exceeds the capacity of timely repair by BER, mammalian cells rely on the actions of poly(ADP-ribose) polymerase 1 (PARP1) to provide temporary protection (Parsons et al., 2005). It is known that SSBs activate PARP family of proteins which are involved in rapid synthesis/disassembly of PAR for damage recognition, chromatin reorganization and DNA repair (Caldecott, 2008). Indeed, loss of PARP1 causes increased SSB to DSB conversion, and simultaneous depletion of PARP1 and BRCA1 leads to synthetic lethality (Bryant et al., 2005). This highlights PARP1 as an important modulator of DNA repair.

1.1.2.3 NER

NER has two mechanisms for DNA lesion detection: global genome NER (GG-NER) and transcription coupled NER (TC-NER) (Marteijn et al., 2014). In GG-NER, bulky DNA adducts, including CPDs and 6-4PPs, as well as DNA intrastrand crosslinks are detected by the XPC complex. In TC-NER, RNA polymerase blocking by the lesions leads to recruitment of CSA and CSB (Cockayne syndrome A and B) proteins. While the initial damage recognition machineries are different, GG-NER and TC-NER converges when the transcription initiation factor IIH (TFIIH) complex is recruited and XPB/D helicases from the complex unwind the DNA and verify the presence of the lesion together with XPA. Then, structure-specific endonucleases ERCC1-XPF and XPG excise the damaged DNA leaving a gap of ssDNA. DNA synthesis and ligation are executed similarly to BER.

1.1.2.4 MMR

The MMR process involves a complex interplay of MMR-specific proteins with the replication and/or HRR machinery. It is activated by the binding of the mismatch-recognition factors, MSH2/3 and MSH2/6, to substrates that contain base–base mismatches and insertion/deletion loops that arise from errors of DNA polymerases or during homology search of the D-loop in HRR (Acharya et al., 1996). The ATP-dependent recruitment of MLH complexes (MLH1/PMS2, MLH1/PMS1, and MLH1/MLH3) to the MSH complex is followed by EXO1-mediated removal of the error-containing strand (Zhang et al., 2005). Remarkably, downstream processes for DNA synthesis and nick ligation that complete the repair process are mediated by the same set of enzymes used in BER. MMR is important because it improves the fidelity of DNA replication and aborts illegitimate recombination.

1.1.2.5 FA

The FA pathway is specialized for removal of DNA interstrand crosslinks (ICL) caused by genotoxins such as mitomycin C (MMC), cisplatin and cyclophosphamide (Deans and West, 2011). There are 14 proteins whose genes are categorized as complementation groups of FA. As many as 7 of them and other accessory proteins form a core complex around FANCM, which detects ICL. The complex is a huge ubiquitin ligase that ubiquitylates FANCD2-FANCI dimer. Following ubiquitylation, FANCD2-FANCI recruits nucleases and polymerases from other pathways, most notable HRR, NER and TLS, to complete the repair.

1.1.2.6 DNA damage tolerance

DNA lesions that have gone unrepaired or generated just before replication initiation can be encountered by the replication machinery and are sometimes bypassed using mechanisms of DNA damage tolerance (DDT), including translesion synthesis (TLS) and template switching. When PCNA-bound error-free DNA polymerases ε and δ are stalled by DNA lesions, PCNA is monoubiquinated by RAD6-RAD18 ubiquitin ligases (Watanabe et al., 2004). This triggers the release of error-free DNA polymerases and the recruitment of error-prone TLS polymerases ζ – κ which are able to replicate across lesions. However, subsequent repair of the lesion would often cause point mutations. An error-free pathway is initiated when PCNA is further polyubiquitinated by UBC13-MMS2-SHPRH complex (Motegi et al., 2006). Although the downstream mechanism is still unclear, it is thought that nascent DNA is unwound from the damaged template and annealed to the newly synthesized sister chromatid for normal replication (Lee and Myung, 2008).

1.1.3 Coordination of cell cycle and DNA repair

In response to DNA damage, the ATM and ATR checkpoint signaling pathway not only arrest cell cycle progression, but also directly participate in and facilitate DNA repair pathways. Conversely, DNA repair proteins process specific lesions into common structures for activation of checkpoint signaling pathway, and may also directly facilitate checkpoint kinase activity. As such, a coordination between cell cycle regulation and DNA repair provides timely control of DDR (Zhou and Elledge, 2000). Listed below are the players involved in the functional coordination between DNA damage checkpoint signaling and DNA repair.

1.1.3.1 Checkpoint proteins facilitate DNA repair

ATM and CHK2 kinases are responsible for the phosphorylation of many proteins directly or indirectly participating in DNA repair (Figure 1.4). Chromatin remodeling protein KAP1 is phosphorylated by ATM at damaged sites to promote chromatin relaxation for better recruitment of repair proteins (Ziv et al., 2006). ATM and CHK2 directly participate in HRR by phosphorylating BRCA1 at different sites, with functional consequences in stimulating its interactions with PALB2, BRCA2 and RAD51 (Cortez, 1999, Roy et al., 2012). In BER, CHK2-dependent phosphorylation of XRCC1 and ATM-dependent phosphorylation of tyrosyl-DNA phosphodiesterase 1 (TDP1) promote recruitment of XRCC1 and TDP1 to AP sites (Chou et al., 2008, Das et al., 2009). ATM also has a role in MMR pathway, specifically in the phosphorylation of MLH1 to promote its stability (Romeo et al., 2011).

Similarly, the activity of ATR and CHK1 kinases regulate several DNA repair pathways (Figure 1.4). CHK1 phosphorylates RAD51 to promote RAD51 foci formation (Sorensen et al., 2005). In NER, ATR phosphorylates XPA at two different sites, one that promote nuclear import

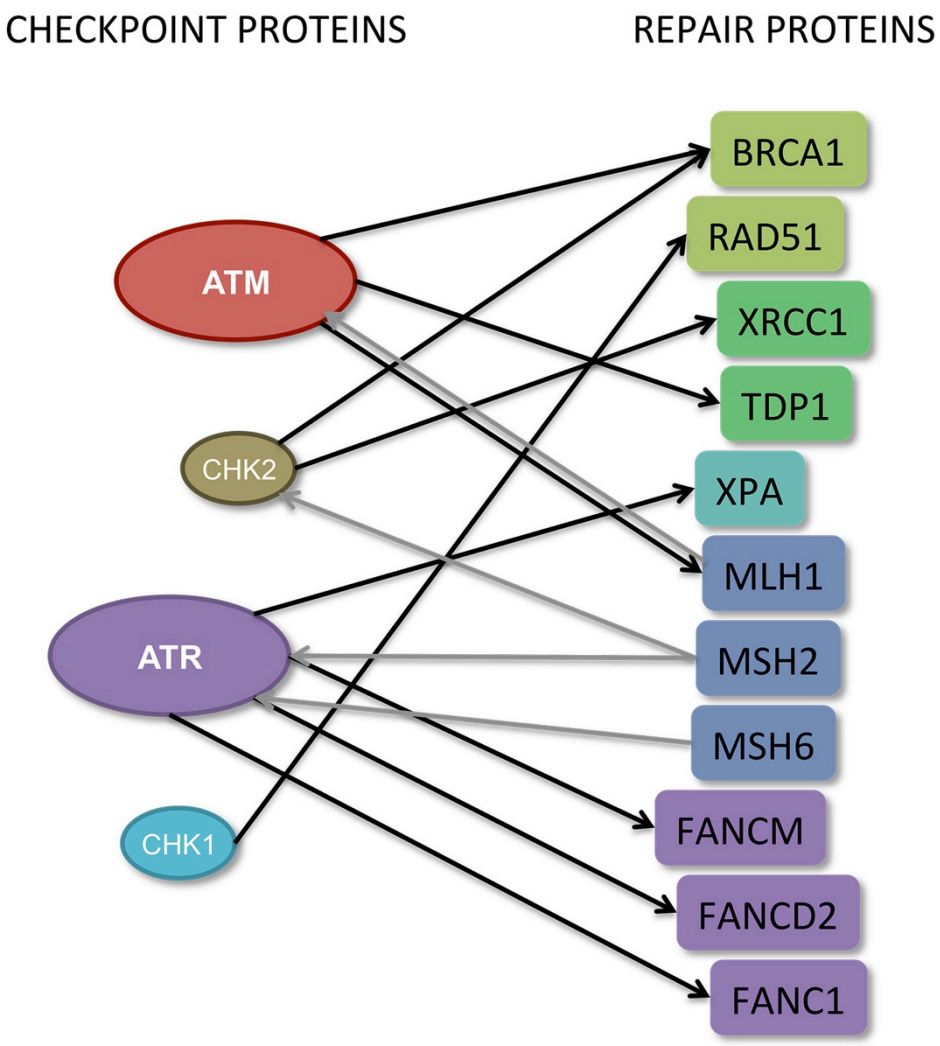

Figure 1.4. Functional interplay between checkpoint proteins and DNA repair proteins. Checkpoint proteins are color-coded similar to Figure 1.2. Repair proteins are color-coded similar to Figure 1.3. Black arrows indicate phosphorylation. Grey arrows indicate direct interaction and recruitment.

of XPA (Wu et al., 2007) and the other for antagonizing interaction of XPA with HERC2 to prevent ubiquitination-mediated degradation of XPA (Lee et al., 2014). Furthermore, ATR plays a major role in FA pathway. It phosphorylates FANCM to promote FANCM recruitment to ICL sites (Singh et al., 2013). ATR also phosphorylates FANCD2 and FANCI to promote FANCD2 monoubiquitination and formation of FANCD2/FANCI complex (Andreassen et al., 2004, Ishiai et al., 2008).

A unique modulation of the BER pathway is mediated by the 9-1-1 complex, a critical component of the ATR checkpoint signaling pathway. 9-1-1 clamp has been shown to interact with many BER proteins, including DNA glycosylases MYH, NEIL1 and TDG, as well as downstream proteins APE1, FEN1, Pol β and DNA ligase I (Table 1.1). However, exactly how the 9-1-1 complex stimulate the BER pathway at almost all steps, and whether the kinase activity of ATR or CHK1 is involved, remains unclear.

1.1.3.2 DNA repair proteins regulate checkpoint pathways

Conversely, DNA repair proteins can promote ATR checkpoint signaling pathway through processing of a variety of DNA lesions into ssDNA, a common substrate for RPA binding and ATR activation. For example, in response to oxidative stress, BER protein APE2 resects and generates ssDNA, and promote RPA-ssDNA formation (Willis et al., 2013). EXO1 functionally couples NER to ATR checkpoint signaling by converting NER intermediates into ssDNA (Giannattasio et al., 2010). The same protein is also involved in resection of DSB into ssDNA. Other than that, some MMR proteins associate directly with the checkpoint kinases and recruit them to DNA lesions (Figure 1.4). Interactions between MSH2 and CHK2 as well as between MLH1 and ATM promote the recruitment of checkpoint proteins to IR-damaged sites

Table 1.1. A list of DNA repair proteins that directly interact with 9-1-1 clamp.

DNA repair component	Repair pathway	Interacting partner(s)	References
SpMYH	BER	SpRad9, SpHus1, SpRad1	(Luncsford et al., 2010, Chang, 2004, Chang et al., 2006)
FEN1	BER	RAD9, HUS1, RAD1	(Friedrich-Heineken et al., 2005, Wang, 2004)
Pol β	BER	RAD9, HUS1, RAD1	(Toueille et al., 2004)
DNA Ligase I	BER	RAD9, HUS1, RAD1	(Smirnova et al., 2005)
APE1	BER	RAD9, HUS1, RAD1	(Gembka et al., 2007)
NEIL1 glycosylase	BER	RAD9, HUS1, RAD1	(Guan et al., 2007a)
TDG glycosylase	BER	RAD9, HUS1, RAD1	(Guan et al., 2007b, Wang et al., 2005)
hOGG1 glycosylase	BER	RAD9, HUS1, RAD1	(Park et al., 2009)
RAD51	HR	RAD9	(Pandita et al., 2006)
EXO1	HR	Mec3 (HUS1)	(Karras et al., 2013)
WRN helicase	HR?	RAD1	(Pichierri et al., 2012)
Metnase	NHEJ	RAD9	(De Haro et al., 2010)
Rad14 (XPA?)	NER	Ddc1 (RAD9)	(Giannattasio et al., 2004)
MSH2	MMR	RAD9, HUS1, RAD1	(Bai et al., 2010)
MSH3	MMR	RAD9, HUS1, RAD1	(Bai et al., 2010)
MSH6	MMR	RAD9, HUS1, RAD1	(Bai et al., 2010)
MLH1	MMR	RAD9	(He et al., 2008)
Rev7	TLS	Mec3 (HUS1) Ddc1 (RAD9)	(Sabbioneda, 2005)
DinB	TLS	SpHus1, SpRad1	(Kai and Wang, 2003)

and facilitate CHK2 phosphorylation by ATM (Brown et al., 2003). MSH2-6 complex also recruits ATR to specific mismatch lesions (Yoshioka et al., 2006, Pabla et al., 2011).

1.2 HUS1 and the 9-1-1 complex

As described in section 1.1.1, the RAD9A-HUS1-RAD1 (9-1-1) complex is extensively studied for its role in ATR checkpoint activation. However, recent studies implicate the 9-1-1 complex in DNA repair too (detailed in sections 1.1.3.1 and 1.2.5), although the mechanisms and physiological significance of these interactions is still unclear. 9-1-1 potentially mediates functional coordination between checkpoint signaling and DNA repair, making it an interesting research subject.

1.2.1 Discovery

Rad9 (radiation-sensitive), *Rad1* and *Hus1* (hydroxyurea-sensitive) genes were first identified in a series of genetic screens for DNA replication checkpoint genes in S. *pombe* (Enoch et al., 1992, Al-Khodairy and Carr, 1992). Mutant fission yeasts deficient in these genes display hypersensitivity to replication stress inducer hydroxyurea (HU) (Enoch et al., 1992), UV (al-Khodairy et al., 1994) and the radiomimetic drug bleomycin (Kostrub et al., 1998). Subsequently, homologs of these genes in higher eukaryotes, including M. *musculus* and H. *sapiens* were identified and cloned (Dean et al., 1998, Weiss et al., 1999). Functional implications of disrupting these genes are discussed in section 1.2.5.

Through DNA sequence BLAST search and subsequent cloning, it was discovered that *Rad9* and *Hus1* have functional paralogs in higher eukaryotes, namely *Rad9b* and *Hus1b* (Dufault et al., 2003, Hang et al., 2002). For clarity, *Rad9* was renamed *Rad9a*. These paralogs are highly expressed in meiotic germline cells, and may have functional implications in meiotic checkpoint signaling and recombination through the formation of alternative 9-1-1-like clamps (Lyndaker et al., 2013b).

1.2.2 9-1-1 Structure

Initially, no one suspected that these 3 seemingly unrelated proteins associate with each other and form a complex, although epistasis analysis in S. *cerevisiae* suggested that they might act in conjunction with each other (Lydall and Weinert, 1995). Subsequent structural prediction experiments suggested that 9-1-1 forms a toroidal heterotrimeric DNA clamp that is structurally similar to proliferating cell nuclear antigen (PCNA) (Venclovas and Thelen, 2000) (Figure 1.5). PCNA is a homotrimeric toroidal complex with a central pore that can encircle duplex DNA (Krishna et al., 1994). Each PCNA subunit consists of two globular domain linked by an interdomain connecting (IDC) loop. The central pore is lined with α-helices which contain highly conserved positively charged residues capable of interaction with DNA backbone (Naryzhny, 2008, McNally et al., 2010). Structure/function relationship studies also reveal that PCNA has a hydrophobic pocket, formed by residues on the second globular domain and the IDL, which is the docking site of most PCNA interacting protein (PIP) box motif-carrying proteins (Naryzhny, 2008). With these features, PCNA provides a DNA-bound scaffold for replicase assembly and processivity. Besides replication, PCNA is also involved in DNA repair pathways, primarily in polymerase switching for translesion synthesis (TLS) (Hishiki et al., 2009) and in recruiting base excision repair (BER) factors (Song et al., 2009, Friedrich-Heineken et al., 2005).

Recent crystal structure resolutions of the 9-1-1 complex have divulged much valuable topological information of the clamp that can be exploited to further investigate its mechanistic function (Xu et al., 2009, Doré et al., 2009, Sohn and Cho, 2009). Most notably, without much sequence homology, each of the 9-1-1 subunits folds into 2 globular domains linked by an IDC loop much like PCNA, although there are slight distinctions in shape and charge (Figure 1.5).

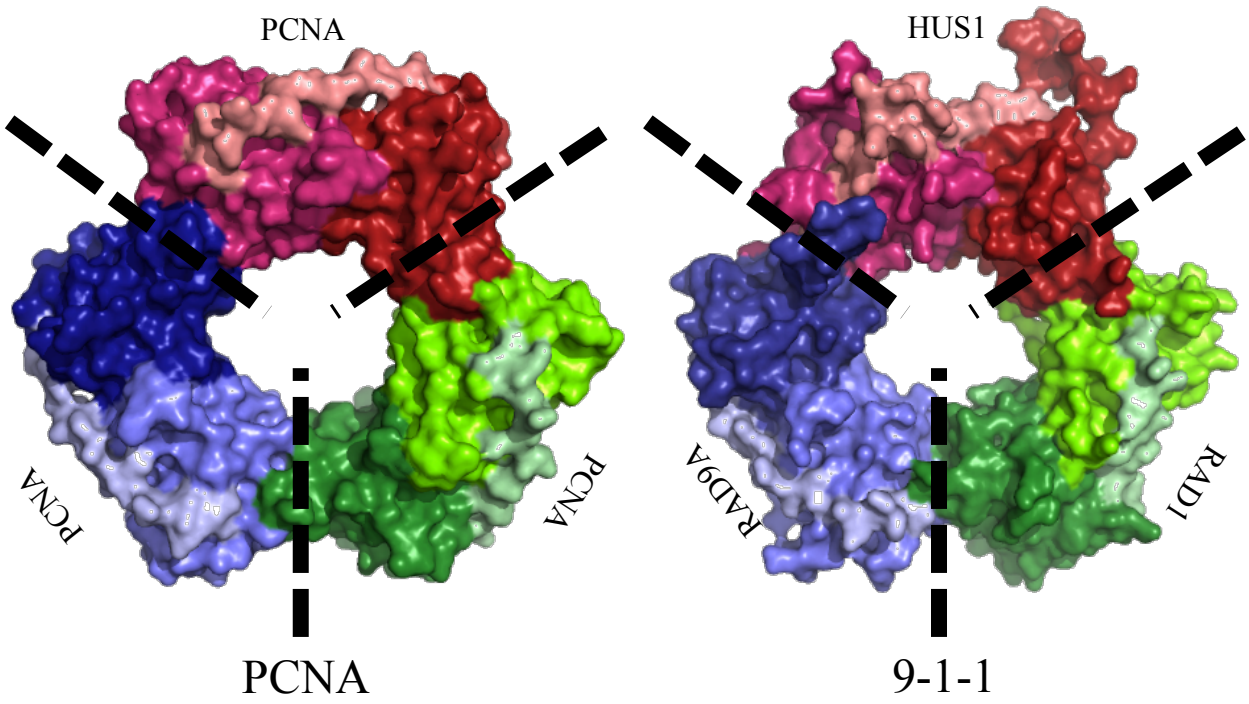

Figure 1.5. Crystal structures of PCNA homotrimer clamp and 9-1-1 heterotrimer clamp. Each subunit is pseudo-colored blue, red or green with 3 intonations to differentiate globular domain 1, globular domain 2 and interdomain connecting (IDC) loop. Images are modified from PDB files 1VYM and 3GGR.

Analogous to PCNA, individual 9-1-1 subunits associate with each other in a head-to-tail manner to form a stable heterotrimeric complex. The central pore of the 9-1-1 complex also contains positively-charged residues for DNA contact (Jordi et al., 2012). Furthermore, the RAD9A and HUS1 subunits are predicted to possess a PCNA-like hydrophobic pocket for protein-protein interactions (Doré et al., 2009), potentiating the 9-1-1 complex for pathway coordination functions.

1.2.3 Expression and subcellular localization

The mRNA and/or protein of *Rad9a*, *Hus1* and *Rad1* are ubiquitously expressed in all tissue types tested, with higher abundance in testes (Hang and Lieberman, 2000, Weiss et al., 1999, Freire et al., 1998, Hang et al., 1998). Intriguingly, there are a few short mRNA isoforms of *Hus1* and *Rad1* found in abundance only in testes samples, suggesting a posttranscriptional regulation of their mRNA expressions. Indeed, Ensembl annotation (http://www.ensembl.org/index.html) and 3'-seq data from Christine Mayr's lab (http://cbio.mskcc.org/leslielab/ApA/atlas/) indicate that *Hus1* and *Rad1* mRNA isoforms are produced by alternative polyadenylation events at the 3'UTR. How this regulation affects protein level is still unclear.

Under normal conditions, RAD9A, HUS1 and RAD1 proteins are mostly located in the cytoplasm throughout the cell cycle. Upon DNA damage or replication stress, RAD9A associates with RAD1 and HUS1 and transports the entire complex into the nucleus via its nuclear localization sequence (Hirai et al., 2004, Hirai and Wang, 2002).

1.2.4 DNA loading mechanism and preference

9-1-1 is loaded by a clamp loader formed by five subunits, RAD17 and RFC2-5. Several lines of evidence indicate that DNA damage induced clamp loading relies on RAD17 interaction with RAD1 (Rauen et al., 2000, Caspari et al., 2000, Parker et al., 1998). Interestingly, RFC2-5 forms another clamp loader with RFC1 that loads PCNA onto DNA (Bermudez et al., 2003). 9-1-1 is preferentially loaded at 5' recessed ends, in contrast to PCNA which prefers loading at 3' recessed DNA ends (Majka et al., 2006). PCNA-DNA interactions are crucial for clamp loading (McNally et al., 2010). Whether the 9-1-1 complex has similar requirements is unknown.

1.2.5 9-1-1 Function

Once loaded at damage sites, one established function of the 9-1-1 complex is to stimulate ATR kinase activation through interactions with DNA topoisomerase 2-binding protein 1 (TOPBP1) (Delacroix et al., 2007). Activated ATR phosphorylates several substrates, including the effector kinase CHK1, which induce cell cycle arrest, stabilize stalled forks and inhibit origin firing (Cimprich and Cortez, 2008).

In addition to its checkpoint signaling functions, 9-1-1 also acts directly in DNA repair through its role as a molecular scaffold (Helt et al., 2005, Eichinger and Jentsch, 2011). The 9-1-1 clamp can physically interact with and stimulate the activity of factors in many DNA repair pathways (Table 1.1). Other than that, the 9-1-1 clamp can interact with HDAC1 as well, possibly promoting chromatin structure reorganization and implicating 9-1-1 complex in transcription regulation during DNA damage (Cai et al., 2000). However, the physiological significance of these interactions is unknown because deletion of 9-1-1 invariably leads to the manifestation of checkpoint signaling defects that complicate assessment of DNA repair defects (Levitt et al., 2005, Weiss et al., 2003, Weiss et al., 2000).

1.2.6 Physiological significance

Mouse HUS1 protein (mHUS1) shares 31% amino acid identity with fission yeast HUS1 (SpHUS1), but 84% identity with human HUS1 (hHUS1). *mHus1* has functionally diverged from *SpHus1* based on several observations. *SpHus1* is not required for essential cellular processes in fission yeast (Enoch et al., 1992), but *mHus1* constitutive knockout causes midgestational embryonic lethality which is accompanied by severe DNA damage (Weiss et al., 2000, Levitt et al., 2005). Genotoxin sensitivity studies using stable *Hus1* deficient ($Hus1^{-/-}$ $p21^{-/-}$) mouse embryonic fibroblast (MEF) reveal that *Hus1* deficiency in mouse cells causes hypersensitivity towards HU and UV, but not to ionizing radiation (IR) (Weiss et al., 2000), in contrast to *SpHus1* null fission yeast which is sensitive to all three genotoxins (section 1.2.1). Further studies on this cell line show that *mHus1* is crucial for intra-S DNA damage cell cycle checkpoint but not for G2/M checkpoint (Weiss et al., 2003), unlike *SpHus1* which is required for both checkpoints (Enoch et al., 1992). Therefore, *in vivo Hus1* studies using the mouse model may be essential to reflect a more accurate picture of DDR mechanisms in higher eukaryotes.

Since complete *mHus1* inactivation causes severe genomic instability and embryonic lethality, *in vivo* and *in vitro* studies of *Hus1* were conducted using two methods: 1) generation of *Hus1* allelic series or 2) conditional/cell specific *Hus1* knockout. In the first method, a hypomorphic allele that is partially impaired for *Hus1* gene function ($Hus1^{neo}$) is paired with wildtype ($Hus1^{+}$) or null ($Hus1^{\Delta 1}$) *Hus1* alleles to generate an allelic series of *Hus1* expression in mice ($Hus1^{+/+}$, $Hus1^{+/neo}$, $Hus1^{+/\Delta 1}$, $Hus1^{neo/neo}$, $Hus1^{neo/\Delta 1}$) (Levitt et al., 2007). Mice with the lowest level of *Hus1* expression ($Hus1^{neo/\Delta 1}$) have elevated GIN evidenced by micronucleus formation in peripheral blood cells and $Hus1^{neo/\Delta 1}$ primary MEF show premature senescence,

increased spontaneous and aphidicolin-induced chromosomal instability, as well as hypersensitivity towards oxidative stress (Levitt et al., 2007). The most common types of chromosomal aberration associated with partial loss of *Hus1* function are chromatid breaks and radial chromosomes, a common phenotype for aberrant DSB repair.

In the second method, a cre-lox system is utilized to create *Hus1* conditional knockout (CKO) in a cell-specific manner. This is achieved by delivering adenovirus carrying cre-recombinase or by cell-specific promoter-driven expression of cre-recombinase to delete *Hus1* exons 2 and 3 which are flanked by loxP sites. CKO of mHus1 in primary MEFs lead to impaired cell proliferation, DSB accumulation, increased common fragile site breakage and apoptosis (Zhu and Weiss, 2007). Similarly, *Hus1* CKO in murine mammary epithelium *in vivo* increased DNA damage in those cells and induce p53-mediated apoptosis and clearance (Yazinski et al., 2009). *Hus1* deficiency not only affects the viability of mitotic cells but also that of meiotic cells, as evidenced from *Hus1* CKO in murine testis leading to germ cell depletion (Lyndaker et al., 2013a).

It is indisputable that *Hus1* plays an important role in checkpoint signaling, but some phenotypes caused by *Hus1* deficiency can be attributed to defective DSB repair too. Chromosomal breaks and radial formations are increased in *Hus1* hypomorph and *Hus1* null MEFs, the types of chromosomal aberrations similarly found in *Brca1* or *Brca2* deficient cells which are defective in homologous recombination repair (HRR) (Farmer et al., 2005). There are a few other lines of evidences that suggest *Hus1* role in HRR. It is reported that *Hus1* siRNA knockdown in mouse kidney fibroblast cells reduced HR efficiency (Wang et al., 2005). Also, RAD9 is implicated in HRR because it interacts with RAD51 (Pandita et al., 2006)(Table 1.1). It is further shown that RAD9 colocalizes with RAD51 during meiotic recombination, and loss of

HUS1 leads to persistent RAD51 foci past the pachytene stage of prophase I in meiosis (Lyndaker et al., 2013a). These data implies that the 9-1-1 complex directly participates in HRR.

1.3 Genomic instability, heritable diseases and cancer

Checkpoint signaling and DNA repair proteins are the guardians of genomic integrity, preventing chromosomal aberrations such as deletion and amplification, translocation, breaks, fusion, and whole chromosome gain or loss. Mutations in these proteins usually lead to genomic instability and cause heritable diseases and tumorigenesis. In fact, inherent instability of the genomic contents is one of the hallmarks of cancer, and heritable diseases caused by DNA damage response defect are often associated with susceptibility to tumorigenesis (Hanahan and Weinberg, 2011). Below details the pathological consequences of checkpoint and DNA repair defects, as well as current strategies to target DNA damage response pathways as means for effective anticancer therapy.

1.3.1 Checkpoint defects

Deregulation of the ATM and ATR checkpoint pathways lead to diseases with characteristic phenotypes caused by genomic instability. *Atm* recessive mutation causes Ataxia-telangiectasia (A-T, OMIM #208900) characterized by ataxia, cerebellar degeneration and oculomotor apraxia. Patients of the Nijmegen breakage syndrome (NBS, OMIM #251260), characterized by microcephaly, facial dysmorphism and growth defects, harbor autosomal recessive mutation in *Nbs1*. The Li-Fraumeni syndrome (LFS) is linked to autosomal dominant mutations of *Tp53* (LFS1, OMIM #151623) and germline mutations in *Chek2* (LFS2, OMIM #609625). Interestingly, all these diseases are associated with infertility, immunodeficiency and increased predisposition to tumor malignancy, suggesting the underlying importance of the ATM pathway to maintain proper meiotic DSB repair, V(D)J/immunoglobin class switch recombination and tumor suppression.

On the other hand, it is less clear if the components of the ATR pathway are implicated in human genetic diseases, other than *Atr* mutation which causes Seckel syndrome (SCKL1, OMIM #210600), a rare mental retardation disorder accompanied by dwarfism and facial defects. The limited number of naturally occurring mutations may perhaps allude to the notion that the ATR pathway is indispensable for genome maintenance and normal cell proliferation. As such, targeted disruption of *Atr*, *Chk1*, *Hus1*, *Rad9, Rad1* or *Rad17* in mice results in embryonic lethality at different stages, and the lethality phenotype is associated with massive chromosomal aberrations (Brown and Baltimore., 2000, Weiss et al., 2000, Budzowska et al., 2004, Takai et al., 2000, Hopkins et al., 2004). Curiously, SCKL1 patients do not display elevated cancer risk as seen in A-T, NBS and LFS patients. However, conditional inactivation studies on the ATR pathway components report contradicting observations. Conditional *Atr* knockout in cultured cells (Brown, 2003), as well as mammary gland-specific *Chk1* and *Hus1* loss (Lam et al., 2004, Yazinski et al., 2009) do not cause predisposition to tumor formation, but increasing tumorigenic events are observed in the case of *Atr* heterozygosity (Brown and Baltimore., 2000), *Chk1* haploinsufficiency (Lam et al., 2004) and keratinocyte-specific *Rad9* loss (Hu et al., 2008). This suggests that the ATR pathway may have roles in both tumor suppression and progression, but the distinctive mechanisms are unclear.

1.3.2 DNA repair defects

Many mutations of DNA repair proteins are implicated in GIN-related heritable diseases and cancer predisposition. Mutations in *Brca1* and *Brca2,* two key genes for homologous recombination repair, lead to susceptibility to breast cancer (OMIM#113705 and #600185). Heraditary nonpolyposis colorectal cancer (HNPCC) is predisposed by mutations in almost all

key genes involved in mismatch repair (*mlh1*, OMIM#120436; *mlh3*, OMIM#604395; *msh2*, OMIM#609309; *msh6*, OMIM#600678). Various nucleotide excision repair genes are implicated in 3 autosomal recessive diseases: xeroderma pigmentosum (XP), which cause skin sensitivity to UV exposure (OMIM#278700); Cockayne syndrome (CS), which impairs nervous system development and causes premature aging on top of photosensitivity (OMIM#216400); and trichothiodystrophy (TTD), characterized by brittle hair and impaired nervous system development (OMIM#601675). XP patients are usually predisposed to melanoma and squamous cell carcinoma, but for reasons unknown no cancer is associated to CS and TTD patients. Fanconi anemia (FA) is a genetically heterogeneous disorder that is caused by mutations in any of the genes in 13 complementation groups, all of which are involved in DNA crosslink repair. FA patients often exhibit symptoms like pancytopenia, bone marrow failure and high predisposition to leukemia.

1.3.3 Targeting checkpoint and DNA repair pathways for anticancer therapy

Traditional chemotherapy utilizes platinum-based drugs, nitrogen mustards and other crosslinking agents to create replication stress that affects highly proliferative cancer cells. There are two important recent breakthroughs in understanding fundamental aspects of cancer cell biology, with important implications for cancer therapy (Lord and Ashworth, 2012). Firstly, it has emerged that stress phenotypes are basic characteristics of cancer cells. The malignant transformation of cells give rise to a set of stress phenotypes such as metabolic stress, proteotoxic stress, mitotic stress, oxidative stress and DNA damage stress (Hanahan and Weinberg, 2011). Therefore, cancer cells are highly dependent on stress response pathways to tolerate the consequences of severe genomic instability. This dependency is termed ‘non-

oncogene addiction' of cancer and may be an important point of susceptibility for cancer cells (Luo et al., 2009). Secondly, cancer cells often harbor defects in DNA repair or other DNA damage response (DDR) pathways. One common example is breast cancer, which is predisposed by the loss of function of *Brca1* and *Brca2* genes pertinent for HRR (Farmer et al., 2005). Hence, cancer cells are highly dependent on other redundant and overlapping DDR mechanisms.

The established strategy for antitumor therapies was to exploit tumor hypersensitivity towards DNA damage (Jackson and Bartek, 2009). However, tumors can develop intrinsic or acquired resistance against genotoxins, thereby reducing the efficacy of the therapy. This is due to the fact that tumors defective in certain specific repair mechanism can shift its dependence to another repair pathway for survival. Therefore, DDR components are potential novel therapeutic targets that can be utilized in two ways (Helleday et al., 2008, Deans and West, 2011). Firstly, DNA repair and DDR inhibitors can be combined with traditional genotoxins in antitumor therapy to produce synergistic results. For example, inhibitors of CHK1 have been proven effective for sensitizing cancer cells towards any chemotherapy that creates replication stress (Guzi et al., 2011). Similarly, inhibitors of ATM, ATR and PCNA are at various stages of clinical trials and show promising signs of effective cancer suppression. Secondly, DNA repair and DDR inhibitors can further be developed into monotherapies by exploiting synthetic lethality interactions between two crosstalking DNA repair pathways. For example, the discovery of synthetic lethal relationship between *Parp1* and *Brca1* led to clinical studies of using PARP1 inhibitors to treat breast cancer with *Brca1* mutations (Reinhardt et al., 2009).

1.4 Summary

The DDR machinery protects cells from DNA insults. Checkpoint signaling activation and DNA repair are two key elements of the DDR, and there are multiple signaling pathways that higher eukaryotes have evolved to deal with many types of DNA lesions. Initial discovery of checkpoint and repair genes and the studies for their functions brought about detailed molecular pathways within each gene onthology or 'interactome'. Soon, the need for proper spatiotemporal and molecular coordination between these signaling events becomes apparent. Key proteins in the checkpoint signaling pathways have been discovered to regulate DNA repair proteins, and vice versa. Understanding how these pathways are connected is crucial for appreciating genome maintenance mechanisms in normal cells and in cancer.

Checkpoint protein HUS1 and the 9-1-1 complex is potentially a key component for the regulation of cell cycle and DNA repair. In the ATR pathway, the canonical function of HUS1 in the 9-1-1 complex is to recruit TOPBP1 for ATR activation and checkpoint signaling. HUS1 interactions with some DNA repair components have been described but the physiological implications are unknown. HUS1 is also suggested to have roles in HR repair. Therefore, it is tempting to hypothesize that HUS1-mediated DNA repair, in addition to checkpoint signaling, is essential for DNA damage survival.

Given the central role for DDR pathways in cancer therapy, understanding the interactions between components of checkpoint signaling pathway and those of various different DNA repair pathways is important for designing effective therapeutics. HUS1 and the 9-1-1 complex is unique among components of the ATR checkpoint signaling pathway because of its structure that is optimized for molecular scaffolding, potentiating a function in coordinating checkpoint signaling and DNA repair. HUS1, in particular, has PCNA-like topology and several

unique features that require further investigation to map potential Hus1 residues for specific functions in DNA and protein interactions. The proposed study has the potential to reveal many significant roles of Hus1 acting as a processivity factor facilitating protein-DNA interactions. I combine molecular and genetic tools in my approach to study HUS1 functions. My approach utilizes stable *Hus1* deficient cells (*Hus1*$^{-/-}$ *p21*$^{-/-}$) (Weiss et al., 2000) to perform complementation tests for structure/function analysis of HUS1 (chapter 2). I will also use *Hus1* hypomorph mice (Levitt et al., 2007) for *in vivo* studies of genetic relationship between *Hus1* and HR repair (chapter 3). These approaches will expand the understanding of HUS1/9-1-1 function in DNA repair and highlight potential targets that can be exploited clinically.

CHAPTER 2

GENOME PROTECTION BY THE 9-1-1 SUBUNIT HUS1 REQUIRES CLAMP FORMATION, DNA CONTACTS AND ATR SIGNALING-INDEPENDENT EFFECTOR FUNCTIONS[1]

Pei Xin Lim, Darshil R. Patel, Kelsey E. Poisson, Manpreet Basuita, Charlton Tsai, Amy M. Lyndaker, Robert S. Weiss

Department of Biomedical Sciences, Cornell University, Ithaca, NY, 14853 USA

2.1 Abstract

The RAD9A-HUS1-RAD1 (9-1-1) complex is a heterotrimeric clamp that promotes checkpoint signaling and DNA repair at damage sites. In this study, we elucidated HUS1 functional residues that drive clamp assembly, DNA interactions, and downstream effector functions. First, we mapped a HUS1-RAD9A interface residue that was critical for 9-1-1 assembly and DNA loading. Next, we identified multiple positively charged residues in the inner ring of HUS1 that were crucial for genotoxin-induced 9-1-1 chromatin localization and ATR signaling. Finally, we found two hydrophobic pockets on the HUS1 outer surface that were important for cell survival after DNA damage. Interestingly, these pockets were not required for 9-1-1 chromatin localization or ATR-mediated CHK1 activation, suggesting that they may serve as interaction domains for the recruitment and coordination of downstream effectors at damage sites. Together, these results indicate that, once properly loaded onto damaged DNA, the 9-1-1 complex executes multiple, separable functions that promote genome maintenance.

[1]Work presented in this chapter has been submitted for publication. Authors' contributions: R.S.W. conceived the research; R.S.W., P.L., and A.M.L. designed the research; P.L., D.R.P., K.E.P., M.B., and C.T. performed

2.2 Introduction

Cells must protect genomic integrity in the face of a myriad of insults from both exogenous and endogenous sources. Failure of genome maintenance can lead to premature aging, developmental defects, and tumorigenesis (Ciccia and Elledge, 2010, Jackson and Bartek, 2009). To prevent these deleterious outcomes, cells have evolved DNA damage response (DDR) pathways that trigger cell cycle arrest and afford cells the means for DNA repair, senescence or apoptosis (Hoeijmakers, 2001, Zhou and Elledge, 2000, Jackson and Bartek, 2009). Central to DDR pathways are checkpoint proteins which function in the regulation of DNA repair, cell cycle transitions, replication fork stability, transcriptional programs and apoptosis (Matsuoka et al., 2007, Cimprich and Cortez, 2008).

The RAD9A-HUS1-RAD1 (9-1-1) clamp is a torroidal heterotrimeric DNA clamp that regulates checkpoint signaling after DNA damage (Eichinger and Jentsch, 2011). It is essential for cell survival in various contexts, such as during embryonic development, adult tissue homeostasis, and spermatogenesis as well as following genotoxin exposure (Hopkins et al., 2004, Han et al., 2010, Weiss et al., 2000, Yazinski et al., 2009, Lyndaker et al., 2013a, Vasileva et al., 2013, Freire et al., 1998). The 9-1-1 clamp is evolutionarily and structurally related to proliferating cell nuclear antigen (PCNA), a homotrimeric processivity factor for DNA replication and repair (Moldovan et al., 2007). Like PCNA, each of the 9-1-1 subunits folds into 2 globular domains linked by an interdomain connecting (IDC) loop. Individual subunits associate with each other in a head-to-tail manner to form a stable heterotrimeric complex (Xu et al., 2009, Doré et al., 2009, Sohn and Cho, 2009). PCNA is loaded onto DNA by a clamp loader composed of RFC1-5, whereas 9-1-1 is loaded by RAD17/RFC2-5 (Bermudez et al., 2003). PCNA associates with 3' recessed DNA ends, in contrast to 9-1-1 which is preferentially loaded

at 5' recessed ends (Majka et al., 2006).

Upon DNA damage, RAD9A associates with RAD1 and HUS1 and transports the entire complex into the nucleus via its nuclear localization sequence (Hirai et al., 2004, Hirai and Wang, 2002). Once loaded at damage sites by the RAD17/RFC2-5 clamp loader, one established function of the 9-1-1 complex is to stimulate ATR kinase activation through interactions with DNA topoisomerase 2-binding protein 1 (TOPBP1) (Delacroix et al., 2007). Activated ATR phosphorylates several substrates, including the effector kinase CHK1, which induce cell cycle arrest, stabilize stalled forks and inhibit origin firing (Cimprich and Cortez, 2008).

In addition to its checkpoint signaling functions, 9-1-1 also acts directly in DNA repair through its role as a molecular scaffold (Helt et al., 2005, Eichinger and Jentsch, 2011). The 9-1-1 clamp can physically interact with and stimulate the activity of factors in many DNA repair pathways, including base excision repair (BER), mismatch repair (MMR), nucleotide excision repair (NER), homologous recombination repair (HRR), non-homologous end joining (NHEJ) and translesion synthesis (TLS). However, the physiological significance of these interactions is unknown because deletion of 9-1-1 invariably leads to the manifestation of checkpoint signaling defects that complicate assessment of DNA repair defects (Levitt et al., 2005, Weiss et al., 2003, Weiss et al., 2000).

In order to resolve the relative importance of the DNA repair and checkpoint signaling functions of the 9-1-1 complex, it is necessary to identify residues that are essential for either or both functions. In this study, we report the identification of several functional residues in murine HUS1 (mHUS1) that mediate three critical 9-1-1 activities: clamp formation, DNA association, and interaction with downstream effectors. We used published crystal structures of the human 9-1-1 clamp (Xu et al., 2009, Doré et al., 2009, Sohn and Cho, 2009), computational modeling of

9-1-1 subunit (Xu et al., 2013) and DNA interactions (Jordi et al., 2012), and evolutionary conservation analysis to predict mHUS1 residues that are functionally important. We then experimentally tested the contributions of each residue in functional assays and defined several key features HUS1 that are critical for genome maintenance, including domains that are dispensable for 9-1-1-induced checkpoint signaling but nevertheless required for genotoxic stress resistance.

2.3 Materials and Methods

2.3.1 Plasmids and mutagenesis

All mutations were introduced into the *mHus1* gene using the QuikChange Lightning Multi Site-Directed Mutagenesis kit (Agilent technologies, cat#210515) and the primers listed in Table 2.1. Most mutagenesis was performed on the pBP2-mHus1 retroviral plasmid (Weiss et al., 2002) as the template, with 2 exceptions. In the first case where compound mutations had to be made sequentially, pBP2-mHus1 plasmids with intermediate mutations were used as the template. In the second case, residues K2, F3, R4 and K6 of mHUS1 were mutagenized with the pGEX2T-mHus1 plasmid (cloned in lab) as the template because 5' retroviral long terminal repeats in the pBP2-mHus1 plasmid interfered with mutagenesis. Subsequently, the pGEX2T-mHus1 mutants were subcloned into pBP2 plasmid using restriction digestion (BamHI and EcoRI) and ligation. All mutations were verified by DNA sequencing.

Due to insufficient HUS1 expression from the pBP2-mHus1 plasmid for Western blot detection, all mutant constructs were further subcloned into pCMV-neo-Bam_3 plasmid (courtesy of Bert Vogelstein). pBP2-mHus1 mutants were digested with BamHI and EcoRI and cloned into BamHI-digested CMV-neo-Bam3 via blunt-end ligation to yield CMV-mHus1 mutant

Table 2.1. Primers used for site-directed mutagenesis of *mHus1*

Mutations	Primer [a]
RAD9-interacting residue	
R128E	5'-gtctccatcgagcagcagcgaaatcgtggtgcatgatatc-3'
Inner ring hydrophobic cleft	
V19A, M22A, I23A	5'-cttgtctgaatcatttcacacgagccagtaacgcggcagccaagcttgccaaaacctgc ac-3'
V247A	5'-gccggacagcaagcgactcccaccaag-3'
V271A, L273A	5'-atttgctcctggaagacgcctccgctcagtatttcatcccagc-3'
R18A	5'-ctatcatgttactgactgctgtgaaatgattcagacaagccagg-3' [b]
R18Q	5'-cttgtctgaatcatttcacacaagtcagtaacatgatagccaa-3'
R18Q M22T	5'-cttgtctgaatcatttcacacaagtcagtaacacgatagccaagcttgcca-3'
Inner ring positively charged residues	
R18A	5'-ctatcatgttactgactgctgtgaaatgattcagacaagccagg-3' [b]
K25A	5'-ggtgcaggttttggcaagcgcggctatcatgttactgact-3' [b]
K25A K28A	5'-atgcggagggtgcaggttgcggcaagcgcggctatcatgttactgac-3' [b]
K93A	5'-tctggagttctgggcagttgccaaggctcgagataagttt-3' [b]
R90A, K93A	5'-tggagttctgggcagttgccaaggctgcagataagttttccgacgttaattctaa-3' [b]
K165A	5'-ccacaacactcttcatcatcgccaaggctggtaagcaaatac-3' [b]
K165A, K168A	5'-gtttctcatttttccacaacactcgccatcatcgccaaggctggtaagcaaatactgacg-3' [b]
K173A, R175A	5'-ttcaatcacaagctgattgctgatgtttgccattgcttccacaacactcttcatcatcttcaag-3' [b]
K236A, K237A	5'-aagaaactggaggagtgccgctatgtcaatgtgcaccttggccatgtcttct-3' [b]
Outer ring primary hydrophobic pocket	
P150A	5'-gtggaaggacttacaagaagcctccatcccagac-3'
P150A, I152A, P153A, C155A	5'-gactgtggaaggacttacaagaagcctccgccgcagacgctgacgtcagtatttgctt-3'
V257A, T261A	5'-caaggcagtgtgcaatattgcgaataacagagctgttcattttgatttgctc-3'
F276A, P278A	5'-aagacgtctcccttcagtatgccatcgcagccttgtcctagg-3'
S53R	5'-gctcacaccacatcctcacgcctccac-3' [b]
I152R	5'-gacttacaagaaccctccagaccagactgtgacgtcag-3'
I152Y	5'-aaggacttacaagaaccctcctacccagactgtgacgtcagtatt-3'
I152F	5'-cttacaagaaccctccttcccagactgtgacgt-3'
Outer ring secondary hydrophobic pocket	
F3A	5'-[ccgcgtggatcc]atgaaggctcgcgccaagatcg-3' [c]
F3R	5'-cgcgtggatccatgaagcgtcgcgccaagatcgtggacc-3'
F3R, R4A	5'-cgcgtggatccatgaaggctgccgccaagatcgtggacct-3'
G71W	5'-gaacttttttagtgaatttcaaatggaatgggtctctgaagaaaacaacgagattt-3'
I79A	5'-aggagtctctgaagaaaacaacgaggcttatttagaattaacgtcggaaaac-3'
L105A	5'-ccagagccttgaaaatcaaggcgactaacaaacactttccct-3'
K104A, L105A, T106A	5'-ccagaactccagagccttgaaaatcgcggcggctaacaaacactttccctgtcttac-3'
V138A, L139D	5'-gcatgatatccccataaaggctgatccgagaagactgtggaagg-3'
L105R	5'tccagagccttgaaaatcaagaggactaacaaacactttccctg-3'
L139R	5'-tcgtggtgcatgatatccccataaaggttagaccgagaagactgtgg-3'
R4D	5'-[cgcgtggatcc]atgaagtttgacgccaagatcgtggacc-3' [c]
F3R, R4D	5'-[cgcgtggatcc]atgaagcgtgacgccaagatcgtggacc-3' [c]

Table 2.1 (continued)

Outer ring positively charged residues	
K2A, R4A, K6A	5'-gacaagccaggtccacgatcgcggcggcaaacgccat[gaatccacgcgg]-3' [b,c]
R99A, K102A, K104A	5'-gggaaagtgtttgttagtcagcgcgattgccaaggctgcggagttctgggcagttttcaag g-3' [b]
K108A, H109A	5'-cagacacggtaagacagggaaaggctgcgttagtcagcttgattttcaagg-3' [b]
K137A, R141A, R142A, K145A	5'-ggttcttgtaagtccgcccacagtgctgccggaagaaccgctatggggatatcatgcaccacgattc -3' [b]
BII4-6 loop	
Δ215-227	5'-gtgcaccttggccat()taatagagggttttcaagatccttaaaa-3' [b,d]
Δ215-227::hHus1 loop	5'-attttaaggatcttgaaaaccctctattagcctctgaaagtacccatgaaaacagacacccagaagaca tggcca-3' 5'-gcctctgaaagtacccatgaagacagaaacgtagaacacatggccaaggtgcaca-3'
Δ215-227::PCNA loop	5'-cattttaaggatcttgaaaaccctctattacaaactagcaatgtcgataaagaagaagaggcagtagacatggccaag acatggccaag-3' 5'-cttgaaaaccctctattacaaactagcaatgtcgataaagaagaagaggcagtagacatggccaagg tgcacat-3'

[a] The positions of nucleotides altered to create desired mutations are underlined.
[b] antisense primers. Primer orientation was chosen based on lower energy cost of mismatches.
[c] [pGEX-2T sequences]
[d] (39 nucleotides deleted)

constructs. All mutations were verified by DNA sequencing.

In order to attach a C-terminal 3XFLAG epitope tag to the mHUS1 mutants, full length mutant mHus1 sequences were PCR-amplified from pBP2-mHus1 mutant plasmids. The PCR products were digested with BamHI and ligated into BamHI-digested p3XFLAG-CMV^{TM}-14 (Sigma-Aldrich cat#E7908) to yield pCMV-mHus1-3XFLAG mutant constructs. Ligation products were confirmed with restriction digests and the mutations were once again verified by DNA sequencing.

2.3.2 Cell culture, retroviral infection and plasmid transfection

Hus1$^{-/-}$ *p21*$^{-/-}$ mouse embryonic fibroblasts (MEFs) previously described in (Weiss et al., 2000) and (Weiss et al., 2002), and HEK293T cells (ATCC, cat#CRL-3216) were used. All cultured cells were grown on gelatinized dishes in Dulbecco's Modified Eagle's Medium (Corning Cellgro, cat#15-013-CV) supplemented with 10% Bovine Calf Serum (Thermo Scientific Hyclone, cat#SH30072), 1% nonessential amino acids (Corning Cellgro, cat#25-025-CI), 1% L-glutamate (Corning Cellgro, cat#25-005-CI) and 1% penicillin and streptomycin (Corning Cellgro, cat#30-002-CI).

Expression of the various *mHus1* constructs in *Hus1*-deficient MEFs was done in two ways. The first method was pBabe-based retroviral infection for low-level ectopic *Hus1* expression. Retrovirus was produced from filter sterilized supernatant of phoenix ecotropic viral packaging cells (courtesy of Gary Nolan) 24 hours post co-transfection with p(psi)2 helper plasmid and pBP2-GFP, pBP2-mHus1 wildtype or mutant plasmids using FuGENE transfection reagent (Promega, cat#E2691). 100µl of the virus and 10µg of polybrene were used to infect 2X10^5 *Hus1*$^{-/-}$ *p21*$^{-/-}$ MEFs seeded the day before in a 6-well dish format. A day after infection,

the virus was removed and the cells were grown in fresh media for another day before passaging to 10cm dishes for selection in culture medium containing 1.83μg/ml puromycin, replaced every other day for a week. The second method was plasmid transfection of CMV-mHus1 and pCMV-mHus1-3XFLAG high expression constructs. A mix of 575μl of DMEM, 40μg of polyethyleneimine, 4μg of CMV construct and 1μg of pGK-puro was dripped onto 10^6 *Hus1*$^{-/-}$ *p21*$^{-/-}$ MEFs seeded the day before in a 10cm dish. Transfected cells were selected in culture medium containing 1.83μg/ml puromycin, replaced every other day for a week. Stable drug-resistant cells made from both methods were cultured according to the 3T3 passaging protocol for maintenance and experimental use.

HEK293T cells were used to transiently express CMV-mHus1, pCMV-mHus1-3XFLAG and the corresponding mutant constructs. Briefly, a mix of 575μl of DMEM, 24μg of polyethyleneimine and 6μg of construct(s) (2μg for each construct when co-transfected with CMV-hRad9a-Myc and CMV-hRad1-HA) was dripped onto HEK293T cells seeded the day before in a 10cm dish. Transfected cells were scraped and lysed for coimmunoprecipitation and Western blot.

2.3.3 Short term viability and clonogenic survival assays

In the short term viability assay, 10^4 cells of each cell line were seeded in 6-well plates in triplicates and incubated overnight. Cells were either left untreated or treated with 50ng/ml 4-nitroquinoline oxide (4NQO) or 0.5uM aphidicolin for 24 hours. For HUS1 pocket mutants, cells were treated with 15, 30 or 60ng/ml of 4NQO (or 0.75, 1.5 and 3.0uM of aphidicolin) for 24 hours. The cells were then washed with PBS and cultured in fresh media for 3 days, at which point the cells were collected by trypsinization and counted using a Moxi^{TM} Z mini automated

cell counter (ORFLO technologies). Percent survival was calculated by dividing the number of cells after treatment by the number of untreated cells. Statistical analysis was by Student's T-test, and p-values of <0.05 were considered significant.

In the clonogenic survival assay, 10^3 cells of each cell line were seeded in 6-well plates and incubated overnight. Cells were either left untreated or treated for 24 hours with 10 or 30ng/ml 4NQO, or 1.25 or 5uM aphidicolin. The cells were then washed with PBS and cultured in fresh media for 6 days, at which point the cells were fixed with methanol and stained with crystal violet (0.1% in 95% EtOH) overnight. The plates were then washed, dried and scanned for quantification.

2.3.4 Co-immunoprecipitation and immunoblotting

HEK293T cells transiently transfected with CMV-mHus1 (wild-type or mutants), CMV-hRad9a-Myc and CMV-hRad1-HA were irradiated with $100J/m^2$ UVC (Spectroline Spectrolinker^{TM} XL-1000 UV crosslinker) two days after transfection. Two hours post UV, the cells were scrapped from the plates and lysed with NETN buffer (20mM Tris pH8.0, 10mM NaCl, 1mM EDTA and 0.5% NP-40) supplemented with aprotinin, leupeptin, sodium orthovanadate and phenylmethylsulfonyl fluoride (PMSF) and sonicated at 24-30W for 1 min (Misonix Sonicator 3000). Lysates were centrifuged at 14,000 rpm for 30 min and the supernatants were collected for immunoprecipitation. Briefly, 500µg of lysates were incubated with 3µl of anti-MYC (Santa Cruz, cat#sc-40) or anti-HA (Covance, cat#mms-101p) antibodies for 2 h at 4°C. The mixture was then incubated with 30µl of pre-washed protein A/G resin (Thermo Scientific, cat#53132) for 1 h at 4°C. Pellets were washed 3 times with NETN buffer and boiled in loading buffer for SDS-PAGE and Western analysis. Immunoprecipitates or total

cell lysates were resolved in 10% or 12% SDS-PAGE gels and transferred to PVDF membranes (Pall Corporation, cat#BSP0161) for Western blotting following standard procedures. Antibodies specific for HUS1 (Lyndaker et al., 2013a), RAD9A (Lyndaker et al., 2013a), MYC (Santa Cruz, cat#sc-40), HA (Covance, cat#mms-101p), FLAG (Sigma, cat#F1804) pCHK1 Ser345 (Cell Signaling, cat#2341), Histone 3 (Abcam, cat#ab1791), GAPDH (Advanced ImmunoChemical Inc., cat#MAb6C5) and β-actin (Sigma, cat#A5441) were used. Blots were imaged using a VersaDoc Imaging System (Bio-Rad Laboratories).

2.3.5 ConSurf evolutionary conservation and surface electrostatic potential analyses

Amino acid sequences of PCNA, RAD9A, HUS1 and RAD1 from 44 organisms that represent a broad range of taxa were curated from UniProtKB database (http://www.uniprot.org) (Table 2.2). Multiple sequence alignments were created with ClustalX ver2.1 (Julie D. et al., 1997) and uploaded to the ConSurf server (http://consurf.tau.ac.il) (Ashkenazy et al., 2010) for calculation of evolutionary conservation scores (Bayesian method) with reference to the human counterparts of each protein. The scores were projected on available protein structures of PCNA (PDB 1VYM) and RAD9A-HUS1-RAD1 (PDB 3GGR) to identify functional surface residues. All images were created using PyMOL.

The surface electrostatic potential of HUS1 was calculated and displayed using the Adaptive Poisson-Boltzmann Solver (APBS) plugin in PyMOL. In the calculations, dielectric constants of 1.0 and solvent ionic strength equivalent to 75mM KCl were used. Side chains lysine and arginine residues were given a net positive charge, aspartate and glutamate negative, and other residues neutral. Positive and negative color contours were set at +/- 10kT/e.

Table 2.2. List of UniProtKB accession numbers of the PCNA, RAD9A, HUS1 and RAD1 sequences used for evolutionary conservation analysis.

		Accession numbers			
Organism	Symbol	PCNA	RAD9A	HUS1	RAD1
Ailuropoda melanoleuca (Giant panda)	AILME	D2HQS7	G1L1M9	G1LDT0	G1L9B8
Arabidopsis thaliana (Mouse-ear cress)	ARATH	Q9M7Q7	F4J7B7	Q709F6	Q8L7G8
Bos taurus (Bovine)	BOVIN	Q3ZBW4	Q5EAC3	E1BG06	E1BB72
Caenorhabditis elegans (Nematode worm)	CAEEL	O02115	Q9NBJ6	G5EFI9	G5EC44
Callithrix jacchus (White-tufted-ear marmoset)	CALJA	F7GZC8	U3DMA2	F7G3C8	F7I3N9
Canis familiaris (Dog)	CANFA	E2R0D6	F6XPS6	F1Q245	E2QYH8
Cavia porcellus (Guinea pig)	CAVPO	H0VE65	H0VIK1	H0WC14	H0VEA3
Ceratitis capitata (Mediterranean fruit fly)	CERCA	W8B157	W8C9F2	W8C4C2	W8B5C0
Gallus gallus (Chicken)	CHICK	Q9DEA3	R4GG06	E1C8I4	E1C4I3
Chlamydomonas reinhardtii (Chlamydomonas smithii)	CHLRE	A8JHX0	A8IS48	A8J5N4	A8IFX0
Dictyostelium discoideum (Slime mold)	DICDI	Q54K47	Q869Q1	Q54NC0	Q55E62
Drosophila melanogaster (Fruit fly)	DROME	P17917	O96533	Q9VN60	Q9VQD4
Felis catus (Cat)	FELCA	M3WAR4	M3W096	M3XC14	M3WY16
Equus caballus (Horse)	HORSE	F6R950	F6QXP4	F7BM24	F6YZW4
Homo sapiens (Human)	HUMAN	P12004	Q99638	O60921	O60671
Hydra vulgaris (Hydra)	HYDVU	T2MHJ2	T2M799	T2MIV2	T2MID6
Lepisosteus oculatus (Spotted gar)	LEPOC	W5NF42	W5MKE2	W5N6Y6	W5N1G5
Loxodonta africana (African elephant)	LOXAF	G3SY50	G3T2S3	G3TJN6	G3SZN1
Macaca mulatta (Rhesus macaque)	MACMU	F6ZD63	H9FXY2	F7F1Y2	F7A5K9
Mus musculus (Mouse)	MOUSE	P17918	Q9Z0F6	Q8BQY8	Q9QWZ1
Mustela putorius furo (European domestic ferret)	MUSPF	M3Y491	M3XXF9	M3Z395	M3YUM0
Myotis lucifugus (Little brown bat)	MYOLU	G1NW67	G1P3Z2	G1NTI5	G1PS54
Neovison vison (American mink)	NEOVI	U6DX35	U6D1D1	U6CPZ2	U6CY10
Nomascus leucogenys (Northern white-cheeked gibbon)	NOMLE	G1R863	G1R3F3	G1QWZ3	G1RWE2
Oreochromis niloticus (Nile tilapia)	ORENI	I3KAK2	I3JC68	I3K6T5	I3JLK1

Table 2.2 (continued)

Ornithorhynchus anatinus (Duckbill platypus)	ORNAN	F7BRC7	F6REC2	F7BS27	F6UI60
Otolemur garnettii (Small-eared galago)	OTOGA	H0XLL4	H0XWZ7	H0X7H9	H0XC10
Pan troglodytes (Chimpanzee)	PANTR	H2QJX3	K7DL38	H2QUJ9	K7BUE0
Sus scrofa (Pig)	PIG	I3L813	F1RUX7	B6UV60	F1SND5
Polysphondylium pallidum (Cellular slime mold)	POLPA	D3BSY5	D3BA05	D3BR17	D3BPJ7
Pongo abelii (Sumatran orangutan)	PONAB	H2P1A0	H2NCN7	H2PXG5	Q5R7X9
Oryctolagus cuniculus (Rabbit)	RABIT	G1SKZ3	G1TKX6	G1TRN1	G1T7G8
Rattus norvegicus (Rat)	RAT	P04961	D3ZXM2	D3ZNA8	D3ZC52
Sarcophilus harrisii (Tasmanian devil)	SARHA	G3WDY3	G3VT27	G3W0W1	G3WBB6
Schizosaccharomyces pombe (Fission yeast)	SCHPO	Q03392	P26306	P78955	P22193
Ovis aries (Sheep)	SHEEP	W5Q6P4	W5PNJ1	W5PS82	W5PPP9
Spermophilus tridecemlineatus (Thirteen-lined ground squirrel)	SPETR	I3NDE1	I3NF38	I3MYM9	I3MDU2
Strongylocentrotus purpuratus (Purple sea urchin)	STRPU	W4Z5C9	W4YCU0	W4ZAK8	W4ZIN8
Tetraodon nigroviridis (Spotted green pufferfish)	TETNG	H3DD39	H3D6H6	H3D7M2	H3BWC7
Wickerhamomyces ciferrii (Yeast)	WICCF	K0KS34	K0KG77	K0KFL9	K0KTE1
Xenopus laevis (African clawed frog)	XENLA	P18248	Q7ZZU5	Q8JHD8	Q8AY27
Xenopus tropicalis (Western clawed frog)	XENTR	Q66KJ8	Q6DJ26	Q6DF51	A9ULD8
Xiphophorus maculatus (Southern platyfish)	XIPMA	M4AKD0	M4A625	M4AET7	M3ZPZ4
Saccharomyces cerevisiae (Baker's yeast)	YEAST	P15873	Q08949	Q02574	P48581

2.3.6 Chromatin fractionation

Hus1$^{-/-}$ *p21*$^{-/-}$ MEFs stably expressing WT or mutant mHUS1-3XFLAG proteins were irradiated with 100J/m^2 UVC and fractionated 2 hours post-treatment using a previously described extraction protocol (Abmayr et al., 2006) with modifications. In short, cells were swollen in hypotonic buffer (10mM HEPES pH7.9, 1.5mM $MgCl_2$, 75mM KCl, 0.2mM PMSF and 0.5M DTT) for 6 min in 37°C and lysed with Dounce homogenizer. After centrifugation at 14,000 rpm for 15 min, the supernatant was separated for cytoplasmic extract preparation. The nuclei pellet was resuspended in equal volumes of low-salt and high-salt buffers (20mM HEPES pH7.9, 25% glycerol, 1.5mM $MgCl_2$, 0.2M or 1.2M KCl, 0.2mM EDTA, 0.2mM PMSF and 0.5M DTT) in sequential order to extract the soluble nuclear fraction. After centrifugation at 14,000 rpm for 30 min, the supernatant was separated for nuclear extract preparation. The pellet was resuspended in RIPA buffer (50mM Tris pH8.0, 150mM NaCl, 5mM EDTA, 50mM NaF, 0.5% DOC, 1% NP-40 and 0.1% SDS) supplemented with aprotinin, leupeptin, sodium orthovanadate and phenylmethylsulfonyl fluoride (PMSF), sonicated at 24-30W for 1 min (Misonix Sonicator 3000), and centrifuged to produce the chromatin fraction in the supernatant. The cytoplasmic and nuclear fractions were dialyzed in dialysis buffer (20mM HEPES pH7.9, 20% glycerol, 100mM KCl, 0.2mM EDTA, 0.2mM PMSF and 0.5M DTT) overnight before use. 20μg of each fraction was resuspended and boiled in loading buffer for SDS-PAGE and Western analysis.

2.3.7 Immunofluorescence

Hus1$^{-/-}$ *p21*$^{-/-}$ MEFs stably expressing WT or mutant mHUS1-3XFLAG proteins were grown on gelatinized cover slips overnight and treated with 2μg/ml mitomycin C (MMC) for 15

hrs, followed by an additional 2μg/ml MMC for 8 hrs. Cells were fixed in 4% paraformaldehyde and 4% sucrose in PBS for 15 min at RT. They were permeabilized in 0.5% NP-40 in PBS for 5 min at RT, then blocked with 10% bovine serum albumin (BSA) in PBS for 45 min at 37°C. Primary antibody incubation with FLAG (1:250) and RAD9 (1:500) specific antibodies was done overnight at 4°C. Secondary antibody incubation with Alexa Fluor 488 goat anti-mouse (1:250) and 555 goat anti-rabbit (1:500) (Life Technologies, cat#A-11001 and A-21428, respectively) was done for 45 min at 37°C. Coverslips were mounted on microscope slides with mounting medium containing DAPI. Cells were visualized using a Leica DMRE fluorescence microscope (Leica Microsystems), and images were collected with an RT Slider camera (Diagnostic Instruments) and were processed using SPOT Advanced software (Diagnostic Instruments). Overlapping FLAG and RAD9A foci in 50 randomly picked cells from each sample were quantified and presented in a box plot overlapped with dot plot. Statistics were done using one-way ANOVA, and p-value <0.05 was considered as significant.

2.4 Results

2.4.1 A systematic structure/function analysis of HUS1.

We used published crystal structure analyses of human 9-1-1 (Xu et al., 2009, Doré et al., 2009, Sohn and Cho, 2009), computational modeling of 9-1-1 subunit and DNA interactions (Jordi et al., 2012, Xu et al., 2013), and evolutionary conservation analysis to predict functionally important mHUS1 residues. Initially we screened mHUS1 mutants with targeted mutations in 7 specific regions (Table 2.3) for their ability to complement the genotoxin sensitivity of *Hus1*$^{-/-}$ *p21*$^{-/-}$ mouse embryonic fibroblasts (MEFs), which are previously reported to be hypersensitive to ultraviolet (UV) irradiation and hydroxyurea, a replication stress-inducing ribonucleotide

reductase inhibitor (Weiss et al., 2000). As detailed below, 3 HUS1 regions emerged as having the greatest functional significance in complemented cells challenged with 4NQO, a UV mimetic, or aphidicolin, a replication stress-inducing DNA polymerase inhibitor.

2.4.2 HUS1-RAD9A interaction is critical for 9-1-1 clamp formation and function.

9-1-1 clamp assembly is predicted to require stable interactions between residues in the αI2+βI9 and αII1+βII4 regions of each subunit that form surface contacts at subunit interfaces (Xu et al., 2009, Doré et al., 2009, Sohn and Cho, 2009). We sought to identify important HUS1 residues necessary for 9-1-1 clamp formation. One candidate residue was Arginine 128 (127 in hHUS1) located at the HUS1-RAD9A interface (Figure 2.1A), as its polar interactions were predicted to make the greatest contributions to the interaction between these subunits (Xu et al., 2013). Indeed, a mutation of N121, the orthologous residue in fission yeast HUS1 (spHUS1), impairs association with spRAD9A, resulting in a dominant negative phenotype (Kaur et al., 2001). Hence, we mutated mHUS1 arginine 128 to glutamic acid (R128E) to investigate the effects of polar charge reversal on 9-1-1 clamp formation. The R128E mutant was stably expressed (Figure 2.1B). mHUS1 R128E-expressing *Hus1*$^{-/-}$ *p21*$^{-/-}$ MEFs were subjected to short term viability and clonogenic survival assays to determine whether the mutation disrupts HUS1 function and cell survival after genotoxin treatment (Figures 2.1C and 1D). We found that the mHUS1 R128E mutant failed to rescue the genotoxin hypersensitivity phenotype of *Hus1*-deficient MEFs in both the acute and long-term viability assays. Next, co-immunoprecipitation (co-IP) assays were performed to determine if mHUS1 R128E is defective for interaction with RAD9A (Figure 2.1E). Consistent with previous reports, wild-type mHUS1 co-IP'd with hRAD9A-MYC and hRAD1A-HA. As expected, mHUS1 R128E was not detected in hRAD9A-

Table 2.3. Summary of clonogenic survival and short-term viability assay results for all mHUS1 mutants analyzed.

Mutations	Expression	Clonogenic survival[a]		Short term viability[a]	
		4NQO	Aphidicolin	4NQO	Aphidicolin
RAD9-interacting residue					
R128E	Yes	Null	Null	Null	Null
Inner ring hydrophobic cleft					
V19A, M22A, I23A	Partial	WT	WT	WT	WT
V247A, V271A, L273A	Partial	WT	WT	WT	WT
V19A, M22A, I23A, V247A, V271A, L273A	Partial	WT	Partial	Partial	Null
R18A	Yes	N/A[b]	N/A	WT	WT
R18Q	Yes	N/A	N/A	WT	WT
R18Q M22T	Yes	N/A	N/A	WT	WT
Inner ring positively charged residues					
R90, K93	Yes	WT	WT	WT	Partial
K165, K168, K173, R175	Yes	WT	Partial	WT	Partial
K25, K93	Yes	WT	WT	WT	WT
K25, K236, K237	Yes	Partial	Partial	Partial	WT
K173, R175, K236, K237	Yes	WT	Partial	Partial	Partial
K25, K93, K236, K237	Yes	Null	Null	Null	Null
K25, K93, K173, R175, K236, K237	Yes	Null	Null	Null	Null
R18, K93, K165	Yes	WT	Partial	Partial	WT
K93	N/A	WT	WT	WT	WT
K25	N/A	WT	WT	WT	WT
R18, K25, K28	N/A	WT	WT	WT	WT
K236, K237	N/A	WT	WT	WT+	WT
K173, R175	N/A	WT	WT	WT+	WT
K165, K168	N/A	WT	WT	N/A	N/A
K25A K28A K165A	Not stable	N/A	N/A	N/A	N/A
Outer ring primary hydrophobic pocket					
P150A, I152A, P153A, C155A	Partial	WT	WT	Partial	Partial
V257A, T261A, F276A, P278A	Yes	WT	WT	WT	WT
P150A, I152A, P153A, C155A, V257A, T261A, F276A, P278A	Partial	WT	Partial	N/A	N/A
P150A, V257A, T261A, F276A, P278A	Partial	WT	Partial	WT	Partial
P150A, I152A, P153A, C155A, F276A, P278A	Not stable	Partial	Partial	Partial	Partial
S53R	Yes	N/A	N/A	WT	WT
I152R	Partial	N/A	N/A	Partial	Partial
I152Y	Yes	Partial	Partial	Partial	Partial
I152F	Yes	N/A	N/A	WT	WT

Table 2.3 (continued)

Outer ring secondary hydrophobic pocket					
F3A, G71W, I79A, L105A	Not stable	Null	Null	N/A	N/A
F3A, G71W	N/A	WT	WT	N/A	N/A
F3A, I79A	N/A	WT	WT	N/A	N/A
F3A, L105A	N/A	WT	WT	N/A	N/A
F3A, I79A, L105A	Not stable	WT	Null	N/A	N/A
F3R	Not stable	Partial	Partial	Partial	WT
F3R, R4A	N/A	Partial	Partial	Partial	WT
K104A, L105A, T106A	N/A	WT	WT	WT	Partial
K104A, L105A, T106A, V138A, L139D	Not stable	Null	Null	Null	Null
L105R	Not stable	N/A	N/A	N/A	N/A
L139R	Not stable	N/A	N/A	N/A	N/A
R4D	Yes	Partial	Partial	Partial	Partial
Combined outer ring primary and secondary hydrophobic pockets					
R4D+I152Y	Yes	Partial	Partial	Partial	Partial
Outer ring positively charged residues					
K2A, R4A, K6A	N/A	WT	WT	N/A	N/A
R99A, K102A, K104A	N/A	WT	WT	N/A	N/A
K108A, H109A	N/A	WT	WT	N/A	N/A
K137A, R141A, R142A, K145A	N/A	WT	WT	N/A	N/A
BII4-6 loop					
Δ215-227	Not stable	Null	Null	N/A	N/A
Δ215-227::hHus1 loop	N/A	WT	WT	N/A	N/A
Δ215-227::PCNA loop	N/A	WT	WT	N/A	N/A

[a] Survival outcomes were categorized into: WT+ (better than WT mHUS1 complemented cells), WT (similar to WT mHUS1 complemented cells), Partial (worse than WT mHUS1 complemented cells but better than *Hus1* null cells), and Null (similar to *Hus1* null cells).
[b] Not tested

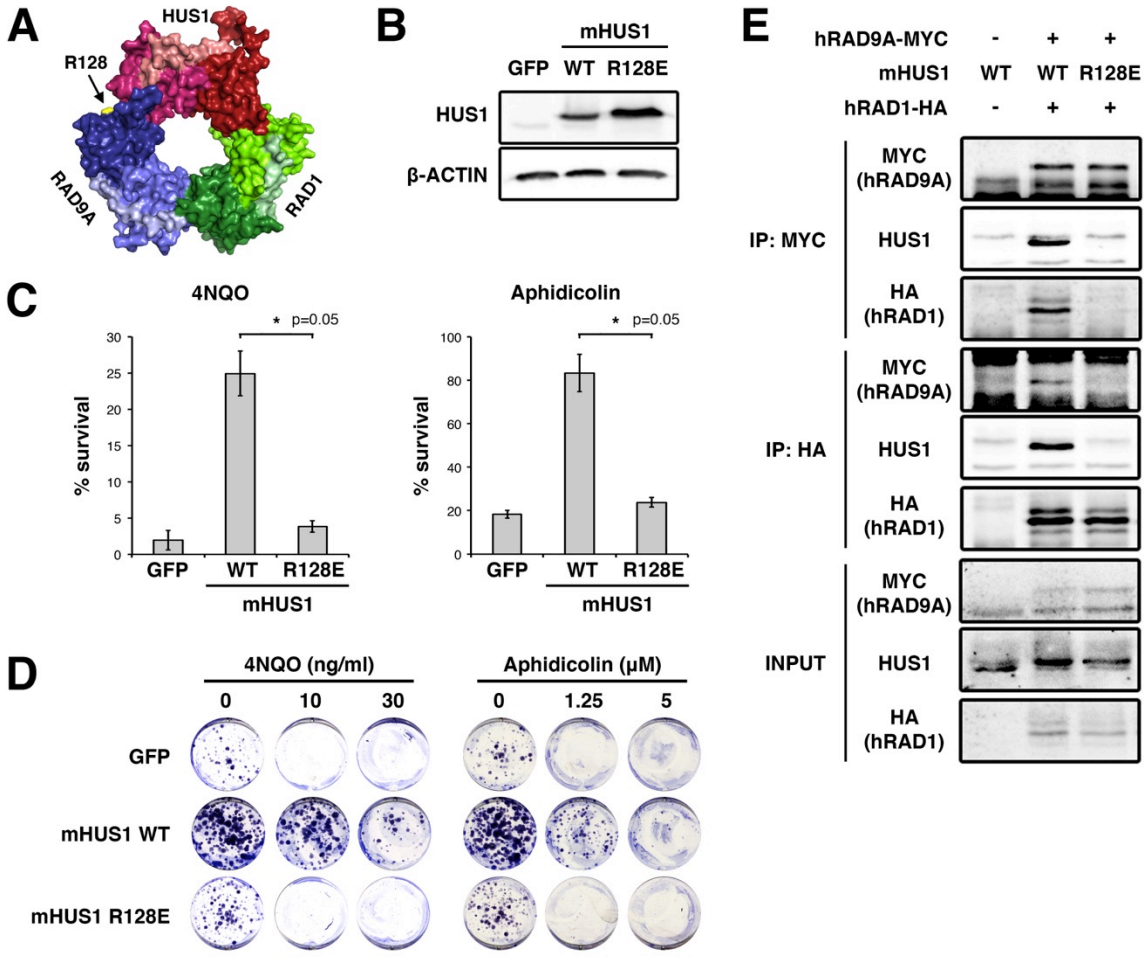

Figure 2.1. mHUS1 residue R128 is crucial for 9-1-1 clamp formation. (A) R128 (arrow) is located at the HUS1-RAD9A interface (PDB 3GGR). (B) Immunoblot using antibodies specific for HUS1 or β-ACTIN was performed to compare the stability of WT and R128E mHUS1 proteins in HEK293T. (C-D) Short term viability and clonogenic survival were measured for *Hus1*-null MEFs stably expressing mHUS1 R128E after 4NQO or aphidicolin treatments. MEFs expressing GFP or WT mHUS1 served as negative and positive controls, respectively. Each experiment in (C) was repeated 5 times with 2 independently generated cell lines. Error bars indicate standard deviation. (E) Interaction of mHUS1 R128E with hRAD9 and hRAD1 was assessed by co-IP.

MYC pulldown. Interestingly, hRAD1-HA also was not detected in the same IP, and neither mHUS1 R128E nor hRAD9A-MYC was detected in reciprocal hRAD1-HA IPs. These results suggest that the mutation not only disrupts mHUS1-hRAD9A interaction but also destabilizes the other clamp interfaces, preventing proper 9-1-1 complex formation and function.

2.4.3 Multiple positively charged residues in the inner ring of HUS1 facilitate HUS1-DNA interactions in a synergistic manner.

Like PCNA and bacterial β-clamp, 9-1-1 is thought to physically interact with the negatively charged DNA phosphate backbone, affording proper loading and complex formation on chromatin (McNally et al., 2010, Georgescu et al., 2008, Jordi et al., 2012). The inner surface of HUS1 consists of 4 parallel α-helices containing 11 positively charged residues (Figure 2.2A). In order to determine the contribution of mHUS1-DNA contacts to overall 9-1-1 function, alanine mutations of these residues (K25, K93, K173, R175, K236 and K237) were generated in various combinations and tested for complementation (Figure 2A). These mutations did not disrupt proper expression of mHUS1 (Figure 2.2B), but all of them caused mHUS1 loss of function as evidenced by partial sensitivity phenotypes of mutants 3A and 4A-1, and hypersensitivity phenotypes of mutants 4A-2 and 6A (Figures 2.2C and 2D). The severe functional defects in these mutants were not due to the disruption of 9-1-1 clamp formation, as both mHUS1 4A-2 and 6A co-immunoprecipitated with hRAD9A-MYC and hRAD1-HA to the same extent as wild-type HUS1 (Figure 2.2E). Interestingly, the human HUS1 residues equivalent to those mutated in 4A-2 and 6A were predicted by computational modeling to be in direct contact with DNA (Jordi et al., 2012). These results suggest that mHUS1 mutants 4A-2 and 6A could form the 9-1-1 clamp but not interact with DNA. We generated additional mutants

Figure 2.2. Multiple positively-charged residues on the HUS1 inner ring are synergistically important for genotoxic stress responses. (A) mHUS1 has 11 arginines and lysines (black circles) distributed on 4 α-helices in the inner ring surface (PDB 3GGR). Alanine substitutions of these residues (3A-6A) were made. (B) Protein expression was measured as in Figure 2.1B. (C-D) Genotoxin sensitivity was measured as in Figures 2.1C and 1D. Each experiment in (C) was repeated 3 times with 3 independently generated cell lines. Error bars indicate standard deviation. (E) Interaction of mHUS1 mutant proteins with hRAD9 and hRAD1 was assessed by co-IP.

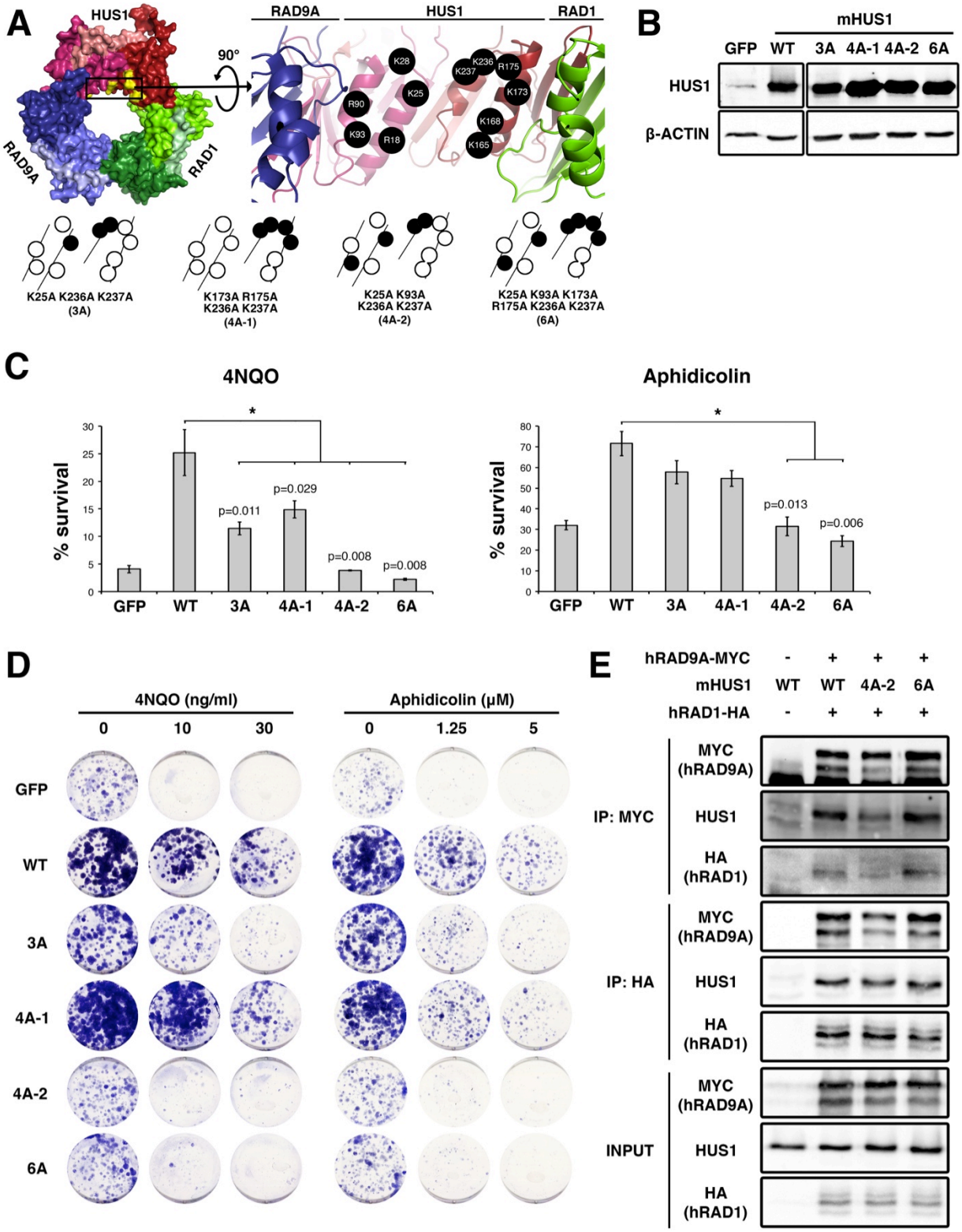
A
HUS1
RAD9A
RAD1
90°
RAD9A
HUS1
RAD1
K28
K25
R90
K93
R18
K236
K237
R175
K173
K168
K165
K25A K236A K237A
(3A)
K173A R175A
K236A K237A
(4A-1)
K25A K93A
K236A K237A
(4A-2)
K25A K93A K173A
R175A K236A K237A
(6A)
B
mHUS1
GFP WT 3A 4A-1 4A-2 6A
HUS1
β-ACTIN
C
4NQO
Aphidicolin
% survival
*
p=0.011
p=0.029
p=0.008
p=0.008
p=0.013
p=0.006
GFP WT 3A 4A-1 4A-2 6A
D
4NQO (ng/ml)
0 10 30
Aphidicolin (μM)
0 1.25 5
GFP
WT
3A
4A-1
4A-2
6A
E
hRAD9A-MYC - + + +
mHUS1 WT WT 4A-2 6A
hRAD1-HA - + + +
IP: MYC
MYC (hRAD9A)
HUS1
HA (hRAD1)
IP: HA
MYC (hRAD9A)
HUS1
HA (hRAD1)
INPUT
MYC (hRAD9A)
HUS1
HA (hRAD1)

in different alignments (Figure 2.3A and Table 2.3) to investigate the possibility that mHUS1 can utilize different DNA contact surfaces. However, short term viability assays showed that these mutants complemented the genotoxin hypersensitivity phenotype of *Hus1*-deficient MEFs to the same extent as wild-type mHUS1, except for R18A K93A K165A (C5) that caused only a mild sensitivity phenotype (Figure 2.3B). Taken together, these results indicate that six specific positively charged HUS1 residues, namely K25, K93, K173, R175, K236 and K237, cooperatively facilitate HUS1-DNA contacts and are functionally important for cell survival.

2.4.4. Identification of a novel hydrophobic pocket on the HUS1 outer surface.

Akin to PCNA, the 9-1-1 clamp coordinates and stimulates the activity of many DNA repair factors via direct physical interaction. 9-1-1 structural analyses indicated that HUS1 contains a PCNA-like hydrophobic pocket based on topological and electrostatic similarities in the regions between the IDC loop and globular domain 2 of PCNA and HUS1 (Xu et al., 2009, Doré et al., 2009, Sohn and Cho, 2009). We conducted an evolutionary conservation analysis as an independent approach to identify HUS1 functional domains for protein-protein associations (details in Supplemental Experimental Procedures). As a proof of principle, we performed this analysis on PCNA using amino acid sequences from 44 organisms selected across a wide range of taxa (Figure 2.4A and Table 2.3). Two clusters of conserved residues were apparent on the outer ring surface of PCNA, one for the well-characterized PIP-box-binding primary pocket (dotted line circle) as expected, and the other for a secondary pocket (dotted line rectangle) that also participates in interactions with some PCNA binding partners through sequences C-terminal to the PIP box motif (Gulbis et al., 1996, Shigeru et al., 2005). Some inner ring positively charged residues that are functionally important for PCNA also were found to be conserved (data

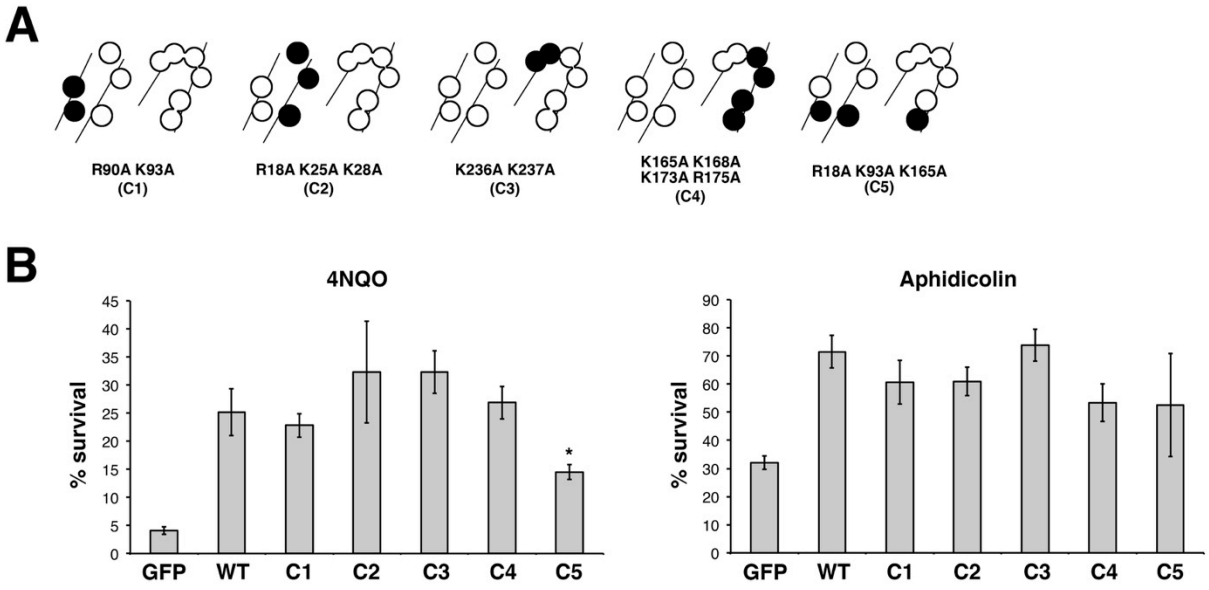

Figure 2.3. Certain configurations of positively charged residues in the inner ring of HUS1 are dispensable for genotoxic stress responses. (A) Alanine substitutions of the positively charged residues were made in various combinations (C1-C5), as indicated by the filled circles. (B) Short term viability of *Hus1*$^{-/-}$ *p21*$^{-/-}$ MEFs stably expressing mHUS1 inner ring mutants C1-C5 after 4NQO or aphidicolin treatments was measured. Each experiment was repeated 4 times using 3 independently generated cell lines. No significant differences in survival between wild-type mHUS1 and mutants C1-C5 were identified, except for C5 with 4NQO treatment ($p=0.045$).

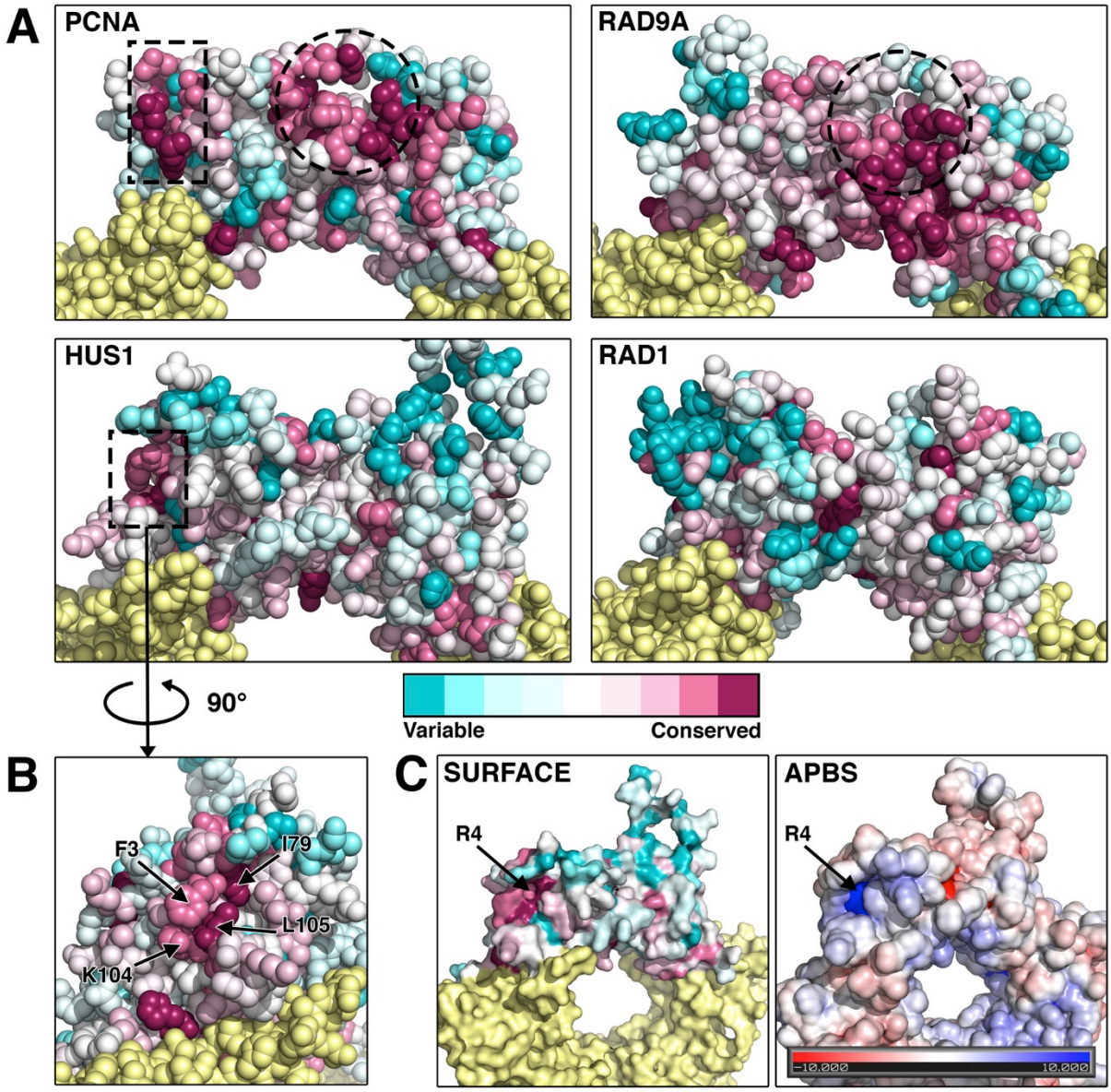

Figure 2.4. The identification of a novel conserved hydrophobic pocket in the outer ring of HUS1. (A, B) The evolutionary conservation values of each amino acid position in the protein structures of PCNA, RAD9A, HUS1 and RAD1 were calculated using the Consurf bioinformatics server. Multiple sequence alignments of 44 organisms that encompass a wide range of taxa were used (see Table S3). Residues pseudo-colored in cyan have diverged and are variable, whereas those in magenta are conserved. Dotted lines outline conserved regions that potentially mediate protein-protein associations. The circled regions correspond to the primary PIP box-binding hydrophobic pocket of PCNA and the analagous conserved region of RAD9A. A second conserved region for PCNA and HUS1 is outlined with a rectangle and in the case of HUS1 corresponds to a secondary pocket on the side of globular domain 1 comprised of 3 conserved hydrophobic residues. (C) HUS1 atomic surface and surface electrostatic potential models reveal a positively charged groove at the base of the secondary pocket. The charge is contributed by an arginine at position 4.

not shown).

The same analysis was then applied to RAD9A, HUS1 and RAD1 (Figure 2.4A and Table 2.3). Intriguingly, the distribution of conserved domains for each subunit was different from PCNA and from each other. RAD9A showed evolutionary conservation of the PCNA-like hydrophobic pocket (dotted line circle) but HUS1 and RAD1 did not. This result implicates RAD9A in PIP box protein interactions. However, in a separate analysis using only mammalian sequences, conservation of HUS1 residues that form the PCNA-like hydrophobic pocket became evident (data not shown), suggesting a possible functional role. A small cluster of conserved HUS1 residues in the topologically equivalent region of the PCNA secondary binding site (dotted line rectangle) also stood out in these analyses. This pocket is formed by 3 hydrophobic residues (F3, I79 and L105) (Figure 2.4B) and an arginine (R4) at the base of the pocket, creating a strong positive electrostatic potential surrounded by a neutral field (Figure 2.4C). Together, these features suggest that this HUS1 secondary pocket may possess functional significance.

2.4.5. HUS1 has two functional hydrophobic pockets that are important for genome maintenance.

To identify HUS1 outer surface residues that are functionally important, we first targeted hydrophobic residues that form the primary and secondary pockets but various combinations of alanine mutants either disrupted HUS1 protein stability or did not cause loss of function in survival assays (Table 2.3). We then generated mutations predicted to physically or electrostatically block the pockets (Figure 2.5A). For the PCNA-like primary pocket, we changed isoleucine 152 (valine 151 in hHUS1) to tyrosine (I152Y) to block the pocket with the bulky polar side chain of tyrosine. For the secondary pocket, arginine 4 was mutated to aspartic

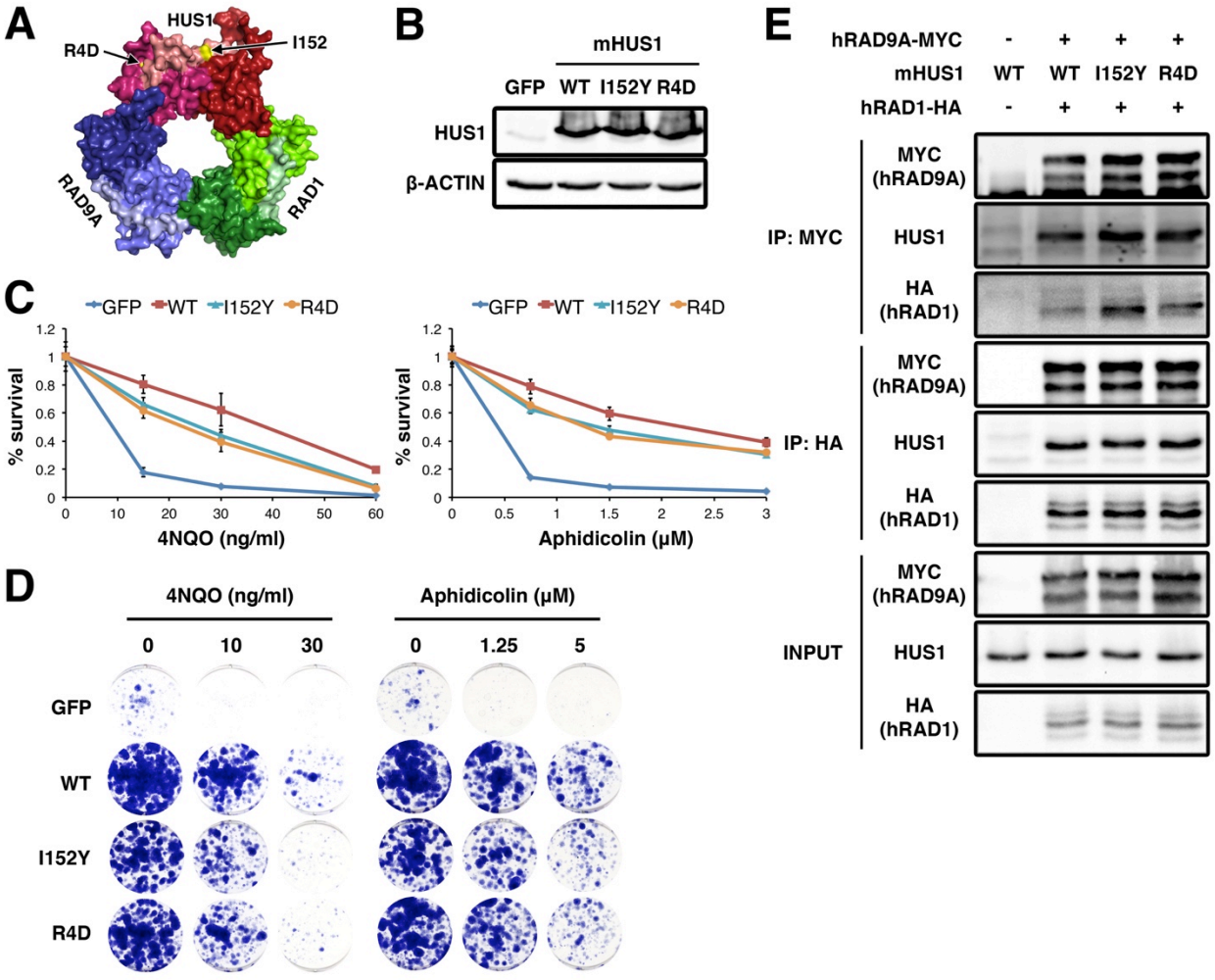

Figure 2.5. Two hydrophobic pockets on the outer surface of HUS1 are required for genotoxic stress responses. (A) R4 and I152 (arrows) are located on the outer ring surface (PDB 3GGR). (B) Protein expression was measured as in Figure 1B. (C-D) Genotoxin sensitivity was measured as in Figures 1C and 1D. Each experiment in (C) was repeated 2 times with 2 independently generated cell lines. Error bars indicate standard deviation. (E) Interaction of the pocket mutants with hRAD9 and hRAD1 was assessed by co-IP.

acid (R4D) to reverse the charge at the base of the pocket. Both mutants were stably expressed (Figure 2.5B). In genotoxin survival assays, both pocket mutants were partially sensitive to acute 4NQO and aphidicolin treatments, whereas survival was largely normal in longer term assays with aphidicolin treatment (Figures 2.5C and 5D). Combined mutant R4D+I152Y did not show increased sensitivity relative to the single pocket mutants in the 4NQO and aphidicolin treatments, but interestingly show synergistic increase in hypersensitivity to mitomycin C (MMC), a DNA interstrand crosslinking agent (data not shown). The genotoxin hypersensitivity phenotype was not due to disruption of 9-1-1 clamp formation, as these mHUS1 pocket mutants co-immunoprecipitated with hRAD9A and hRAD1 (Figure 2.5E). These data suggest that mHUS1 possesses two outer surface hydrophobic pockets that contribute to genome protection, likely through interactions with binding partners.

2.4.6. DNA damage-induced mHUS1 chromatin localization and CHK1 phosphorylation are disrupted in clamp destabilizing and DNA interaction mutants, but occurs normally in mHUS1 pocket mutants.

In order to determine how the different classes of HUS1 mutations affected the ability of HUS1 to enter the nucleus and localize on chromatin after DNA damage, we performed immunofluorescence and chromatin fractionation assays in cells complemented with 3XFLAG epitope-tagged mHUS1 constructs, including mutants R128E (RAD9A interface), 4A-2 or 6A (DNA binding), or I152Y or R4D (outer surface pockets). The epitope-tagged versions of the mutants displayed similar protein expression and loss of function characteristics as their untagged counterparts (data not shown). We performed immunofluorescent staining with DAPI, FLAG antibody and RAD9A antibody and quantified the number of co-stained foci in the

nucleus (Figure 2.6A). This experiment was done with MMC treatment, which, unlike 4NQO or aphidicolin (data not shown), induces the formation of punctate 9-1-1 nuclear foci as detailed below. Under untreated conditions, none of the cell lines displayed any nuclear foci (data not shown). After MMC treatment, RAD9A foci were absent in *mHus1*-deficient MEFs (empty vector) but were present in wild-type mHUS1 complemented cells. In MEFs expressing wild-type mHUS1-3XFLAG, the RAD9A foci colocalized with FLAG foci (mean of 8.22 foci/cell), likely representing accumulation of 9-1-1 clamps at damaged DNA. We next analyzed foci formation by the mHUS1-3XFLAG mutants and their impact on RAD9A foci. As expected, the clamp destabilizing mutant, R128E-3XFLAG, failed to form foci and disrupted RAD9A foci formation as well (0 foci/cell, average = 0 foci/cell). Similar results were observed in cells expressing 4A2-3XFLAG and 6A-3XFLAG mutants (mean of 0.12 or 0.14 foci/cell, respectively). These data suggest that unstable subunit-subunit and mHUS1-DNA interactions prevent the 9-1-1 clamp from stably localizing on damaged DNA. By contrast, mHUS1 pocket mutants I152Y-3XFLAG and R4D-3XFLAG retained the ability to form MMC-induced foci and colocalize with RAD9A to the same extent as WT mHUS1-3XFLAG (mean of 8.73 or 9.26 foci/cell, respectively). Thus, disabling either mHUS1 outer surface pocket impairs 9-1-1 function without affecting its chromatin localization.

To verify the immunofluorescence assay results, the same set of cells was fractionated into cytoplasmic, nuclear and chromatin fractions after UV irradiation (Figure 2.6B). Lysates were immunoblotted with antibodies specific to FLAG for HUS1 detection, GAPDH as a cytoplasmic marker, and histone H3 as a chromatin marker. As expected, WT mHUS1-3XFLAG was detected in the nuclear and chromatin compartments after UV damage. This response was ablated in MEFs expressing R128E-3XFLAG, 4A2-3XFLAG and 6A-3XFLAG, which were not

Figure 2.6. DNA damage-induced HUS1 localization is defective in HUS1 clamp forming and DNA interacting mutants, but not in HUS1 pocket mutants. (A) MMC-treated *Hus1*-null MEFs stably expressing the indicated constructs were stained with DAPI (blue), and α-FLAG (green) and α-RAD9A (red) antibodies. Scale bar=10μm. Quantification is presented in quartile box and dot plots. NS=not significant. (B) Cells were UV-treated, fractionated into cytoplasmic (cyt), nuclear (nuc) and chromatin (chr) fractions, and immunoblotted. GAPDH and Histone 3 served as fractionation controls. Arrows indicate HUS1 band; asterisks denote a non-specific band. (C) DNA damage-induced CHK1 phosphorylation is hampered in HUS1 clamp formation and DNA interaction mutants, but is intact for HUS1 outer surface pocket mutants. Lysates from cells treated with 0 or 100 J/m^2 UV were immunoblotted using antibodies specific for phospho-CHK1 or β-ACTIN.

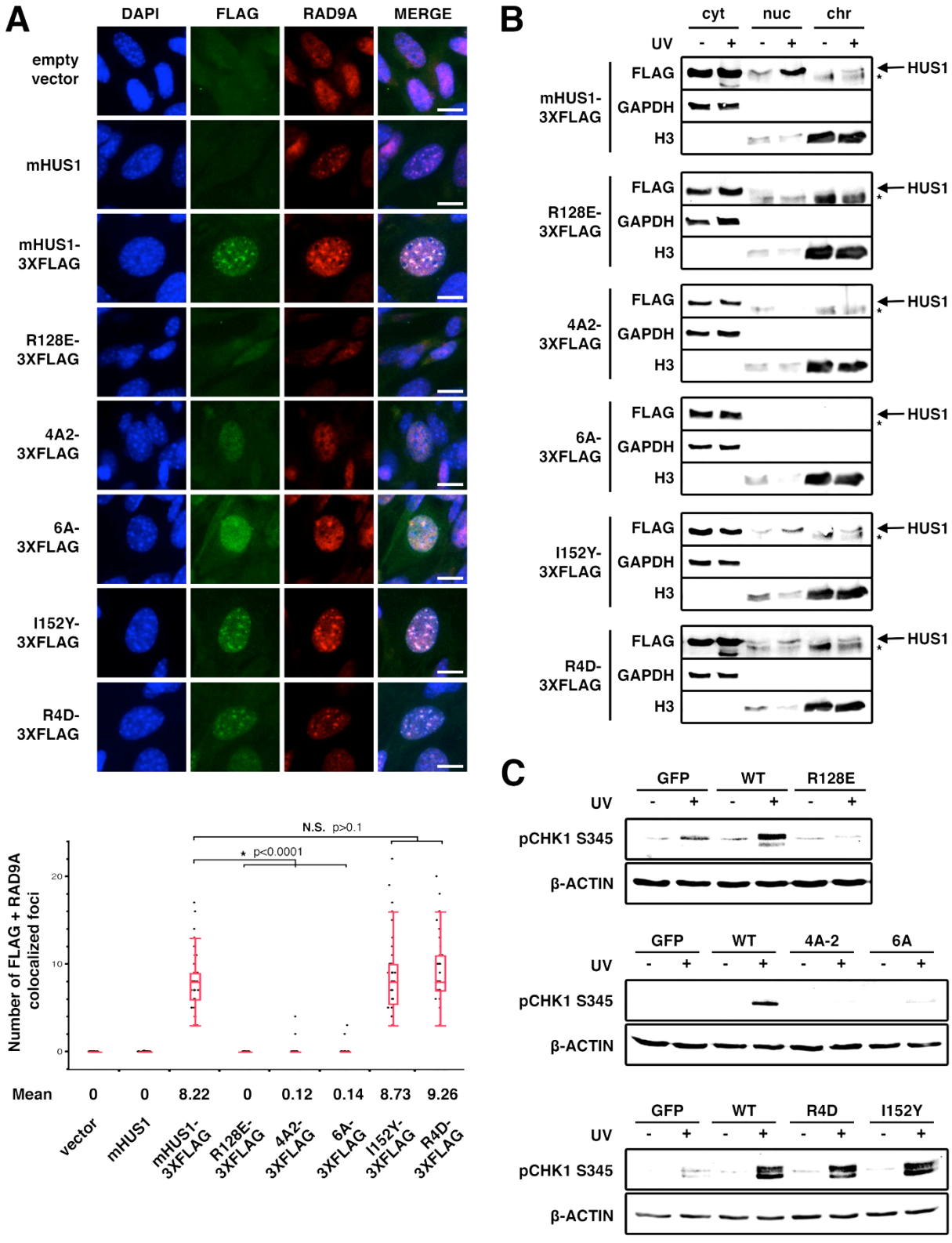
A
DAPI
FLAG
RAD9A
MERGE
empty vector
mHUS1
mHUS1-3XFLAG
R128E-3XFLAG
4A2-3XFLAG
6A-3XFLAG
I152Y-3XFLAG
R4D-3XFLAG
N.S. p>0.1
* p<0.0001
Number of FLAG + RAD9A colocalized foci
Mean 0 0 8.22 0 0.12 0.14 8.73 9.26
vector
mHUS1
mHUS1-3XFLAG
R128E-3XFLAG
4A2-3XFLAG
6A-3XFLAG
I152Y-3XFLAG
R4D-3XFLAG
B
cyt
nuc
chr
UV
FLAG
GAPDH
H3
HUS1
C
GFP
WT
R128E
4A-2
6A
R4D
I152Y
pCHK1 S345
β-ACTIN

detected in the nuclear or chromatin fractions. Thus, defects in 9-1-1 clamp formation and DNA interactions lead to loss of mHUS1 nuclear localization. On the other hand, the pocket mutants I152Y-3XFLAG and R4D-3XFLAG were detected in the nuclear and chromatin fractions after UV damage in a similar manner as for wild-type HUS1, indicating that the pocket mutations disrupt mHUS1 function without disturbing its localization to damage sites.

The best established function of the 9-1-1 clamp is activation of ATR kinase through interactions between RAD9A and TOPBP1. In order to determine if the various mHUS1 mutants affected ATR activation and subsequent downstream checkpoint signaling events, we assessed phosphorylation of CHK1 (pCHK1), an ATR substrate (Figure 2.6C). As previously reported (Weiss et al., 2002), *mHus1*-deficient MEFs failed to upregulate pCHK1 upon UV treatment. This defect was rectified by complementation with wild-type mHUS1. However, in cells complemented with the mHUS1 R128E clamp assembly mutant or the 4A-2 or 6A DNA interaction mHUS1 mutants, the pCHK1 response was abrogated to the same extent as with complete *mHus1* deficiency. These data indicate that unstable subunit-subunit and mHUS1-DNA interactions significantly impair ATR activation, consistent with the observations that these mutant proteins failed to properly localize to DNA damage sites. By contrast, cells expressing mHUS1 pocket mutants I152Y or R4D retained normal levels of UV-induced CHK1 phosphorylation (Figure 2.6C). Together, these results indicate that the partially defective mHUS1 pocket mutants properly localize to damage sites and support ATR-mediated checkpoint signaling, highlighting ATR-independent effector functions downstream of HUS1.

2.5 Discussion

Checkpoint signaling in coordination with appropriate DNA repair is crucial for a successful DDR. Understanding this concerted action is important for appreciating how normal cells are protected from the deleterious effects of genomic instability and how malignant cells proliferate in the face of numerous physiological stresses (Hanahan and Weinberg, 2011). In this study, we sought to understand the molecular interactions that underlie a robust DDR involving the 9-1-1 clamp and in doing so defined the molecular requirements for both stimulation of ATR-induced CHK1 phosphorylation and CHK1-independent functions for the 9-1-1 complex mediated by outer surface residues of the HUS1 subunit.

Maintaining sufficient inter-subunit contacts is the most crucial initial step for 9-1-1 clamp formation, failure of which abrogates all downstream clamp functions. Remarkably, reversing the polarity of a single residue (R128 of mHUS1) at the RAD9A/HUS1 interface fully disrupted 9-1-1 clamp integrity and function, even though there are at least 8 other HUS1 residues predicted to contribute to RAD9A-HUS1 interactions (Xu et al., 2013). Interestingly, the RAD9A/HUS1 interface mutation also disrupted HUS1-RAD1 and RAD1-RAD9A associations. One possibility is that mHUS1 R128E causes active repulsion from RAD9A, indirectly weakening HUS1-RAD1 interactions due to unstable inter-subunit conformations. Alternatively, the findings with the HUS1 R128E mutant may reflect that all three 9-1-1 interfaces function cooperatively during trimerization, or an ordered, stepwise process for 9-1-1 clamp assembly. Precedent for such a mechanism comes from analysis of the heterotrimeric PCNA from the hyperthermophilic archaeon *Sulfoflobus solfataricus* (*Sso*PCNA), in which PCNA1-PCNA2 heterodimer formation is a prerequisite for PCNA3 recruitment (Dionne et al., 2003). Failure of stable clamp formation may happen either early during nuclear localization or

later during clamp loading, when clamp stability is challenged by conformational changes at subunit interfaces associated with clamp opening and closing (Xu et al., 2013, Dionne et al., 2003).

The inner surface of PCNA consists of four parallel alpha-helices that contain positively charged residues, some of which contact the negatively charged DNA sugar-phosphate backbone and are necessary for efficient clamp loading and mobility on DNA (McNally et al., 2010). Similarly, the HUS1 inner surface also is comprised of four parallel alpha-helices containing numerous positively charged residues, and here we report that HUS1 function requires a specific set of synergistically important residues that are aligned in a transhelical manner analogous to those of PCNA. Notably, our findings are consistent with predicted HUS1-DNA contacts from computational modeling (Jordi et al., 2012). It is remarkable that loss of DNA contacts for the HUS1 subunit alone leads to severe checkpoint signaling defects and hypersensitivity to genotoxins, since modeling of 9-1-1 on DNA indicates that the three subunits contribute almost equally for DNA backbone associations (Jordi et al., 2012). We suspect that similar to PCNA, clamp-DNA interactions are important for 9-1-1 loading onto DNA. Consistent with this idea, the HUS1 inner surface mutants stably associate with the other 9-1-1 subunits but do not show substantial DNA damage-induced accumulation on chromatin.

Much knowledge about PCNA function was gained by structure/function studies that identified a PCNA hydrophobic pocket as the docking site for most PCNA interacting protein (PIP) box motif-carrying proteins (Naryzhny, 2008). Based on the structural similarity between the 9-1-1 complex and PCNA, we hypothesized that the outer surface of HUS1 would mediate physical interactions with downstream effectors. Our evolutionary conservation analysis revealed that among all 9-1-1 subunits, RAD9A showed the greatest conservation of the hydrophobic

pocket that is analogous to the site where PCNA interacts with PIP box motifs, consistent with the idea that RAD9A is the subunit most closely related to PCNA (Doré et al., 2009). The same region was conserved among mammalian HUS1 and RAD1 proteins but not in a broader representation of species. This suggests that while the RAD9A primary hydrophobic pocket is evolutionarily conserved, HUS1 and RAD1 hydrophobic pockets have undergone greater divergence, potentially reflecting specialization and coevolution of subunit-effector associations. Consurf analysis of HUS1 additionally revealed a secondary hydrophobic pocket on the outer surface that showed substantial evolutionary conservation. Disruption of these two HUS1 outer surface pockets caused partial loss of function without disturbing clamp formation or its recruitment to chromatin following DNA damage. That cells expressing these pocket mutants showed only intermediate levels of genotoxin hypersensitivity likely relates to the fact that they remain functional for genotoxin-induced CHK1 activation, as would be expected since interactions between 9-1-1 and the ATR activator TOPBP1 occur through the C-terminal tail of RAD9A (Delacroix et al., 2007). It also remains possible that RAD9A and RAD1 provide some level of redundancy when HUS1 is dysfunctional, as in some cases, RAD9A, HUS1 and RAD1 can all interact with the same repair protein albeit with different binding affinities (Friedrich-Heineken et al., 2005, Smirnova et al., 2005, Gembka et al., 2007, Guan et al., 2007b, Park et al., 2009, Bai et al., 2010). In contrast, each 9-1-1 subunit may bind to distinct players of the same repair pathway to coordinate the repair process in a spatiotemporal manner. This concept stems from the ability of *Sso*PCNA to coordinate Okazaki fragment maturation through distinct specificity of each PCNA subunit in binding to enzymes involved in early to late functions (Beattie and Bell, 2012).

PCNA-effector interactions invariably involve PIP box sequences (QXXΨXXΦΦ), but

there is mixed evidence regarding a role for PIP box motifs in 9-1-1-effector interactions (Friedrich-Heineken et al., 2005, Shi et al., 2006, Guan et al., 2007a, Guan et al., 2007b, Xu et al., 2009, Doré et al., 2009, Eichinger and Jentsch, 2010). While HUS1 primary hydrophobic pocket may associate with PIP box-containing proteins, the role of the secondary pocket is unknown. We found that combining the outer surface mutations (R4D+I152Y) did not further increase hypersensitivity to 4NQO or aphidicolin beyond that for either single mutant (Table 2.3) suggesting that the secondary pocket contribute equally in stabilizing interactions with the same effector that bind the primary pocket, resembling PCNA interactions with FEN1 and p21 (Sakurai et al., 2005, Gulbis et al., 1996). However, cells expressing the double mutant R4D+I152Y showed increased sensitivity to the crosslinking agent mitomycin C (MMC) (Balmus et al., submitted manuscript), implying that at certain DNA lesions the two HUS1 pockets can have separate roles that cooperatively improve cell survival. In such circumstances, the secondary HUS1 pocket might interact with distinct effectors independently of the primary pocket, through a different motif, like the recently reported Mec3-Mcm10 interaction (Alver et al., 2014). Binding of individual clamp subunits to unique downstream effectors occurs with *Sso*PCNA (Beattie and Bell, 2012) and would provide a means to diversify and possibly coordinate clamp function. With its close proximity to the RAD9A primary PCNA-like pocket, the secondary HUS1 pocket also may be involved in RAD9A-HUS1 intersubunit-effector binding, as has been reported for the interaction between the equivalent budding yeast proteins (DDC1-MEC3) and their partner RED1 (Eichinger and Jentsch, 2010). Bacterial β-clamp and *Sso*PCNA similarly display intersubunit interactions with TLS polymerases (Bunting et al., 2003, Xing et al., 2009).

Loss of individual 9-1-1 components leads to severe DDR defects and chromosomal instability (Hopkins et al., 2004, Weiss et al., 2000, Han et al., 2010). Genetic approaches to ablate 9-1-1 function typically involve complete gene deletion or knockdown, which fully compromise both checkpoint signaling and all other functions executed by the clamp. Thus, an open question has been to what extent the requirement for the 9-1-1 complex reflects its role in TOBP1-induced ATR activation achieved through interaction between the clamp and TOPBP1, versus direct functions for 9-1-1 subunits in other processes. By mutating the HUS1 outer surface pockets, we have successfully separated these 9-1-1 functions and demonstrate that HUS1 has roles apart from checkpoint signaling that also are crucial for cell survival following DNA damage. Continued analysis of this collection of HUS1 mutants holds promise for shedding light on 9-1-1 functions in genome maintenance and highlighting potential targets that can be exploited clinically for anti-cancer therapies.

2.6 Acknowledgement

This work was supported by National Institutes of Health grant R01 CA108773 (R.S.W.). Additionally, we thank Dr. Ivaylo Ivanov from Georgia State University and Dr. Alba Guarne from McMaster University for suggestions on strategies for mutagenesis. We also thank Joseph Peters and Marcus Smolka from Cornell University for helpful discussions and comments on the manuscript.

CHAPTER 3

HUS1 MODULATES THE EFFICIENCY OF DNA DOUBLE STRAND BREAK REPAIR THROUGH THE HOMOLOGOUS RECOMBINATION PATHWAY[2]

3.1 Abstract

Previous studies suggested that *Hus1* may play an important role in the error-free branch of double strand break repair (DSBR) in mitotic and meiotic cells. In order to test the functional implications of 9-1-1 complex in DSBR pathways, a genetic approach was undertaken by crossing *Hus1* hypomorph mice with *Rad54*$^{-/-}$ mice, which are mildly perturbed for HR repair. In this study, we found that simultaneous *Hus1* and *Rad54* disruption (*Rad54*$^{-/-}$;*Hus1*$^{neo/\Delta 1}$) caused synergistic effects on spontaneous and genotoxin induced genomic instability, both in vivo and ex vivo. As predicted, *Rad54*$^{-/-}$;*Hus1*$^{neo/\Delta 1}$ double mutant mice sustained higher spontaneous genomic instability as measured by micronucleus assay and showed hypersensitivity to the crosslinking agent mitomycin C, and ionizing radiation. Consistent with these findings, *Rad54*$^{-/-}$;*Hus1*$^{neo/\Delta 1}$ MEFs proliferated poorly and senesced early in culture. Furthermore, these MEFs have higher percentage of chromosomal aberrations in the presence of replication stress. While Rad54 and Hus1 single mutants are fertile, *Rad54*$^{-/-}$;*Hus1*$^{neo/\Delta 1}$ males were subfertile, with reduced sperm counts and significant germ cell loss, suggesting that HR defects due to loss of *Rad54* and *Hus1* also affected spermatogenesis. Taken together, these results indicate that HUS1 and the 9-1-1 complex synergistically cooperate with HR machinery for effective double strand break repair, and HUS1 inhibition could potentially hypersensitize HR-inefficient tumors to radiotherapy.

[2]Dr Robert Weiss, Mark Riccio, Dr. Amy Lyndaker, Dr. Gabriel Balmus and Cindy Luan contributed to the work presented in this chapter. Full acknowledgement can be found in section 3.6.

3.2 Introduction

Double-strand breaks (DSBs) are arguably the most lethal type of DNA damage cells could sustain. DSBs arise from direct damage from ionizing radiation, unrepaired single-strand breaks (SSBs), replication fork collapse or programmed DSBs in meiotic cells. If left unrepaired, DSBs will lead to genomic instability, cell death or tumorigenesis. DSBs can be repaired by two major repair pathways, which are the homologous recombination repair (HRR) and the non-homologous end joining (NHEJ). HRR begins with resection of DSB ends into long stretches of single-strand DNA (ssDNA), which is bound by RAD51. RAD51, with a few accessory proteins, mediate strand invasion onto undamaged sister chromatid or homologous chromosome to form a displacement loop (D-loop) to allow DNA synthesis and faithful restoration of the damaged DNA. On the other hand, NHEJ mediates direct ligation of DSB ends, which is a much faster repair than HRR, and absolutely essential for immunoglobulin class switch recombination. However, NHEJ can create insertion/deletion mutations or, even worse, aberrant interchromosomal fusions, particularly when HRR pathway is misregulated.

RAD54, an ATPase related to the SWI2/SNF2 family of chromatin remodeling proteins, is established to mediate HRR by interacting with RAD51 to assist the latter in ssDNA coating and in strand invasion by D-loop formation (Mazin et al., 2010). *Rad54*-deficient embryonic stem cells show hypersensitivity towards ionizing radiation (IR), DNA crosslinker mitomycin C (MMC) and DNA alkylating agent methylmethane sulfonate (MMS) but not towards ultraviolet (UV) treatment, consistent with a DSB repair defect (Essers et al., 1997). Low HRR efficiency and reduced MMC-induced sister chromatid exchange in these *Rad54*-deficient ES cells suggest that Rad54 plays a major role in HRR (Dronkert et al., 2000). Surprisingly, *Rad54*$^{-/-}$ mice do not show increased IR sensitivity compared to wildtype mice at the adult stage, suggesting that HRR

pathway is indispensable for cells at early developmental stage, and less so in more differentiated cells (Essers et al., 1997, Essers et al., 2000). They still retain hypersensitivity towards MMC, suggesting a mild perturbation of HRR pathway by inactivation of *Rad54*. In contrast, deletion of central components of the HRR pathway such as *Rad51* leads to embryonic lethality (Symington, 2002). This makes the *Rad54* mouse model suitable for the study of gene function in HRR, as already done for Blm (Chu et al., 2010), as well as HRR-NHEJ crosstalk study with Ku80 (Couëdel et al., 2004).

The 9-1-1 complex is a heterotrimeric toroidal DNA clamp that is important for DNA damage checkpoint signaling and repair. Once loaded at damage sites, one established function of the 9-1-1 complex is to stimulate ATR kinase activation through interactions with DNA topoisomerase 2-binding protein 1 (TOPBP1) (Delacroix et al., 2007). Activated ATR phosphorylates several substrates, including the effector kinase CHK1, which induce cell cycle arrest, stabilize stalled forks and inhibit origin firing (Cimprich and Cortez, 2008). In addition to its checkpoint signaling functions, 9-1-1 also acts directly in DNA repair through its role as a molecular scaffold (Helt et al., 2005, Eichinger and Jentsch, 2011). Since complete *mHus1* inactivation causes severe genomic instability and embryonic lethality, *in vivo* studies of *Hus1* were conducted using a hypomorphic allele that is partially impaired for *Hus1* gene function ($Hus1^{neo}$) in combination with wildtype *Hus1* ($Hus1^{+}$) and a null allele ($Hus1^{\Delta 1}$) to generate an allelic series of *Hus1* expression in mice ($Hus1^{+/+}$, $Hus1^{+/neo}$, $Hus1^{+/\Delta 1}$, $Hus1^{neo/neo}$, $Hus1^{neo/\Delta 1}$) (Levitt et al., 2007). $Hus1^{neo/\Delta 1}$ mice are grossly normal and fertile, but they have increased spontaneous genomic instability and are hypersensitive to MMC. An alternative method is by cre recombinase-mediated conditional knockout of *Hus1*, which has been used to reveal tissue-specific *Hus1* functions (Lyndaker et al., 2013a, Yazinski et al., 2009).

There are several lines of evidence that suggest the participation of HUS1 and the 9-1-1 complex in DSB repair. Previous study of $Hus1^{neo/\Delta 1}$ primary mouse embryonic fibroblasts (MEFs) shows that partial loss of Hus1 causes spontaneous chromatid breaks which can be aggravated into radial structures by replication stress (Levitt et al., 2007). These aberrations are reminiscent to those sustained by *Brca1* or *Brca2* deficient cells, which are defective in homologous recombination (HR), the error-free DSB repair pathway (Farmer et al., 2005). Furthermore, reports have shown interactions of 9-1-1 clamp with RAD51 and EXO1, both important components of the HR repair pathway (Pandita et al., 2006, Karras et al., 2013). In meiosis, RAD9A colocalizes with RAD51 foci during pachytene stage of prophase I, and *Hus1* conditional knockout leads to persistent RAD51 foci and increased DSBs (Lyndaker et al., 2013a). Also, *Hus1* siRNA knockdown reduced HR efficiency in mouse kidney fibroblast cells (Wang et al., 2005). These observations suggest that *Hus1*, and by extent the 9-1-1 complex, may play an important role in the error-free branch of DSB repair pathways like HRR. By combining the *Hus1* allelic series with targeted *Rad54* deletion, we identify an essential cooperative relationship between *Hus1* and HRR for proper DSB repair and genome maintenance.

3.3 Materials and Methods

All animals used in this study were handled in accordance with federal and institutional guidelines, under protocols approved by the Cornell University Institutional Animal Care and Use Committee (IACUC).

3.3.1 Mouse strains and breeding

First, *Rad54*$^{+/-}$ C57BL/6 mice (provided by Dr. R. Kanaar, Erasmus University Rotterdam) were backcrossed with wildtype 129 mouse up to ten generations to unify the genetic background of our Hus1 hypomorphic mice. Then *Rad54*$^{+/-}$ 129 mice were crossed with *Hus1*$^{+/neo}$ and *Hus1*$^{+/\Delta 1}$ 129 mice individually to generate *Rad54*$^{+/-}$*;Hus1*$^{+/neo}$ and *Rad54*$^{+/-}$*;Hus1*$^{+/\Delta 1}$ mice. Finally, these two genotypes were mated to breed all wanted genotypic groups. *Rad54*$^{-/-}$*;Hus1*$^{neo/\Delta 1}$ is designated as the experimental genotype, *Rad54*$^{-/-}$*;Hus1*$^{+/+}$, *Rad54*$^{-/-}$*;Hus1*$^{+/neo}$ and *Rad54*$^{-/-}$*;Hus1*$^{+/\Delta 1}$ as the *Rad54* single mutant controls, *Rad54*$^{+/-}$*;Hus1*$^{neo/\Delta 1}$ and *Rad54*$^{+/+}$*;Hus1*$^{neo/\Delta 1}$ as the *Hus1* hypomorph controls, and the rest as wildtype controls. The number of viable mice from each genotypic group was recorded and Mendelian ratio was calculated. Averaged weekly weights of mice from each genotypic group were also recorded and graphed (error bar = standard error of mean). Cohorts were observed for any developmental abnormalities that might occur, including spontaneous tumor development, accelerated aging phenotypes, and diseases. At 18 months adults of each genotype category were euthanized and dissected to identify any subtle pathological abnormalities.

3.3.2 Micronucleus assay

Micronucleus assay was performed as described (Levitt et al., 2007). Briefly, peripheral

blood was collected from the mandibular vein of 6-8 week-old female mice and kept in methanol at -80°C overnight. Blood samples were then washed with ice cold bicarbonate buffer and incubated with CD71-FITC diluted in RNAse A-containing bicarbonate buffer at 4°C for 45 minutes for reticulocyte labeling. The samples will then be washed with ice cold bicarbonate buffer, resuspended in propidium iodide (PI) for DNA labeling, and analyzed on a flow cytometer (BD LSR II). CD71 was detected with FITC channel whereas DNA was detected by PerCP channel. As controls, wildtype control blood sample labeled with CD71-FITC only and the same sample labeled with PI only were prepared for FACS gating. Percentage of $FITC^{-}DNA^{+}$ population over total gated population were calculated. Error bar = standard error of mean. Statistics were done using Student's T test. P-value<0.05 was considered significant.

3.3.3 In vivo genotoxin treatment

The experiment was performed as previously described (Balmus et al., 2012). Briefly, cohorts of female mice with representation from each genotypic group was selected and aged to 6-8 weeks old. They were injected with 3mg/kg of mitomycin C via intraperitoneal route, or were subjected to 8 Gy dose of gamma irradiation from ^{137}Cs source (JL Shepherd & Associates Mark I Model 68). The mice were weighed and monitored daily for up to 20 days or until reaching humane endpoint criteria, including severe weight loss, hunched posture, labored breathing, poor grooming or wasting, at which point they were euthanized.

3.3.4 Micro-CT scan

18-month old mice were anesthesized with isofluorane (4% mixture with oxygen, reduced to 1% during the scan) in an induction chamber. Micro-CT scans of the tail region were

done using GE eXplore CT120 micro-CT scanner with 50mA current and 100kV voltage. Micro-CT images were reconstructed at 50μm^3 voxel dimensions. Scans were converted from the manufacturer's propriety format into DICOM format. 3D reconstruction videos were made using Osirix64 software.

3.3.5 Skeletal staining

Procedure was done as previously described with minor alterations (Balmus et al., 2012). Briefly, 18-month old mice were euthanized, eviscerated, and fixed in 95% ethanol for 2 days. Then, the samples were stained in Alcian blue (Sigma #A3157) solution (150μg/ml in 76% ethanol and 20% acetic acid) for a week. Samples were rinsed in fresh 95% ethanol for 24 hours, twice. Then, samples were cleared in 1% KOH solution for 6 hours and counterstained with Alizarin red solution (50μg/ml in 1% KOH) for 24 hours. Finally, samples were rinsed and kept in 1% KOH for 1-2 months until the desired clarity is reached. The samples were imaged submerged in a tank of water with direct bottom white light with a Canon EOS Rebel XS dSLR camera.

3.3.6 MEF preparation and immortalization

Mouse embryonic fibroblasts (MEFs) were prepared as described (Levitt et al., 2007). Briefly, Rad54$^{+/-}$;Hus1$^{neo/neo}$ female was mated with Rad54$^{+/-}$;Hus1$^{+/ex}$ male. 13 days after female plug was observed, the female mouse was euthanized and uterus removed. Embryos were individually separated from deciduum, yolk sac, placenta and umbilical cord. Next, in a sterile hood, differentiated tissues were removed from the embryos and the remaining chunks of fibroblast tissues were resuspended in sterile PBS. The supernatant was transferred into a 60mm

dish containing 10% FBS media. The remaining solid tissue was used for genotyping.

MEFs were allowed to grow for 5 days with frequent change of medium. Cells were then passaged for Large T antigen immortalization or experimental use. For immortalization, 70% confluent MEFs were infected with retrovirus carrying pBP-LargeT construct (Addgene #14088) overnight and puromycin resistant MEFs were selected with 10% BCS media containing 1.25μg/ml of puromycin. Selected cells were maintained on a 3T3 schedule (Todaro and Green, 1963) and used for short term viability assay and metaphase spread count.

3.3.7 Population doubling assay

Briefly, each cell line was passaged onto 10cm dish in triplicates with 10^6 cells per dish at the first passage after primary MEF preparation. After three days, cells from each individual dish were trypsinized and counted, then pooled and counted again before seeding another triplicate of 10^6 cells per dish. This was repeated until cells entered senescence, upon which cells were fed but not passaged until they become spontaneously immortalized and confluent. Population doubling will be calculated using the formula $PD= \log_2(n_f/n_o)$, where n_o is the initial number of cells and n_f is the final number of cells.

3.3.8 Short term viability assay

The protocol is similar to section 2.3.3. Briefly, 10^4 cells of each cell line were seeded in 6-well plates in triplicates and incubated overnight. Cells were either left untreated or treated with mitomycin C (MMC) at various concentrations for 1 hour. The cells were then washed with PBS and cultured in fresh media for 3 days, at which point the cells were collected by trypsinization and counted using a Moxi^{TM} Z mini automated cell counter (ORFLO

technologies). Percent survival was calculated by dividing the number of cells after treatment by the number of untreated cells. Statistical analysis was by Student's T-test, and p-values of <0.05 were considered significant.

3.3.9 Metaphase spread preparation

Procedure was done as previously described (Levitt et al., 2007). Briefly, cells were either left untreated or treated with 0.1μM of aphidicolin or 60 ng/ml of MMC for 24 hours. Following genotoxin removal and PBS rinse, cells were incubated in fresh culture medium containing 0.15μg/ml of colcemid (Life Technologies #15210-040) for 1 hour. Cells were then trypsinized and centrifuged at 1,500rpm for 5 mins. Then, the cell pellets were resuspended in residual media and swollen in 6ml 75mM KCl solution at 37°C for 6 mins. After that, 1 ml of fixative solution (75% methanol 25% acetic acid) was slowly added while vortexing at a slow speed. Then, the cells were pelleted by centrifugation. Following resuspension in residual solution, 5ml of fresh fixative solution was added and cells were incubated at 4°C for at least 1 hour. After washing 3 times with fixative solution, cells were resuspended in 100-300μl of fixative solution and spotted on charged microscope slides (Fisher #12-550-15). Slides were stained with Giemsa stain (1:50 dilution in Gurr buffer) for 6 mins, washed with nanopure water 3 times, and air dried overnight before coverslipped. For each cell line, total chromosomal aberrations such as breaks/gaps, fusions, acentrics and radials were counted from 40 randomly picked spreads using a standard scoring method (Savage, 1976). Data were presented in tables (aberration type breakdown) and histograms (number of aberrations per spread).

3.3.10 Fertility test, epididymal sperm count and testes H&E staining

The fertility of male *Rad54*$^{-/-}$;*Hus1*$^{neo/\Delta 1}$ mice were evaluated by mating with wild-type female mice and recording the number of litters and pups produced. For sperm counts, both caudal epididymides from each mouse at various ages were minced and incubated in 1ml 37°C PBS for 20 mins to release the sperms. 20µl of the sperm solution were then fixed with 480µl of 10% phosphate-buffered formalin (Fisher #SF100-4) (1:25 dilution). The number of sperms were counted under an inverted microscope using a hemocytometer. Data were presented as mean ± SEM. Student's T test were applied and p-values<0.05 were considered as significant. Testes at various ages were removed, weighed and fixed in Bouin's fixative (VWR #RC112032) overnight, then rinsed with 70% ethanol before sending to the histology laboratory of Animal Health Diagnostic Center (AHDC) at the College of Veterinary Sciences, Cornell University for sectioning and standard hematoxylin and eosin staining. Stained sections were imaged with Aperio Scanscope CS at 10X magnification.

3.4 Results

3.4.1 Combined Rad54 and Hus1 defects cause dwarfism and skeletal defects.

To elucidate the physiological impact of depleting *Hus1* in sensitizing mice to damage caused by DSBs, we generated an allelic series of *Hus1* expressions (*Hus1*$^{+/+}$, *Hus1*$^{+/neo}$, *Hus1*$^{+/\Delta 1}$, *Hus1*$^{neo/neo}$, and *Hus1*$^{neo/\Delta 1}$) in a *Rad54*-deficient background. For the following experiments, we designate *Rad54*$^{-/-}$*Hus1*$^{neo/\Delta 1}$ as the experimental genotype, *Rad54*$^{-/-}$*Hus1*$^{+/+}$, *Rad54*$^{-/-}$*Hus1*$^{+/neo}$ and *Rad54*$^{-/-}$*Hus1*$^{+/\Delta 1}$ as the *Rad54* single mutant controls, *Rad54*$^{+/-}$*Hus1*$^{neo/\Delta 1}$ and *Rad54*$^{+/+}$*Hus1*$^{neo/\Delta 1}$ as the *Hus1* hypomorph controls, and the rest as wildtype controls. Initially we hypothesized that simultaneous deletion of *Rad54* and depletion of Hus1 to the lowest level (*Rad54*$^{-/-}$*Hus1*$^{neo/\Delta 1}$) would cause early embryonal developmental defects that would lead to synthetic lethality. *Rad54*$^{-/-}$*Hus1*$^{neo/\Delta 1}$ mice, however, are viable and were produced at the expected Mendelian ratio (Table 3.1). We first observed the mice for any overt physical defect. We noticed that the *Rad54*$^{-/-}$*Hus1*$^{neo/\Delta 1}$ mice were consistently and significantly underweight compare to the rest of the genotypic groups regardless of gender (Figure 3.1A). We also observed about 65% of our *Rad54*$^{-/-}$*Hus1*$^{neo/\Delta 1}$ mice have curly or kinked tails (Figure 3.1B and C). Additionally, these oddly-shaped tails were observed at birth and remained the same throughout their lives. Suspecting that the tail vertebrae structures may be deformed, we first performed live CT scan on the tail region of a *Rad54*$^{-/-}$*Hus1*$^{neo/\Delta 1}$ mouse (Figure 3.1D) and its wildtype control (not shown). We also performed skeletal staining on these mice (Figure 3.1E). Both the scans and staining revealed that the *Rad54*$^{-/-}$*Hus1*$^{neo/\Delta 1}$ mouse had several vertebrae that were deformed and fused together, forming the 'kinks' we saw. Together, these results suggest that perturbing *Hus1* and *Rad54* leads to mild dwarfism and late vertebrate developmental defect, likely due to elevated basal levels of genomic instability throughout development.

Table 3.1. Distribution of offsprings from *Rad54* and *Hus1* crosses[a].

Rad54	*Hus1*	Observed	Expected
+/+	+/+	16	12.00
	+/neo	54	50.38
	+/Δ1	17	12.00
	neo/Δ1	51	50.38
+/-	+/+	21	24.00
	+/neo	101	100.75
	+/Δ1	22	24.00
	neo/Δ1	95	100.75
-/-	+/+	6	12.00
	+/neo	53	50.38
	+/Δ1	13	12.00
	neo/Δ1	50	50.38

[a] Mice were genotyped by PCR analysis at 3 weeks of age. Expected values represent the combined Mendelian ratios from crosses with different parental genotypes. The observed and expected genotype frequencies are not significantly different (χ^2 test p-value = 0.73).

Figure 3.1. Disruption of *Rad54* and *Hus1* leads to mild dwarfism and tail vertebrae development defect. (A) Weight of mice from multiple cohorts were weighed weekly up to 76 weeks and graphed according to gender. (B) Representative photos of *Rad54*$^{-/-}$*Hus1*$^{neo/\Delta 1}$ mice with kinked tails (white arrows) (C) Number of mice with kinked tails were segregated according to genotypic group. (D) Micro-CT image of the skeletal structure of the tail region of a *Rad54*$^{-/-}$ *Hus1*$^{neo/\Delta 1}$ mouse. Several vertebrae were fused together. (E) The same mouse was prepared for alcian blue and alizarin red staining together with a wildtype mouse from the same cohort.

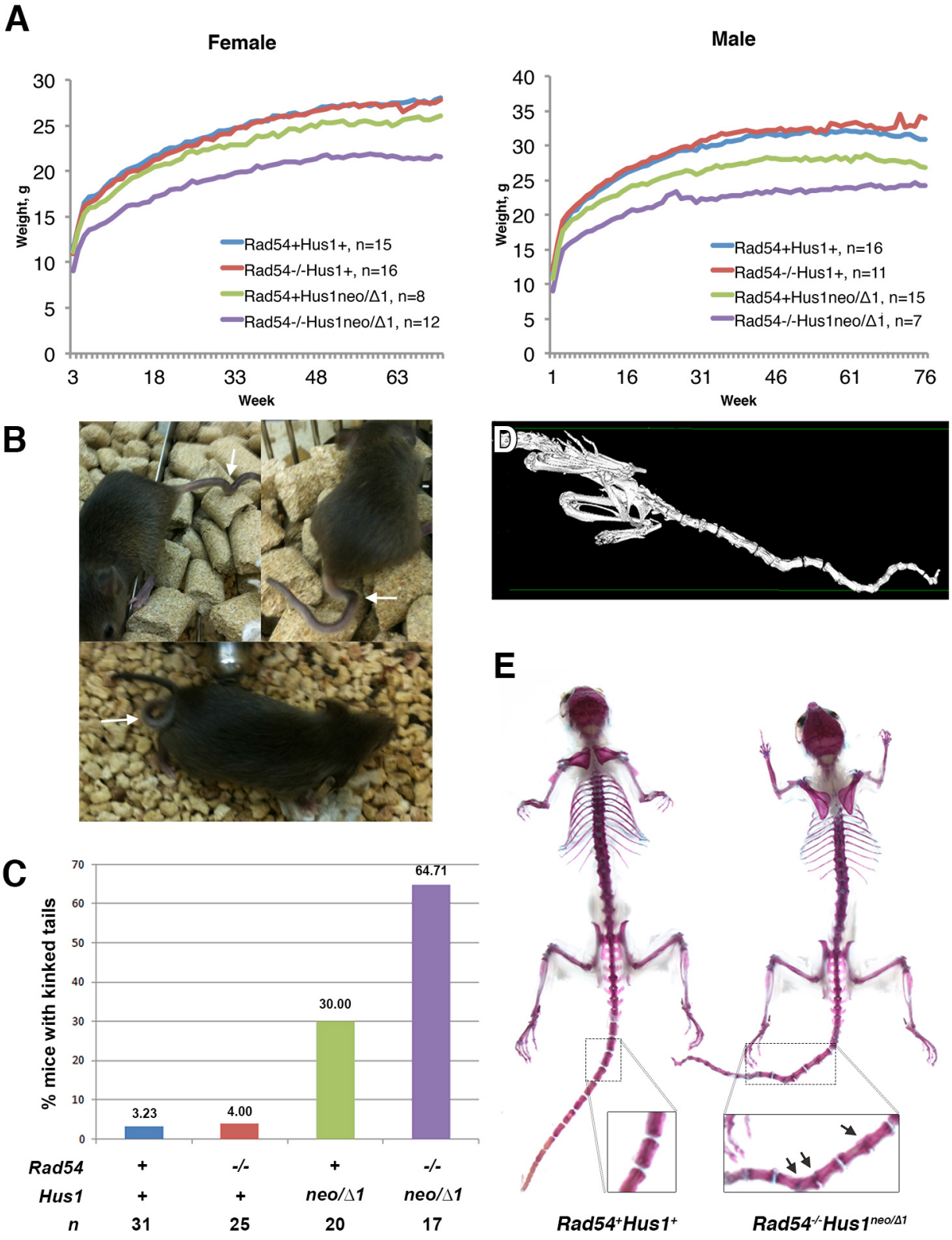
A
Female
Weight, g
Week
Rad54+Hus1+, n=15
Rad54-/-Hus1+, n=16
Rad54+Hus1neo/Δ1, n=8
Rad54-/-Hus1neo/Δ1, n=12
Male
Weight, g
Week
Rad54+Hus1+, n=16
Rad54-/-Hus1+, n=11
Rad54+Hus1neo/Δ1, n=15
Rad54-/-Hus1neo/Δ1, n=7
B
C
% mice with kinked tails
3.23
4.00
30.00
64.71
Rad54 + -/- + -/-
Hus1 + + neo/Δ1 neo/Δ1
n 31 25 20 17
D
E
Rad54+Hus1+
Rad54-/-Hus1neo/Δ1

3.4.2 Disruption of Rad54 and Hus1 leads to elevated spontaneous genomic instability

We tested the impact of combined *Rad54/Hus1* defects on basal genome maintenance by measuring micronucleus formation in peripheral blood cells (Figure 3.2A). Using flow cytometry, micronuclei levels were detected as the percentage of CD71-negative DNA-positive population of cells, signifying DNA fragment-containing mature erythrocytes. Consistent with previous studies (Levitt et al., 2007, Essers et al., 2000), *Rad54*$^{-/-}$ mice have the same level of micronuclei formation as wildtype mice, whereas *Hus1*$^{neo/\Delta 1}$ mice have a significantly higher number of micronuclei compare to wildtype. As expected, the double mutant mice have even higher micronuclei formation than other genotypic groups, suggesting that loss of *Rad54* and *Hus1* lead to synergistic increase in spontaneous genomic instability. We did not observe an intermediate phenotype in *Rad54*$^{+/-}$*Hus1*$^{neo/\Delta 1}$(data not shown), suggesting that elevated genomic instability is independent of *Rad54* dosage. Given that elevated spontaneous genomic instability often lead to early senescence of cells in culture, we isolated primary mouse embryonic fibroblasts (MEFs) and performed population doubling assay (Figure 3.2B). Wildtype MEFs proliferated well for 7 passages before they started to senesce. *Rad54*-deficient MEFs were also able to proliferate at a lower rate, but *Hus1*$^{neo/\Delta 1}$ MEFs began to senesce early at passage 2, as previously reported (Levitt et al., 2007). Importantly, *Rad54*$^{-/-}$*Hus1*$^{neo/\Delta 1}$ MEFs could not proliferate well as early as the first passage, and could never recover from senescing. These data reinforce the notion that combined *Rad54/Hus1* perturbations lead to less efficient genome maintenance that affects cell proliferation.

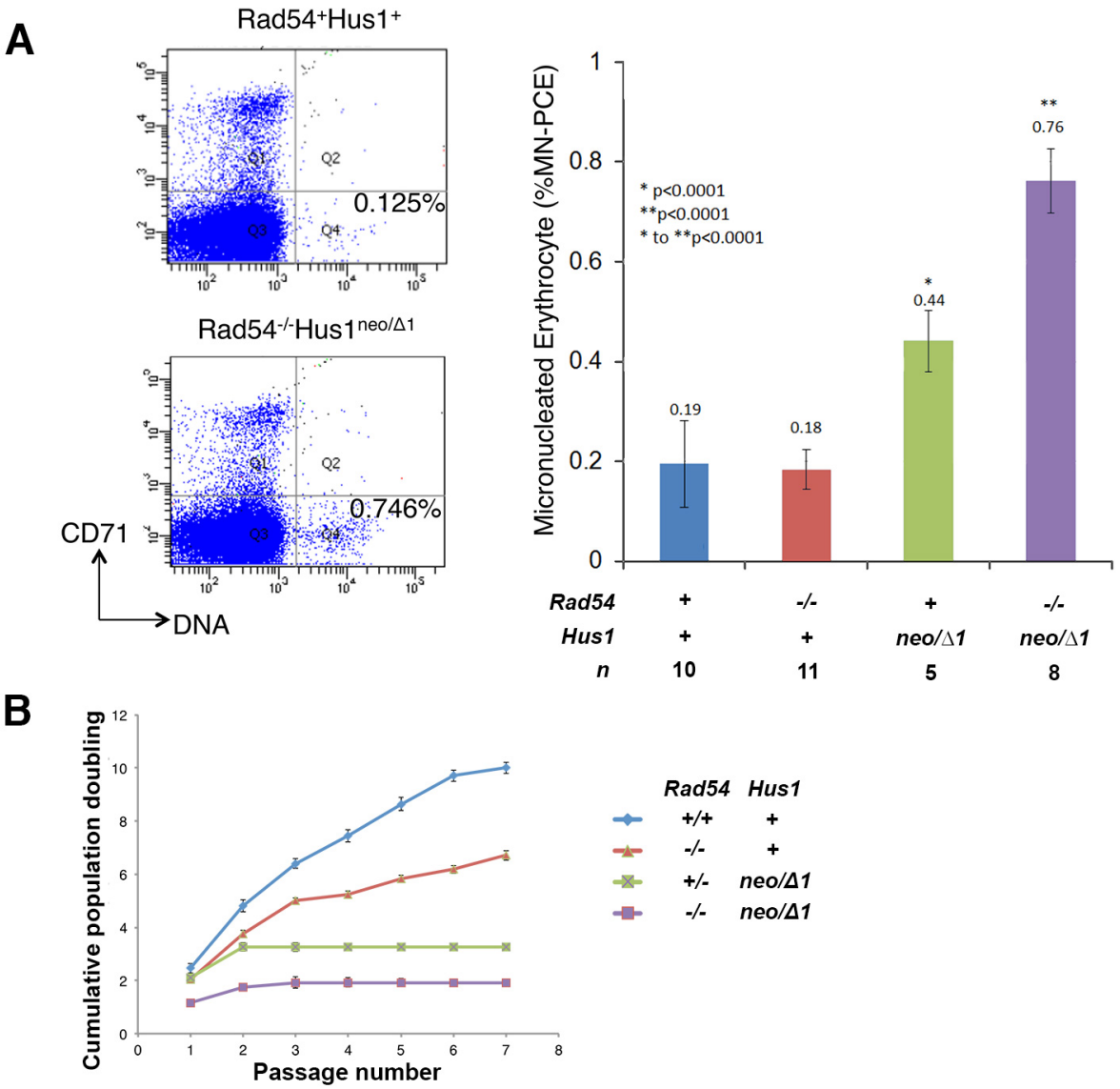

Figure 3.2. Elevated genomic instability is inherent in Rad54-/-Hus1 neo/Δ1 mice and MEFs. (A) Micronucleus assay by flow cytometry. The charts on the left indicate gatings used to isolate and calculate the percentage of CD71+DNA- cells in the population, represented in the graph on the right with mean ± SEM. * and ** are p-values from Student's T-test comparing each with *Rad54*$^{+}$*Hus1*$^{+}$ values. (B) Cumulative population doubling of primary MEFs. Data points indicate mean ± SD.

3.4.3 Partial Hus1 impairment synergizes with Rad54 deficiency to increase hypersensitivity towards genotoxin-induced damage .

We then hypothesized that simultaneous *Hus1* depletion and *Rad54* deletion would also cause synergistic effect on genotoxin-induced genomic instability. *Rad54*$^{-/-}$ mice are sensitive to MMC at 10mg/kg dose but they are not sensitive to IR (Essers et al., 2000). *Hus1*$^{neo/\Delta 1}$ mice are also sensitive to MMC at 4mg/kg but not to IR (Balmus G, et al. paper in review) We first irradiated mice with 8 Gy IR and monitored their survival post irradiation (Figure 3.3A). Kaplan-Meier curve analysis showed that the survival of *Rad54* and *Hus1* single mutant cohorts was not significantly different from the wildtype cohorts, consistent with published and unpublished results. Interestingly, *Rad54*$^{-/-}$*Hus1*$^{neo/\Delta 1}$ mice became hypersensitive to IR treatment and 4 out of 5 mice succumbed to IR-induced damage. This hypersensitivity was also reflected in the severity of weight loss throughout the first two weeks post treatment (Figure 3.3B). We then performed the same experiment but with 3mg/kg of MMC to determine if the reported preexisting sensitivity in the *Rad54* and *Hus1* single mutant mice was amplified in the double mutant (Figure 3.3C). While none of the mice in control and single mutant groups died, 2 out of 5 *Rad54*$^{-/-}$ *Hus1*$^{neo/\Delta 1}$ mice succumbed to MMC-induced damage, while the surviving cohort sustained the worst weight loss difference before recovering (Figure 3.3D).

To further validate the reduced genome maintenance capability of *Rad54*$^{-/-}$*Hus1*$^{neo/\Delta 1}$ mice, we tested MMC sensitivity of MEFs *in vitro*. Because primary *Rad54*$^{-/-}$*Hus1*$^{neo/\Delta 1}$ MEFs senesce very early in culture (Figure 3.2B), we immortalized these cells with Large T antigen (see Section 3.3 for Materials and Methods). Various doses of MMC were given to each cell line, and the amount of surviving cells 3 days after treatment were plotted (Figure 3.3E). As expected, Rad54-deficient MEFs and *Hus1*$^{neo/\Delta 1}$ MEFs were both sensitive to MMC treatment, while

Figure 3.3. Partial loss of Hus1 in combination with Rad54 deficiency leads to heightened sensitivity to genotoxin-induced damage. (A and C) Kaplan-Meier curve for survival of mice of indicated genotypes after IR and MMC treatment, respectively. Log-rank test was performed for statistics. (B and D) Averaged percent weight loss for mice of the indicated genotypes were plotted over time post IR and MMC treatment. (E) Short term viability was measured for MEFs of the indicated genotypes after 1 hour of MMC treatment at indicated dosages. Data was presented in mean ± SD. (F and G) Metaphase spread analyses was performed on MEFs of indicated genotypes after 24 hours of MMC or aphidicolin treatment. Each spread was categorized into one of the four bins for number of chromosomal abnormalities per spread.

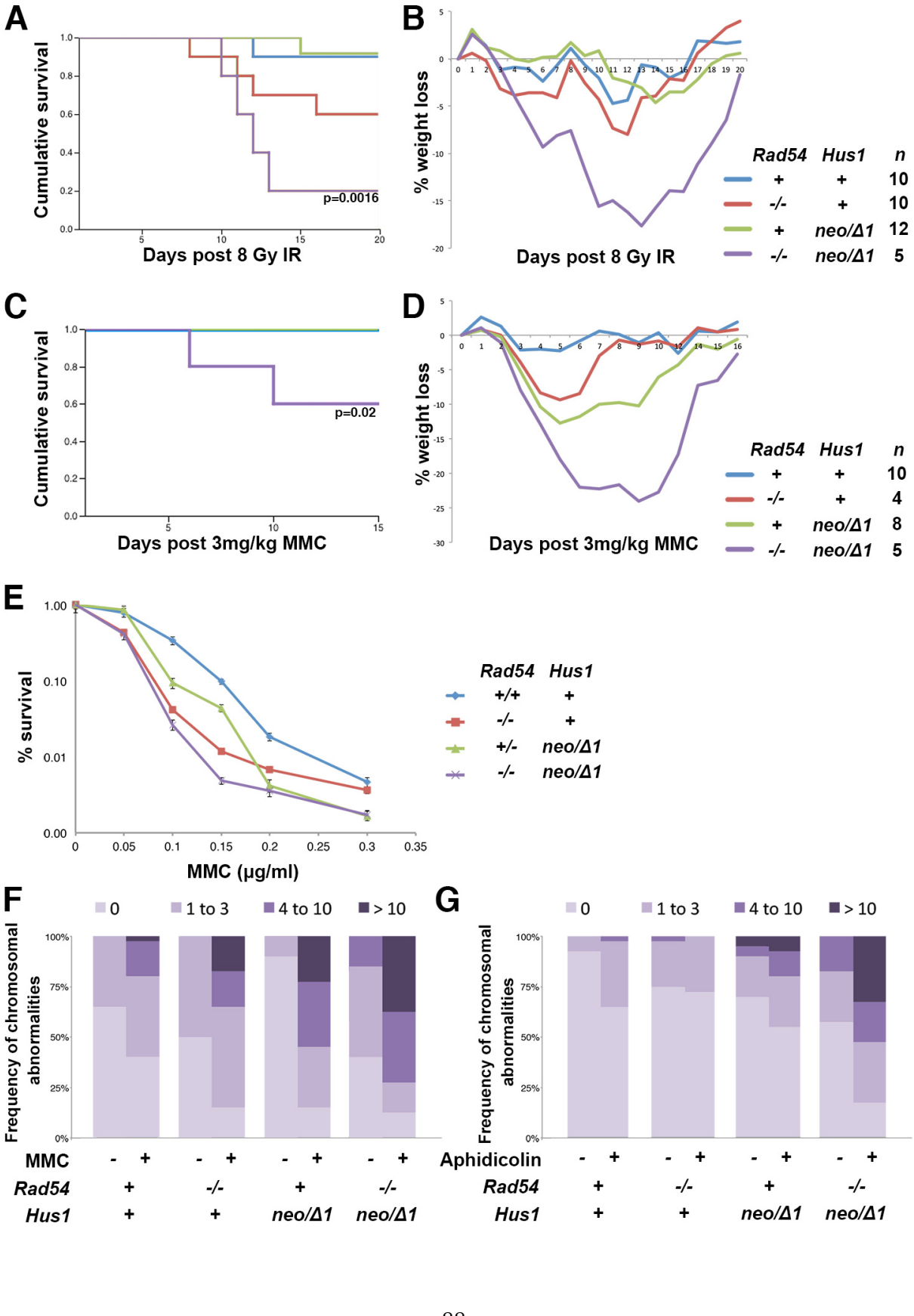
A
Cumulative survival
Days post 8 Gy IR
p=0.0016
B
% weight loss
Days post 8 Gy IR
Rad54 Hus1 n
+ + 10
-/- + 10
+ neo/Δ1 12
-/- neo/Δ1 5
C
Cumulative survival
Days post 3mg/kg MMC
p=0.02
D
% weight loss
Days post 3mg/kg MMC
Rad54 Hus1 n
+ + 10
-/- + 4
+ neo/Δ1 8
-/- neo/Δ1 5
E
% survival
MMC (µg/ml)
Rad54 Hus1
+/+ +
-/- +
+/- neo/Δ1
-/- neo/Δ1
F
0 1 to 3 4 to 10 > 10
Frequency of chromosomal abnormalities
MMC - + - + - + - +
Rad54 + -/- + -/-
Hus1 + + neo/Δ1 neo/Δ1
G
0 1 to 3 4 to 10 > 10
Frequency of chromosomal abnormalities
Aphidicolin - + - + - + - +
Rad54 + -/- + -/-
Hus1 + + neo/Δ1 neo/Δ1

Rad54$^{-/-}$*Hus1*$^{neo/\Delta 1}$ MEFs were significantly hypersensitized at 0.15μg/ml of MMC, showing a similar trend as the in vivo experiment.

In order to understand the underlying cause of genotoxin sensitivity, we examined the chromosomal integrity of the MEF cultures after MMC or aphidicolin treatment. *Hus1*$^{neo/\Delta 1}$ primary MEFs sustain spontaneous chromosome breaks which are aggravated by aphidicolin treatment into more breaks and radial chromosomal structures, indicative of HR repair pathway impairment (Levitt et al., 2007). Similar results were seen with MMC treatment (Joanna Mleczko, unpublished data). No metaphase spread analysis of *Rad54*$^{-/-}$ cells have been published yet. Metaphase spread analyses were quantified as the percentage of spreads with binned number of aberrations per spread (Figure 3.3F and G) or segregated by the types of aberrations found (Tables 3.2 and 3.3). As presented in the graphs, *Rad54*$^{-/-}$*;Hus1*$^{neo/\Delta 1}$ MEFs already had higher basal level of chromosomal abnormalities per spread in untreated condition compare to wildtype or single mutants. After exposure to exogenous DNA damage, the double mutant MEFs sustained even more severe amounts of chromosomal aberrations, with most aggravating type being chromosomal breaks/gaps and radials. Taken together, these results strongly suggest that Hus1 partial loss together with Rad54 deficiency leads to further reduced HRR efficiency, increased error-prone DSB repair and higher genomic instability.

3.4.4. Simultaneous impairment of Rad54 and Hus1 caused subfertility and meiotic defects

We aged the mice to 18 months to identify any age-related phenotypes associated with simultaneous impairment of *Rad54* and *Hus1*. However, through necropsy and analyses of histological sections, we did not observe any abnormalities specific to the *Rad54*$^{-/-}$*Hus1*$^{neo/\Delta 1}$ mice, except for smaller testes (Figure 3.4A). We recorded testes weights for mice at 14-days,

Table 3.2. Distribution of chromosomal aberrations caused by MMC treatment by aberration type[a]

Genotype	Breaks / Gaps	Fusions	Acentrics	Radials
Rad54^{+} *Hus1*$^{+}$	48	20	13	10
Rad54$^{-/-}$ *Hus1*$^{+}$	79	52	34	28
Rad54^{+} *Hus1*$^{neo/\Delta 1}$	177	58	39	29
Rad54$^{-/-}$ *Hus1*$^{neo/\Delta 1}$	224	152	30	90

[a] 40 metaphase spreads per genotype were randomly selected and quantified for the total number of breaks/gaps, fusions, acentrics and radials

Table 3.3. Distribution of chromosomal aberrations caused by aphidicolin treatment by aberration type[a]

Genotype	Breaks / Gaps	Fusions	Acentrics	Radials
Rad54^{+} *Hus1*$^{+}$	15	7	5	2
Rad54$^{-/-}$ *Hus1*$^{+}$	8	6	4	0
Rad54^{+} *Hus1*$^{neo/\Delta 1}$	43	17	25	3
Rad54$^{-/-}$ *Hus1*$^{neo/\Delta 1}$	185	68	56	25

[a] 40 metaphase spreads per genotype were randomly selected and quantified for the total number of breaks/gaps, fusions, acentrics and radials

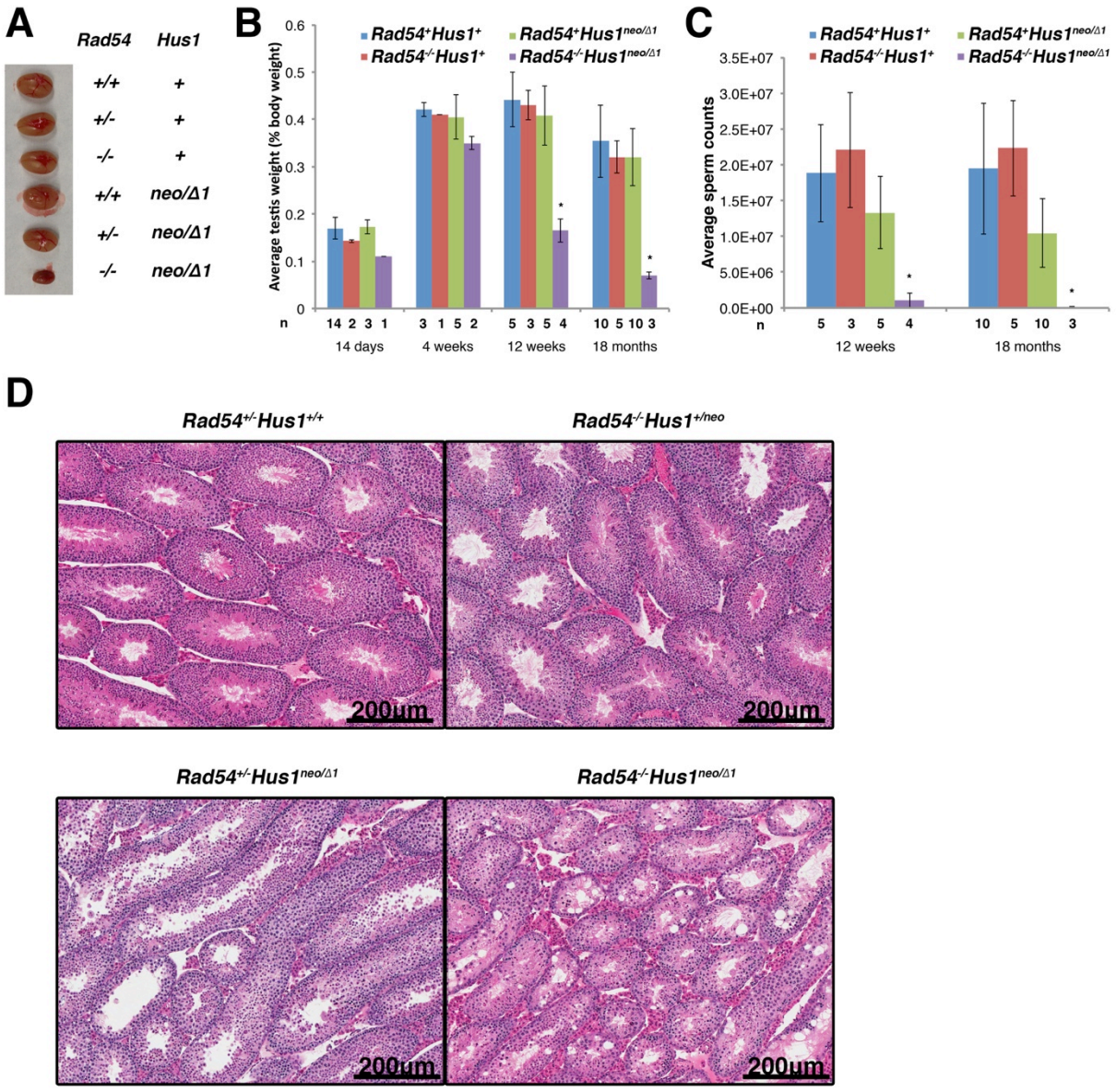

Figure 3.4. Rad54 deficiency coupled with Hus1 partial loss lead to subfertility in male mice. (A) Picture of testes size comparison among genotypes for 18-month old mice. (B) Testes weights of mice with indicated genotypes at 14-day, 4-week, 12-week and 18-month old. Error bar = SEM. *p-values<0.05 (C) Averaged number of sperms stored in caudal epididymis of mice of indicated genotypes at 12-week and 18-month old. Error bar = SEM. *p-values<0.05 (D) H&E sections of testis tubules at 100X magnification.

4-weeks, 12-weeks and 18-months of age and found that at 12-weeks old, *Rad54*$^{-/-}$*Hus1*$^{neo/\Delta 1}$ mice already had significantly smaller testes (Figure 3.4B). In correlation, 12-week old *Rad54*$^{-/-}$ *Hus1*$^{neo/\Delta 1}$ mice have significantly lower sperm counts, and by 18 months they were almost depleted (Figure 3.4C). H&E sections of 12-week old *Rad54*$^{-/-}$*Hus1*$^{neo/\Delta 1}$ mice showed that most testicular tubules were smaller, had lost their cellularity and were filled with large vacuoles (Figure 3.4D). Many tubules also lacked mature spermatids in the lumen, and some had pyknotic nuclei or multinucleated cells. Finally, evaluation of the fertility of male *Rad54*$^{-/-}$*Hus1*$^{neo/\Delta 1}$ mice by mating them with wild-type female mice revealed that indeed simultaneous perturbation of Rad54 and Hus1 leads to subfertility (Table 3.4).

3.5 Discussion

We have conducted a genetic analysis of *Hus1* function in homologous recombination repair (HRR) by combining the *Hus1* allelic series with *Rad54*-null mice. In assessing the impact of depleting Hus1 function in a mild HRR defective background, we identified an essential cooperative relationship between *Hus1* and HRR for proper DSB repair and genome maintenance in both mitotic and meiotic cells.

Initially, we thought that combined disruption of *Hus1* and *Rad54* would lead to embryonic lethality. This is because ATR-mediated cell cycle arrest is crucial for HRR and CHK1, a downstream substrate of ATR, also directly phosphorylates RAD51 to promote its nucleation on ssDNA (Sorensen et al., 2005). Furthermore, there may be higher requirement of HR repair in mouse cells in the embryonic stage (Essers et al., 2000). Moreover, HUS1 and the 9-1-1 complex may play a direct mechanistic role in HRR (Pandita et al., 2006, Karras et al., 2013). However, *Rad54*$^{-/-}$*Hus1*$^{neo/\Delta 1}$ mice are viable. Recent discovery of an alternative mode for

Table 3.4. Fertility tests for male mice[a]

Genotype	# matings	# copulatory plugs	# pregnancies	Total viable pups
Rad54^{+} *Hus1*$^{+}$	13	13	12	103
Rad54$^{-/-}$ *Hus1*$^{+}$	3	3	3	16
Rad54^{+} *Hus1*$^{neo/\Delta 1}$	4	4	3	15
Rad54$^{-/-}$ *Hus1*$^{neo/\Delta 1}$	16	16	2	12

[a] Male mice from the four genotypic groups were mated with wildtype FVB female mice and the number of viable pups born were recorded.

ATR activation may provide partial explanation. The MRN complex from the ATM pathway interacts with TOPBP1 independent of RAD17 and may activate ATR on long stretches of ssDNA inaccessible by the 9-1-1 clamp (Duursma et al., 2013, Lee and Dunphy, 2013, Shiotani et al., 2013). This might alleviate the dampening effects of *Hus1* loss on ATR signaling.

Nevertheless, *Rad54*$^{-/-}$*Hus1*$^{neo/\Delta 1}$ mice produced phenotypes symptomatic of a less effective DNA damage response. They exhibited a mild dwarfism phenotype very similar to *Atm*$^{-/-}$*Hus1*$^{neo/neo}$ mice, which also displayed skeletal abnormalities with unfused skull plates and brachymesophalangy of the fifth digit (Balmus et al., 2012). We did not observe any skull or digit defects in the *Rad54*$^{-/-}$*Hus1*$^{neo/\Delta 1}$ mice. However, a significant number of these mice have kinked tails, which was produced by deformed and fused tail vertebrae. Precedence of tail defects in mice was historically associated with partial loss of *Brachyury* gene expression, in which heterozygous mice exhibit variably shortened tails (Stott et al., 1993) The mechanistic detail of the defect is thought to originate from improper formation of the notochord causing loss of Shh signaling to the paraxial mesoderm, eventually losing somites that would form the tail vertebrates (Pennimpede et al., 2012). Deregulation of Hox gene expression via specific ribosomal mutant protein is also found to affect somite development (Kondrashov et al., 2011). We think that these are not the underlying reason for the phenotype seen in our *Rad54*$^{-/-}$ *Hus1*$^{neo/\Delta 1}$ mice because *Hus1* and *Rad54* genes are not involved in *Shh* signaling, and the total number of vertebrae sections or the rest of the spinal cord was not affected. We favor the notion that intrinsic genomic instability triggers p53-dependent apoptosis of somatic cells (Vlangos et al., 2009, Watkins-Chow et al., 2013) It is also shown that scoliosis, a spinal cord malformation disease, is modulated by hypoxic conditions during development, linking DNA damage and genomic instability to vertebral abnormalities (Sparrow et al., 2012). Further investigation is

warranted to see if this phenotype seen in our mice is associated with persistant DNA damage and apoptosis during somatogenesis.

Spontaneous genomic instability negatively affects cell proliferation capacity and drive early senescence. Our *Rad54*$^{-/-}$*Hus1*$^{neo/\Delta 1}$ mice exhibited synergistic increase in spontaneous genomic instability, which leads to limited cell proliferation in cell culture setting. However, this defect was not severe enough to translate into significant premature aging or early death phenotype *in vivo*. Increased mutation rate due to elevated genomic instability is also a source of increases cancer incidence. However, we did not observe any malignant growth in any of our *Rad54*$^{-/-}$*Hus1*$^{neo/\Delta 1}$ mice up to 18 months of age. The lack of premature aging and tumor burden may hint of heavier reliance of ATM checkpoint pathway and alternative DSB repair pathway like non-homologous end joining to deal with endogenous DNA damage.

Ionizing radiation and DNA interstrand crosslink agents are extremely genotoxic for proliferating cells. The efficacy of these treatments on cancer cells is modulated by the ability of cells to repair the inflicted DNA damage. Here we demonstrated that partial loss of *Hus1* hypersensitizes *Rad54* deficient mice to both IR and MMC treatment. This finding is further validated in cell culture in which *Rad54*$^{-/-}$*Hus1*$^{neo/\Delta 1}$ MEFs are further sensitized to MMC treatment. Both *Rad54* and *Hus1* are synergistically important to prevent deleterious chromosomal aberrations from forming due to error prone DSB repair, as evidenced by accumulation of chromosomal breaks and radials caused by MMC and aphidicolin induced replication stress in the absence of *Rad54* and *Hus1*. This is consistent with the notion that loss of efficient HRR and ATR checkpoint signaling trigger the molecular switch for cells to depend on ATM checkpoint pathway and NHEJ repair instead.

It has been shown that total *Hus1* loss in testes leads to defects in meiotic recombination

in mouse testes (Lyndaker et al., 2013a). Interestingly, we show that partial loss of *Hus1* in combination with loss of *Rad54* can lead to similar physiological defects. These data indicate that in the absence of RAD54-mediated HRR, HUS1 level modulates the efficiency of DSB repair. We speculate that the molecular mechanism of HUS1 function in HRR involves the coordination of checkpoint signaling and repair. HUS1 and the 9-1-1 clamp tightly regulate cell cycle arrest through ATR and CHK1 activation, providing ample time for the lengthy process of HRR to be completed. CHK1 modulation of RAD51 activity may also alleviate loss of HRR efficiency due to *Rad54* deficiency. In addition, HUS1 and the 9-1-1 clamp may also improve HRR efficiency by stimulating EXO1 activity for DSB resection, and RAD9 interaction with RAD51 may further fortify the efficiency of strand invasion.

Taken together, we think that Hus1-mediated checkpoint and DNA repair functions cooperate with HRR pathways to respond to DNA damaging stresses and meiotic recombination. Further experiments are required to understand the mechanistic details of HUS1 function in HRR, and to evaluate the potential of *Hus1* as a therapeutic target to hypersensitize HRR deficient cancer cells to genotoxin treatment.

3.6 Acknowledgement

I would like to thank Dr. Roland Kanaar from Erasmus University for the gracious gift of *Rad54* mice, and Mark Riccio, director of Cornell University's Biotechnology Resource Center Imaging Facility for helping us with micro-CT use. I would also like to thank the lab technicians at the histology laboratory of Animal Health Diagnostic Center (AHDC) at the College of Veterinary Sciences, Cornell University for sectioning and standard hematoxylin and eosin staining of the testis sections. Thank you to fellow former and current lab members for helping

with various parts of the experiments: To Dr. Robert Weiss, who irradiated the mice for in vivo survival; To Dr. Gabriel Balmus, who assisted in the micronucleus assay and MMC in vivo treatment; To Cindy Luan, who did the metaphase spread analyses; and to Dr. Amy Lyndaker, who did part of the sperm counts and scanscope imaging of the testes sections.

CHAPTER 4

SUMMARY AND FUTURE DIRECTIONS

4.1 HUS1-mediated ATR signaling-independent protein-protein interaction for proficient DNA repair

The mechanism for 9-1-1-mediated checkpoint signaling has been extensively elucidated. Each subunit of the 9-1-1 complex has also been reported to directly interact with many repair factors, mostly of which are involved in every step of base excision repair. Base on these observations we believe that the 9-1-1 complex acts as a molecular scaffold to coordinate checkpoint signaling and DNA repair for a robust DNA damage response. We are interested in understanding the functional residues that facilitate 9-1-1 functions, from clamp assembly and nuclear localization to chromatin loading and effector interactions (Figure 4.1). Under normal conditions, HUS1 interacts with RAD9A and RAD1 to form the 9-1-1 clamp which is then loaded onto damaged DNA. Disruption of HUS1-RAD9A interaction prevents clamp formation and perturbs all downstream events. Similarly, weakened HUS1-DNA interactions may prevent proper loading of the clamp onto damaged DNA and subsequently prevent activation of ATR checkpoint signaling and stimulation of DNA repair. And when HUS1-effector interactions are disrupted, upstream events such as clamp assembly, chromatin localization and ATR signaling are not affected. Instead, loss of HUS1-effector interaction function may lead to partial loss of DNA repair efficiency. Together, these results indicate that, once properly loaded onto damaged DNA, the 9-1-1 complex executes multiple, separable functions that promote genome maintenance.

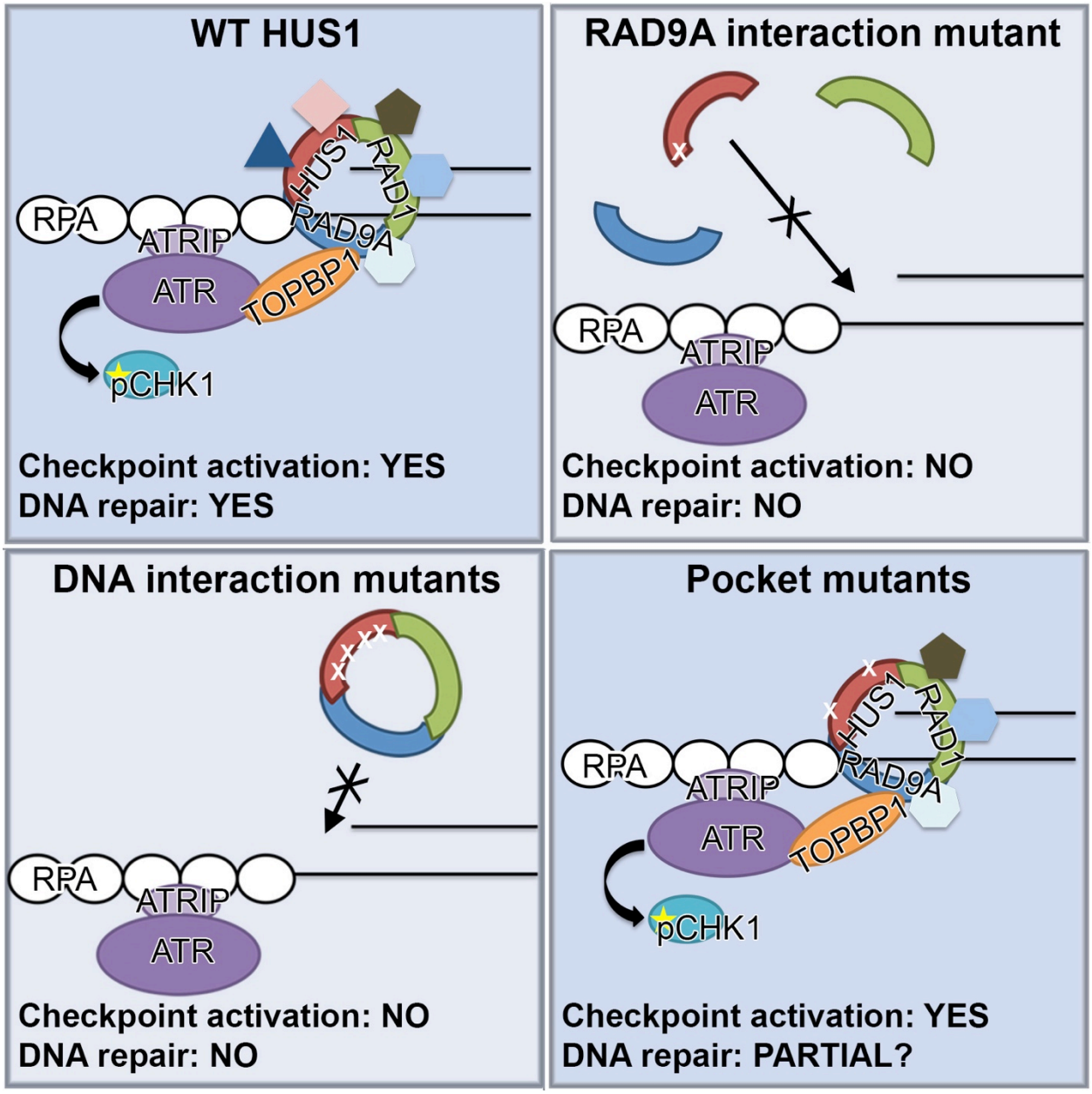

Figure 4.1. Model for HUS1-mediated function in DNA damage response. WT HUS1 forms 911 clamp, localizes on damaged DNA site, and mediates ATR checkpoint signaling and DNA repair functions. When the RAD9A interacting residue is dysfunctional, HUS1 cannot form 911 clamp, causing loss of all downstream functions. HUS1 defective in DNA interactions is still able to form 911 clamp but could not localize to damaged DNA site, similarly causing loss of all downstream functions. Only HUS1 pocket mutants are able to form 911 clamp, localize to DNA lesion and activate ATR for checkpoint signaling. However, checkpoint-independent functions of HUS1 are perturbed, leading to possible partial loss of DNA repair function.

In this study, we have created a library of valuable HUS1 mutants that enabled us to investigate HUS1 molecular functions in a greater detail. The next question is whether these mutants exhibit dominant negative effects when overexpressed in cells expressing wildtype HUS1. We hypothesize that if HUS1-effector interactions are strong and the molarity of the effector is limited, HUS1 mutants defective in clamp assembly and chromatin localization might sequester some DNA repair factors and reduce DNA repair efficiency. We also suspect that 9-1-1 clamp formed with HUS1 pocket mutants may compete with that of wildtype HUS1 to occupy damaged sites and prevent efficient repair, leading to mild dominant negative effect.

For future experiments, we would like to utilize HUS1 pocket mutants to understand the physiological significance of HUS1-mediated DNA repair functions separate from 9-1-1-mediated checkpoint signaling function. We have demonstrated that these pocket mutants did not disrupt ATR-mediated CHK1 phosphorylation at 2 hours post UV treatment. To further validate that these mutants are true separation of function mutants, we will perform the same assay at different time points to understand the effects of these mutants on checkpoint maintenance and dampening post repair. We expect that these mutants will not disrupt checkpoint maintenance but may delay checkpoint deactivation indirectly due to partial loss of repair efficiency. Finally, we would like to identify effectors that could not bind to these HUS1 pocket mutants using quantitative mass spectrometry. This approach will be useful to identify all HUS1 interactors in an unbiased way, as well as to tease apart the relative importance of the two effector-interacting pockets, especially in genotoxin-specific settings. We predict that, in response to bulky DNA adducts and replication stress, both pockets are equally important in binding to the same set of effectors for repair, whereas in response to DNA interstrand crosslinks, each pocket independently binds a different effector that are cooperatively important for repair. These

experiments are crucial to unfold the molecular dynamics of HUS1 function in DNA damage response, and potentially used to design inhibitors for clinical applications. Currently, inhibitors of ATM, ATR, PCNA and CHK1 are in various stages of clinical trial for antitumor treatments. HUS1 may prove to be a good candidate because it has multiple surface areas for targeted inhibition of small or large subset of repair pathways, as well as both repair and checkpoint signaling pathways mediated by HUS1, providing a one-target hit with multiple outcomes. These surface areas are also small and simple enough to conduct drug screening with available libraries of small molecule inhibitors available at pharmaceutical companies such as Roche, GSK and Bayer.

4.2 Hus1 role in DSB repair

The 9-1-1 clamp is implicated in DSB repair as loss of *Hus1* lead to error-prone DSB repair in mitotic and meiotic cells. In order to test the functional implications of 9-1-1 complex in DSBR pathways, a genetic approach was undertaken by crossing *Hus1* hypomorph mice with *Rad54*$^{-/-}$ mice, which are mildly perturbed for homologous recombination repair (HRR). In this study, we found that simultaneous *Hus1* and *Rad54* disruption caused synergistic effects on spontaneous and genotoxin induced genomic instability, both in vivo and ex vivo. Loss of *Rad54* and *Hus1* also affected spermatogenesis. These results suggest that HUS1 and the 9-1-1 complex are physiologically important for HRR. We speculate that HUS1 and RAD54 cooperatively facilitate HRR at different steps of the repair process (Figure 4.2). At the beginning when DSB is detected, HUS1 and the 9-1-1 clamp aid the formation of ssDNA through stimulation of EXO1 activity for DSB resection. At the same time, it regulates cell cycle arrest through ATR and CHK1 activation, providing ample time for the lengthy process of HRR to continue without interruptions. Then, RAD9 interaction with RAD51 and CHK1 modulation of RAD51 activity may further fortify the efficiency of strand invasion and displacement loop formation, which is a key process mediated by RAD54 through stabilization of RAD51 filament and chromatin remodeling of sister chromatid to allow easy access. Whether HUS1 has any direct interaction with other HRR proteins remains unknown, but we are poised to find that out (section 4.1).

To know if HUS1 and the 9-1-1 complex directly participates in HRR, we can measure HRR efficiency in the mutant MEFs using sister chromatid exchange assay or a GFP reporter plasmid. We can also measure known markers for HRR status, such as γH2AX, BRCA1 and RAD51 foci quantification. To understand the fundamental effects of *Hus1* and *Rad54* deficiencies on proliferation profiles of cells, we should also assess the levels of proliferative and

Figure 4.2. Model of HUS1 function in homologous recombination repair. HUS1 and the 9-1-1 clamp aid the formation of ssDNA through stimulation of EXO1 activity for DSB resection. It also regulates cell cycle arrest through ATR and CHK1 activation. Then, RAD9 interaction with RAD51 and CHK1 modulation of RAD51 activity, together with RAD54 function may further fortify the efficiency of strand invasion and displacement loop formation.

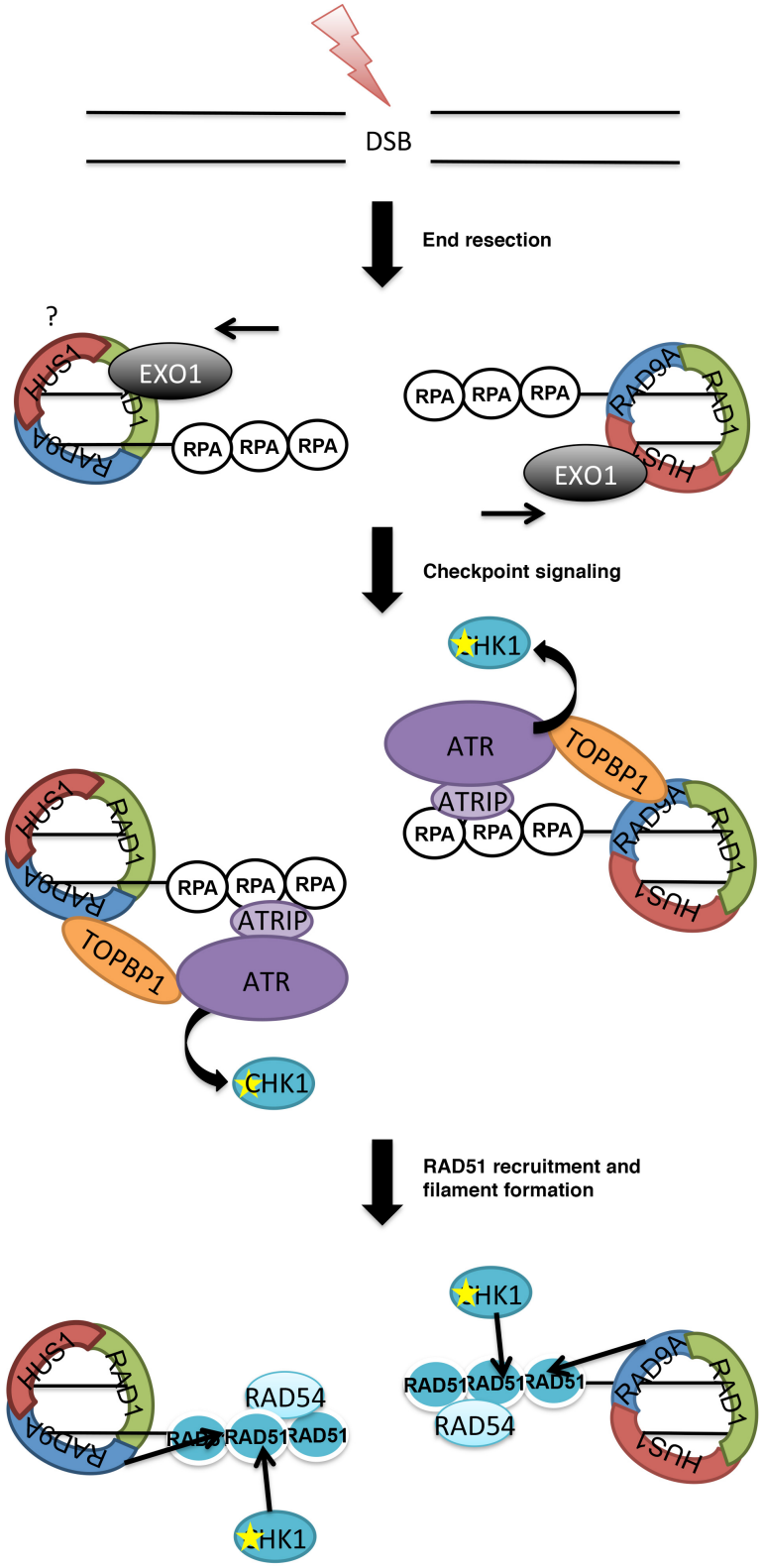
DSB
End resection
?
EXO1
RPA
RPA
RPA
HUS1
RAD1
RAD9A
RAD9A
RAD1
HUS1
EXO1
Checkpoint signaling
CHK1
ATR
TOPBP1
ATRIP
RPA
RPA
RPA
RAD9A
RAD1
HUS1
HUS1
RAD1
RAD9A
RPA
RPA
RPA
ATRIP
TOPBP1
ATR
CHK1
RAD51 recruitment and
filament formation
CHK1
RAD51
RAD51
RAD51
RAD54
RAD9A
RAD1
HUS1
HUS1
RAD1
RAD9A
RAD54
RAD51
RAD51
CHK1

apoptotic cells using markers such as Ki67 and TUNEL staining on tissue sections. To confirm if loss of *Hus1* and *Rad54* causes DDR pathway switch, Western analysis should also be conducted, specifically immunoblots detecting levels of pCHK1, pCHK2, RAD51, BRCA1 and 53BP1. Finally, it is also imperative to investigate *Hus1* genetic interactions with the other choice of DSB repair, the NHEJ pathway. This could be done by crossing our *Hus1* allelic series mice with *prkdc* mice and analyze the double mutants with all similar experiments done in this study. The results from this genetic cross will complement the data we have generated in this study and further validate the genetic relationship of *Hus1* with homologous recombination repair.

In conclusion, using molecular and genetic approaches, we have begun to resolve the HUS1 molecular mechanisms that mediate its physiological function in DNA repair. Taken together, these studies will reveal how HUS1 cooperates with DSB repair pathways to respond to DNA damaging stresses, and evaluate the potential of HUS1 as a therapeutic target to hypersensitize cancer cells to genotoxin treatment.

REFERENCES

ABMAYR, S. M., YAO, T., PARMELY, T. & WORKMAN, J. L. 2006. Preparation of Nuclear and Cytoplasmic Extracts from Mammalian Cells. *Curr Protoc Mol Biol.,* Chapter 12**,** Unit 12.1.

ACHARYA, S., WILSON, T., GRADIA, S., KANE, M., GUERRETTE, S., MARSISCHKY, G., KOLODNER, R. & FISHEL, R. 1996. hMSH2 forms specific mispair-binding complexes with hMSH3 and hMSH6. *Proc Natl Acad Sci U S A,* 93**,** 13629-13634.

AHNESORG, P., SMITH, P. & JACKSON, S. P. 2006. XLF interacts with the XRCC4-DNA ligase IV complex to promote DNA nonhomologous end-joining. *Cell,* 124**,** 301-13.

AL-KHODAIRY, F. & CARR, A. M. 1992. DNA repair mutants defining G2 checkpoint pathways in Schizosaccharomyces pombe. *The EMBO Journal,* 11**,** 1343-1350.

AL-KHODAIRY, F., FOTOU, E., SHELDRICK, K., GRIFFITHS, D., LEHMANN, A. & CARR, A. 1994. Identification and characterization of new elements involved in checkpoint and feedback controls in fission yeast. *Molecular biology of the cell,* 5**,** 147-160.

ALVER, R. C., ZHANG, T., JOSEPHRAJAN, A., FULTZ, B. L., HENDRIX, C. J., DAS-BRADOO, S. & BIELINSKY, A. K. 2014. The N-terminus of Mcm10 is important for interaction with the 9-1-1 clamp and in resistance to DNA damage. *Nucleic Acids Res,* 42**,** 8389-404.

ANDREASSEN, P. R., D'ANDREA, A. D. & TANIGUCHI, T. 2004. ATR couples FANCD2 monoubiquitination to the DNA-damage response. *Genes Dev,* 18**,** 1958-63.

ASHKENAZY, H., EREZ, E., MARTZ, E., PUPKO, T. & BEN-TAL, N. 2010. ConSurf 2010: calculating evolutionary conservation in sequence and structure of proteins and nucleic acids. *Nucleic Acids Res,* 38**,** W529-33.

BAI, H., MADABUSHI, A., GUAN, X. & LU, A. L. 2010. Interaction between human mismatch repair recognition proteins and checkpoint sensor Rad9-Rad1-Hus1. *DNA Repair (Amst),* 9**,** 478-87.

BALMUS, G., ZHU, M., MUKHERJEE, S., LYNDAKER, A. M., HUME, K. R., LEE, J., RICCIO, M. L., REEVES, A. P., SUTTER, N. B., NODEN, D. M., PETERS, R. M. & WEISS,

R. S. 2012. Disease severity in a mouse model of ataxia telangiectasia is modulated by the DNA damage checkpoint gene Hus1. *Hum Mol Genet,* 21**,** 3408-20.

BEATTIE, T. R. & BELL, S. D. 2012. Coordination of multiple enzyme activities by a single PCNA in archaeal Okazaki fragment maturation. *EMBO J,* 31**,** 1556-67.

BERMUDEZ, V. P., LINDSEY-BOLTZ, L. A., CESARE, A. J., MANIWA, Y., GRIFFITH, J. D., HURWITZ, J. & SANCAR, A. 2003. Loading of the human 9-1-1 checkpoint complex onto DNA by the checkpoint clamp loader hRad17-replication factor C complex in vitro. *Proc Natl Acad Sci U S A,* 100**,** 1633-8.

BROWN, E. J. 2003. Essential and dispensable roles of ATR in cell cycle arrest and genome maintenance. *Genes & Development,* 17**,** 615-628.

BROWN, E. J. & BALTIMORE., D. 2000. ATR disruption leads to chromosomal fragmentation and early embryonic lethality. *Genes & Development,* 14**,** 397-402.

BROWN, K. D., RATHI, A., KAMATH, R., BEARDSLEY, D. I., ZHAN, Q., MANNINO, J. L. & BASKARAN, R. 2003. The mismatch repair system is required for S-phase checkpoint activation. *Nat Genet,* 33**,** 80-4.

BRYANT, H. E., SCHULTZ, N., THOMAS, H. D., PARKER, K. M., FLOWER, D., LOPEZ, E., KYLE, S., MEUTH, M., CURTIN, N. J. & HELLEDAY, T. 2005. Specific killing of BRCA2-deficient tumours with inhibitors of poly(ADP-ribose) polymerase. *Nature,* 434**,** 913-917.

BUDZOWSKA, M., JASPERS, I., ESSERS, J., WAARD, H. D., DRUNEN, E. V., HANADA, K., BEVERLOO, B., HENDRIKS, R. W., KLEIN, A. D., KANAAR, R., HOEIJMAKERS, J. H. & MAAS., A. 2004. Mutation of the mouse Rad17 gene leads to embryonic lethality and reveals a role in DNA damage-dependent recombination. *EMBO Journal,* 23**,** 3548-3558.

BUIS, J., WU, Y., DENG, Y., LEDDON, J., WESTFIELD, G., ECKERSDORFF, M., SEKIGUCHI, J. M., CHANG, S. & FERGUSON, D. O. 2008. Mre11 nuclease activity has essential roles in DNA repair and genomic stability distinct from ATM activation. *Cell,* 135**,** 85-96.

BUNTING, K. A., ROE, M. S. & PEARL, L. H. 2003. Structural basis for recruitment of transletion DNA polymerase Pol IV/DinB to the beta-clamp. *EMBO J.,* 22**,** 5883-5892.

BURMA, S. & CHEN, D. J. 2004. Role of DNA-PK in the cellular response to DNA double-strand breaks. *DNA Repair (Amst),* 3**,** 909-18.

CAI, R. L., YAN-NEALE, Y., CUETO, M. A., XU, H. & COHEN, D. 2000. HDAC1, a histone deacetylase, forms a complex with Hus1 and Rad9, two G2/M checkpoint Rad proteins. *J Biol Chem,* 275**,** 27909-16.

CALDECOTT, K. W. 2008. Single-strand break repair and genetic disease. *Nat Rev Genet,* 9**,** 619-31.

CAPPELLI, E., TAYLOR, R., CEVASCO, M., ABBONDANDOLO, A., CALDECOTT, K. & FROSINA, G. 1997. Involvement of XRCC1 and DNA Ligase III Gene Products in DNA Base Excision Repair. *Journal of Biological Chemistry,* 272**,** 23970-23975.

CASPARI, T., DAHLEN, M., KANTER-SMOLER, G., LINDSAY, H. D., HOFMANN, K., PAPADIMITRIOU, K., SUNNERHAGEN, P. & CARR, A. M. 2000. Characterization of Schizosaccharomyces pombe Hus1: a PCNA-Related Protein That Associates with Rad1 and Rad9. *Molecular and Cellular Biology,* 20**,** 1254-1262.

CHANG, D.-Y., SHI, G., CHENG, C.-C., GUAN, X., VENCLOVAS, Č. & LU, A. L. 2006. Physical and functional interactions between MutY glycosylase homologue (MYH) and checkpoint proteins Rad9–Rad1–Hus1. *Biochemical Journal,* 400**,** 53.

CHANG, D. Y. 2004. Interaction of checkpoint proteins Hus1/Rad1/Rad9 with DNA base excision repair enzyme MutY homolog (MYH) in fission yeast, Schizosaccharomyces pombe. *Journal of Biological Chemistry*.

CHEN, L., NIEVERA, C. J., LEE, A. Y. & WU, X. 2008. Cell cycle-dependent complex formation of BRCA1.CtIP.MRN is important for DNA double-strand break repair. *J Biol Chem,* 283**,** 7713-20.

CHOU, W.-C., WANG, H.-C., WONG, F.-H., DING, S.-L., WU, P.-E., SHIEH, S.-Y. & SHEN, C.-Y. 2008. Chk2-dependent phosphorylation of XRCC1 in the DNA damage response promotes base excision repair. *The EMBO Journal,* 27**,** 3140-3150.

CHU, W. K., HANADA, K., KANAAR, R. & HICKSON, I. D. 2010. BLM has early and late functions in homologous recombination repair in mouse embryonic stem cells. *Oncogene,* 29**,** 4705-14.

CICCIA, A. & ELLEDGE, S. J. 2010. The DNA Damage Response: Making It Safe to Play with Knives. *Molecular Cell,* 40**,** 179-204.

CIMPRICH, K. A. & CORTEZ, D. 2008. ATR: an essential regulator of genome integrity. *Nat Rev Mol Cell Biol,* 9**,** 616-27.

CORTEZ, D. 1999. Requirement of ATM-Dependent Phosphorylation of Brca1 in the DNA Damage Response to Double-Strand Breaks. *Science,* 286**,** 1162-1166.

COUËDEL, C., MILLS, K., BARCHI, M., SHEN, L., OLSHEN, A., JOHNSON, R., NUSSENZWEIG, A., ESSERS, J., KANAAR, R., LI, G., ALT, F. & JASIN, M. 2004. Collaboration of homologous recombination and nonhomologous end-joining factors for the survival and integrity of mice and cells. *Genes & Development,* 18**,** 1293-1304.

DAS, B. B., ANTONY, S., GUPTA, S., DEXHEIMER, T. S., REDON, C. E., GARFIELD, S., SHILOH, Y. & POMMIER, Y. 2009. Optimal function of the DNA repair enzyme TDP1 requires its phosphorylation by ATM and/or DNA-PK. *EMBO J,* 28**,** 3667-80.

DE HARO, L. P., WRAY, J., WILLIAMSON, E. A., DURANT, S. T., CORWIN, L., GENTRY, A. C., OSHEROFF, N., LEE, S. H., HROMAS, R. & NICKOLOFF, J. A. 2010. Metnase promotes restart and repair of stalled and collapsed replication forks. *Nucleic Acids Research,* 38**,** 5681-5691.

DEAN, F., LIAN, L. & O'DONNELL, M. 1998. cDNA cloning and gene mapping of human homologs for Schizosaccharomyces pombe rad17, rad1, and hus1 and cloning of homologs from mouse, Caenorhabditis elegans, and Drosophila melanogaster. *Genomics,* 54**,** 424-436.

DEANS, A. J. & WEST, S. C. 2011. DNA interstrand crosslink repair and cancer. *Nat Rev Cancer,* 11**,** 467-80.

DELACROIX, S., WAGNER, J. M., KOBAYASHI, M., YAMAMOTO, K. & KARNITZ, L. M. 2007. The Rad9-Hus1-Rad1 (9-1-1) clamp activates checkpoint signaling via TopBP1. *Genes Dev,* 21**,** 1472-7.

DI VIRGILIO, M., CALLEN, E., YAMANE, A., ZHANG, W., JANKOVIC, M., GITLIN, A. D., FELDHAHN, N., RESCH, W., OLIVEIRA, T. Y., CHAIT, B. T., NUSSENZWEIG, A., CASELLAS, R., ROBBIANI, D. F. & NUSSENZWEIG, M. C. 2013. Rif1 prevents resection of DNA breaks and promotes immunoglobulin class switching. *Science,* 339**,** 711-5.

DIANOV, G. L. & HUBSCHER, U. 2013. Mammalian base excision repair: the forgotten archangel. *Nucleic Acids Res,* 41**,** 3483-90.

DIONNE, I., NOOKALA, R. K., JACKSON, S. P., DOHERTY, A. J. & BELL, S. D. 2003. A Heterotrimeric PCNA in the Hyperthermophilic Achaeon Sulfolobus solfatoricus. *Mol Cell,* 11**,** 275-282.

DOHERTY, A. J. & JACKSON, P. K. 2001. DNA repair: How Ku makes ends meet. *Curr Biol,* 11**,** R920-R924.

DORÉ, A. S., KILKENNY, M. L., RZECHORZEK, N. J. & PEARL, L. H. 2009. Crystal structure of the rad9-rad1-hus1 DNA damage checkpoint complex--implications for clamp loading and regulation. *Mol Cell,* 34**,** 735-45.

DRONKERT, M., BEVERLOO, H., JOHNSON, R., HOEIJMAKERS, J., JASIN, M. & KANAAR, R. 2000. Mouse RAD54 affects DNA double-strand break repair and sister chromatid exchange. *Molecular and Cellular Biology,* 20**,** 3147-3156.

DUCOUX, M., URBACH, S., BALDACCI, G., HUBSCHER, U., KOUNDRIOUKOFF, S., CHRISTENSEN, J. & HUGHES, P. 2001. Mediation of proliferating cell nuclear antigen (PCNA)-dependent DNA replication through a conserved p21(Cip1)-like PCNA-binding motif present in the third subunit of human DNA polymerase delta. *J Biol Chem,* 276**,** 49258-66.

DUFAULT, V. M., OESTREICH, A. J., VROMAN, B. T. & KARNITZ, L. M. 2003. Identification and characterization of RAD9B, a paralog of the RAD9 checkpoint gene. *Genomics,* 82**,** 644-651.

DUURSMA, A. M., DRISCOLL, R., ELIAS, J. E. & CIMPRICH, K. A. 2013. A role for the MRN complex in ATR activation via TOPBP1 recruitment. *Mol Cell,* 50**,** 116-22.

EICHINGER, C. S. & JENTSCH, S. 2010. Synaptonemal complex formation and meiotic checkpoint signaling are linked to the lateral element protein Red1. *Proc Natl Acad Sci U S A,* 107**,** 11370-11375.

EICHINGER, C. S. & JENTSCH, S. 2011. 9-1-1: PCNA's specialized cousin. *Trends Biochem Sci,* 36**,** 563-8.

ENOCH, T., CARR, A. M. & NURSE, P. 1992. Fission yeast genes involved in coupling mitosis to completion of DNA replication. *Genes & Development,* 6**,** 2035-2046.

ESCRIBANO-DIAZ, C., ORTHWEIN, A., FRADET-TURCOTTE, A., XING, M., YOUNG, J. T., TKAC, J., COOK, M. A., ROSEBROCK, A. P., MUNRO, M., CANNY, M. D., XU, D. & DUROCHER, D. 2013. A cell cycle-dependent regulatory circuit composed of 53BP1-RIF1 and BRCA1-CtIP controls DNA repair pathway choice. *Mol Cell,* 49**,** 872-83.

ESSERS, J., HENDRIKS, R., SWAGEMAKERS, S., TROELSTRA, C., DE WIT, J., BOOTSMA, D., HOEIJMAKERS, J. & KANAAR, R. 1997. Disruption of mouse RAD54 reduces ionizing radiation resistance and homologous recombination. *Cell,* 89**,** 195-204.

ESSERS, J., VAN STEEG, H., DE WIT, J., SWAGEMAKERS, S., VERMEIJ, M., HOEIJMAKERS, J. & KANAAR, R. 2000. Homologous and non-homologous recombination differentially affect DNA damage repair in mice. *EMBO Journal,* 19**,** 1703-1710.

FARMER, H., MCCABE, N., LORD, C. J., TUTT, A. N. J., JOHNSON, D. A., RICHARDSON, T. B., SANTAROSA, M., DILLON, K. J., HICKSON, I., KNIGHTS, C., MARTIN, N. M. B., JACKSON, S. P., SMITH, G. C. M. & ASHWORTH, A. 2005. Targeting the DNA repair defect in BRCA mutant cells as a therapeutic strategy *Nature,* 434**,** 917-921.

FORTINI, P. 1996. Two Pathways for Base Excision Repair in Mammalian Cells. *Journal of Biological Chemistry,* 271**,** 9573-9578.

FREIRE, R., MURGUIA, J. R., TARSOUNAS, M., LOWNDES, N. F., MOENS, P. B. & JACKSON, S. P. 1998. Human and mouse homologs of Schizosaccharomyces pombe rad1+ and Saccharomyces cerevisiae RAD17: linkage to checkpoint control and mammalian meiosis. *Genes & Development,* 12**,** 2560-2573.

FRIEDBERG, E. C. 2008. A brief history of the DNA repair field. *Cell Res,* 18**,** 3-7.

FRIEDRICH-HEINEKEN, E., TOUEILLE, M., TANNLER, B., BURKI, C., FERRARI, E., HOTTIGER, M. O. & HUBSCHER, U. 2005. The two DNA clamps Rad9/Rad1/Hus1 complex and proliferating cell nuclear antigen differentially regulate flap endonuclease 1 activity. *J Mol Biol,* 353**,** 980-9.

GEMBKA, A., TOUEILLE, M., SMIRNOVA, E., POLTZ, R., FERRARI, E., VILLANI, G. & HUBSCHER, U. 2007. The checkpoint clamp, Rad9-Rad1-Hus1 complex, preferentially stimulates the activity of apurinic/apyrimidinic endonuclease 1 and DNA polymerase beta in long patch base excision repair. *Nucleic Acids Res,* 35**,** 2596-608.

GEORGESCU, R. E., KIM, S. S., YURIEVA, O., KURIYAN, J., KONG, X. P. & O'DONNELL, M. 2008. Structure of a sliding clamp on DNA. *Cell,* 132**,** 43-54.

GIANNATTASIO, M., FOLLONIER, C., TOURRIERE, H., PUDDU, F., LAZZARO, F., PASERO, P., LOPES, M., PLEVANI, P. & MUZI-FALCONI, M. 2010. Exo1 competes with repair synthesis, converts NER intermediates to long ssDNA gaps, and promotes checkpoint activation. *Mol Cell,* 40**,** 50-62.

GIANNATTASIO, M., LAZZARO, F., LONGHESE, M. P., PLEVANI, P. & MUZI-FALCONI, M. 2004. Physical and functional interactions between nucleotide excision repair and DNA damage checkpoint. *EMBO Journal,* 23**,** 429-438.

GUAN, X., BAI, H., SHI, G., THERIOT, C. A., HAZRA, T. K., MITRA, S. & LU, A. L. 2007a. The human checkpoint sensor Rad9-Rad1-Hus1 interacts with and stimulates NEIL1 glycosylase. *Nucleic Acids Res,* 35**,** 2463-72.

GUAN, X., MADABUSHI, A., CHANG, D. Y., FITZGERALD, M. E., SHI, G., DROHAT, A. C. & LU, A. L. 2007b. The human checkpoint sensor Rad9-Rad1-Hus1 interacts with and stimulates DNA repair enzyme TDG glycosylase. *Nucleic Acids Res,* 35**,** 6207-18.

GULBIS, J. M., KELMAN, Z., HURWITZ, J., O'DONNELL, M. & KURIYAN, J. 1996. Structure of the C-Terminal Region of p21WAF1/CIP1 Complexed with Human PCNA. *Cell,* 87**,** 297-306.

GUZI, T. J., PARUCH, K., DWYER, M. P., LABROLI, M., SHANAHAN, F., DAVIS, N., TARICANI, L., WISWELL, D., SEGHEZZI, W., PENAFLOR, E., BHAGWAT, B., WANG, W., GU, D., HSIEH, Y., LEE, S., LIU, M. & PARRY, D. 2011. Targeting the replication checkpoint using SCH 900776, a potent and functionally selective CHK1 inhibitor identified via high content screening. *Mol Cancer Ther,* 10**,** 591-602.

HAN, L., HU, Z., LIU, Y., WANG, X., HOPKINS, K. M., LIEBERMAN, H. B. & HANG, H. 2010. Mouse Rad1 deletion enhances susceptibility for skin tumor development. *Mol Cancer,* 9**,** 67.

HANAHAN, D. & WEINBERG, R. A. 2011. Hallmarks of cancer: the next generation. *Cell,* 144**,** 646-74.

HANG, H. & LIEBERMAN, H. B. 2000. Physical interactions among human checkpoint control proteins HUS1p, RAD1p, and RAD9p, and implications for the regulation of cell cycle progression. *Genomics,* 65**,** 24-33.

HANG, H., RAUTH, S. J., HOPKINS, K. M., DAVEY, S. K. & LIEBERMAN, H. B. 1998. Molecular Cloning and Tissue-Specific Expression of Mrad9, a Murine Orthologue of the Schizosaccharomyces pombe rad9+ Checkpoint Control Gene. *J Cell Physiol,* 177**,** 241-247.

HANG, H., ZHANG, Y., DUNBRACK, R. L., JR., WANG, C. & LIEBERMAN, H. B. 2002. Identification and characterization of a paralog of human cell cycle checkpoint gene HUS1. *Genomics,* 79**,** 487-92.

HE, W., ZHAO, Y., ZHANG, C., AN, L., HU, Z., LIU, Y., HAN, L., BI, L., XIE, Z., XUE, P., YANG, F. & HANG, H. 2008. Rad9 plays an important role in DNA mismatch repair through physical interaction with MLH1. *Nucleic Acids Research,* 36**,** 6406-6417.

HELLEDAY, T., PETERMANN, E., LUNDIN, C., HODGSON, B. & SHARMA, R. A. 2008. DNA repair pathways as targets for cancer therapy. *Nat Rev Cancer,* 8**,** 193-204.

HELT, C. E., WANG, W., KENG, P. C. & BAMBARA, R. A. 2005. Evidence that DNA Damage Detection Machinery Participates in DNA Repair. *Cell Cycle,* 4**,** 529-532.

HIRAI, I., SASAKI, T. & WANG, H. G. 2004. Human hRad1 but not hRad9 protects hHus1 from ubiquitin-proteasomal degradation. *Oncogene,* 23**,** 5124-30.

HIRAI, I. & WANG, H. G. 2002. A role of the C-terminal region of human Rad9 (hRad9) in nuclear transport of the hRad9 checkpoint complex. *J Biol Chem,* 277**,** 25722-7.

HISHIKI, A., HASHIMOTO, H., HANAFUSA, T., KAMEI, K., OHASHI, E., SHIMIZU, T., OHMORI, H. & SATO, M. 2009. Structural Basis for Novel Interactions between Human Translesion Synthesis Polymerases and Proliferating Cell Nuclear Antigen. *Journal of Biological Chemistry,* 284**,** 10552-10560.

HOEIJMAKERS, J. 2001. Genome maintenance mechanisms for preventing cancer. *Nature,* 411**,** 366-374.

HOPKINS, K. M., AUERBACH, W., WANG, X. Y., HANDE, M. P., HANG, H., WOLGEMUTH, D. J., JOYNER, A. L. & LIEBERMAN, H. B. 2004. Deletion of mouse rad9 causes abnormal cellular responses to DNA damage, genomic instability, and embryonic lethality. *Mol Cell Biol,* 24**,** 7235-48.

HU, Z., LIU, Y., ZHANG, C., ZHAO, Y., HE, W., HAN, L., YANG, L., HOPKINS, K. M., YANG, X., LIEBERMAN, H. B. & HANG, H. 2008. Targeted Deletion of Rad9 in Mouse Skin

Keratinocytes Enhances Genotoxin-Induced Tumor Development. *Cancer Research,* 68**,** 5552-5561.

ISHIAI, M., KITAO, H., SMOGORZEWSKA, A., TOMIDA, J., KINOMURA, A., UCHIDA, E., SABERI, A., KINOSHITA, E., KINOSHITA-KIKUTA, E., KOIKE, T., TASHIRO, S., ELLEDGE, S. J. & TAKATA, M. 2008. FANCI phosphorylation functions as a molecular switch to turn on the Fanconi anemia pathway. *Nat Struct Mol Biol,* 15**,** 1138-46.

JACKSON, S. P. & BARTEK, J. 2009. The DNA-damage response in human biology and disease. *Nature,* 461**,** 1071-1078.

JORDI, Q.-A., CHUNLI, Y., XIAOJUN, X., SUSAN E., T., MIAW-SHEUE, T., JOHN A., T., PRISCILLA K., C., EVA, N. & IVAYLO, I. 2012. Repair complexes of FEN1 endonuclease, DNA, and Rad9-Hus1-Rad1 are distinguished from their PCNA counterparts by functionally important stability. *Proc Natl Acad Sci U S A,* 109**,** 8528-8533.

JULIE D., T., TOBY J., G., FREDERIC, P., FRANCOIS, J. & DESMOND G., H. 1997. The CLUSTAL_X windows interface: flexible strategies for multiple sequence alignment aided by quality analysis tools. *Nucleic Acids Res,* 25**,** 4876-4882.

KAI, M. & WANG, T. S.-F. 2003. Checkpoint activation regulates mutagenic translesion synthesis. *Genes & Development,* 17**,** 64-76.

KARRAS, G. I., FUMASONI, M., SIENSKI, G., VANOLI, F., BRANZEI, D. & JENTSCH, S. 2013. Noncanonical role of the 9-1-1 clamp in the error-free DNA damage tolerance pathway. *Mol Cell,* 49**,** 536-46.

KAUR, R., KOSTRUB, C. & ENOCH, T. 2001. Structure-Function Analysis of Fission Yeast Hus1- Rad1-Rad9 Checkpoint Complex. *Mol Biol Cell,* 12**,** 3744-3758.

KEDAR, P. S., KIM, S. J., ROBERTSON, A., HOU, E., PRASAD, R., HORTON, J. K. & WILSON, S. H. 2002. Direct interaction between mammalian DNA polymerase beta and proliferating cell nuclear antigen. *J Biol Chem,* 277**,** 31115-23.

KLUNGLAND, A. & LINDAHL, T. 1997. Second pathway for completion of human DNA base excision-repair: reconstitution with purified proteins and requirement for DNase IV (FEN1). *The EMBO Journal,* 16**,** 3341-3348.

KONDRASHOV, N., PUSIC, A., STUMPF, C. R., SHIMIZU, K., HSIEH, A. C., XUE, S., ISHIJIMA, J., SHIROISHI, T. & BARNA, M. 2011. Ribosome-mediated specificity in Hox mRNA translation and vertebrate tissue patterning. *Cell,* 145**,** 383-97.

KOSTRUB, C., KNUDSEN, K., SUBRAMANI, S. & ENOCH, T. 1998. Hus1p, a conserved fission yeast checkpoint protein, interacts with Rad1p and is phosphorylated in response to DNA damage. *EMBO Journal,* 17**,** 2055-2066.

KRISHNA, T. S. R., KONG, X.-P., GARY, S., BURGERS, P. M. & KURIYAN, J. 1994. Crystal structure of the eukaryotic DNA polymerase processivity factor PCNA. *Cell,* 79**,** 1233-1243.

KURZ, E. U. & LEES-MILLER, S. P. 2004. DNA damage-induced activation of ATM and ATM-dependent signaling pathways. *DNA Repair,* 3**,** 889-900.

LAM, M. H., LIU, Q., ELLEDGE, S. J. & ROSEN, J. M. 2004. Chk1 is haploinsufficient for multiple functions critical to tumor suppression. *Cancer Cell,* 6**,** 45-59.

LEE, J. & DUNPHY, W. G. 2013. The Mre11-Rad50-Nbs1 (MRN) complex has a specific role in the activation of Chk1 in response to stalled replication forks. *Mol Biol Cell,* 24**,** 1343-53.

LEE, K.-Y. & MYUNG, K. 2008. PCNA Modifications for Regulation of Post-Replication Repair Pathways. *Mol Cells,* 25**,** 5-11.

LEE, T. H., PARK, J. M., LEEM, S. H. & KANG, T. H. 2014. Coordinated regulation of XPA stability by ATR and HERC2 during nucleotide excision repair. *Oncogene,* 33**,** 19-25.

LEVITT, P., LIU, H., MANNING, C. & WEISS, R. 2005. Conditional inactivation of the mouse cell cycle checkpoint gene. *Genomics,* 86**,** 212-224.

LEVITT, P. S., ZHU, M., CASSANO, A., YAZINSKI, S. A., LIU, H., DARFLER, J., PETERS, R. M. & WEISS, R. S. 2007. Genome maintenance defects in cultured cells and mice following partial inactivation of the essential cell cycle checkpoint gene Hus1. *Mol Cell Biol,* 27**,** 2189-201.

LORD, C. J. & ASHWORTH, A. 2012. The DNA damage response and cancer therapy. *Nature,* 481**,** 287-94.

LUNCSFORD, P. J., CHANG, D.-Y., SHI, G., BERNSTEIN, J., MADABUSHI, A., PATTERSON, D. N., LU, A. L. & TOTH, E. A. 2010. A Structural Hinge in Eukaryotic MutY Homologues Mediates Catalytic Activity and Rad9–Rad1–Hus1 Checkpoint Complex Interactions. *Journal of Molecular Biology,* 403**,** 351-370.

LUO, J., SOLIMINI, N. L. & ELLEDGE, S. J. 2009. Principles of Cancer Therapy: Oncogene and Non-oncogene Addiction. *Cell,* 136**,** 823-837.

LYDALL, D. & WEINERT, T. A. 1995. Yeast Checkpoint Genes in DNA Damage Processing: Implications for Repair and Arrest. *Science,* 270**,** 1488-91.

LYNDAKER, A. M., LIM, P. X., MLECZKO, J. M., DIGGINS, C. E., HOLLOWAY, K. J., HOLMES, R. J., KAN, R., SCHLAFER, D. H., FREIRE, R., COHEN, P. E. & WEISS, R., S. 2013a. Conditional Inactivation of the DNA Damage Response Gene Hus1 in Mouse Testis Reveals Separable Roles for Components of the RAD9-RAD1-HUS1 Complex in Meiotic Chromosome Maintenance. *PLoS Genet,* 9.

LYNDAKER, A. M., VASILEVA, A., WOLGEMUTH, D. J., WEISS, R. S. & LIEBERMAN, H. B. 2013b. Clamping down on mammalian meiosis. *Cell Cycle,* 12**,** 3135-45.

MAJKA, J., BINZ, S. K., WOLD, M. S. & BURGERS, P. M. 2006. Replication protein A directs loading of the DNA damage checkpoint clamp to 5'-DNA junctions. *J Biol Chem,* 281**,** 27855-61.

MARTEIJN, J. A., LANS, H., VERMEULEN, W. & HOEIJMAKERS, J. H. 2014. Understanding nucleotide excision repair and its roles in cancer and ageing. *Nat Rev Mol Cell Biol,* 15**,** 465-81.

MATSUOKA, S., BALLIF, B. A., SMOGORZEWSKA, A., MCDONALD, E. R., 3RD, HUROV, K. E., LUO, J., BAKALARSKI, C. E., ZHAO, Z., SOLIMINI, N., LERENTHAL, Y., SHILOH, Y., GYGI, S. P. & ELLEDGE, S. J. 2007. ATM and ATR substrate analysis reveals extensive protein networks responsive to DNA damage. *Science,* 316**,** 1160-6.

MAZIN, A. V., MAZINA, O. M., BUGREEV, D. V. & ROSSI, M. J. 2010. Rad54, the motor of homologous recombination. *DNA Repair,* 9**,** 286-302.

MCNALLY, R., BOWMAN, G. D., GOEDKEN, E. R., O'DONNELL, M. & KURIYAN, J. 2010. Analysis of the role of PCNA-DNA contacts during clamp loading. *BMC Struct Biol,* 10**,** 3.

MOLDOVAN, G. L., PFANDER, B. & JENTSCH, S. 2007. PCNA, the maestro of the replication fork. *Cell,* 129**,** 665-79.

MONTECUCCO, A., ROSSI, R., LEVIN, D. S., GARY, R., PARK, M. S., MOTYCKA, T. A., CIARROCCHI, G., VILLA, A., BIAMONTI, G. & TOMKINSON, A. E. 1998. DNA ligase I is recruited to sites of DNA replication by an interaction with proliferating cell nuclear antigen: identification of a common targeting mechanism for the assembly of replication factories. *The EMBO Journal,* 17**,** 3786-3795.

MOTEGI, A., SOOD, R., MOINOVA, H., MARKOWITZ, S. D., LIU, P. P. & MYUNG, K. 2006. Human SHPRH suppresses genomic instability through proliferating cell nuclear antigen polyubiquitination. *J Cell Biol,* 175**,** 703-8.

MOYNAHAN, M. E. & JASIN, M. 2010. Mitotic homologous recombination maintains genomic stability and suppresses tumorigenesis. *Nat Rev Mol Cell Biol,* 11**,** 196-207.

NARYZHNY, S. N. 2008. Proliferating cell nuclear antigen: a proteomics view. *Cellular and Molecular Life Sciences,* 65**,** 3789-3808.

NIMONKAR, A. V., OZSOY, A. Z., GENSCHEL, J., MODRICH, P. & KOWALCZYKOWSKI, S. C. 2008. Human exonuclease 1 and BLM helicase interact to resect DNA and initiate DNA repair. *Proc Natl Acad Sci U S A,* 105**,** 16906-11.

PABLA, N., MA, Z., MCILHATTON, M. A., FISHEL, R. & DONG, Z. 2011. hMSH2 recruits ATR to DNA damage sites for activation during DNA damage-induced apoptosis. *J Biol Chem,* 286**,** 10411-8.

PANDITA, R. K., SHARMA, G. G., LASZLO, A., HOPKINS, K. M., DAVEY, S., CHAKHPARONIAN, M., GUPTA, A., WELLINGER, R. J., ZHANG, J., POWELL, S. N., ROTI ROTI, J. L., LIEBERMAN, H. B. & PANDITA, T. K. 2006. Mammalian Rad9 plays a role in telomere stability, S- and G2-phase-specific cell survival, and homologous recombinational repair. *Mol Cell Biol,* 26**,** 1850-64.

PARK, M. J., PARK, J. H., HAHM, S. H., KO, S. I., LEE, Y. R., CHUNG, J. H., SOHN, S. Y., CHO, Y., KANG, L. W. & HAN, Y. S. 2009. Repair activities of human 8-oxoguanine DNA glycosylase are stimulated by the interaction with human checkpoint sensor Rad9-Rad1-Hus1 complex. *DNA Repair (Amst),* 8**,** 1190-200.

PARKER, A. E., WEYER, I. V. D., LAUS, M. C., VERHASSELT, P. & LUYTEN, W. H. M. L. 1998. Identification of a Human Homologue of the Schizosaccharomyces pombe rad17+ Checkpoint Gene. *J Biol Chem,* 273**,** 18340-6.

PARSONS, J. L., DIANOVA, II, ALLINSON, S. L. & DIANOV, G. L. 2005. Poly(ADP-ribose) polymerase-1 protects excessive DNA strand breaks from deterioration during repair in human cell extracts. *FEBS J,* 272**,** 2012-21.

PENNIMPEDE, T., PROSKE, J., KONIG, A., VIDIGAL, J. A., MORKEL, M., BRAMSEN, J. B., HERRMANN, B. G. & WITTLER, L. 2012. In vivo knockdown of Brachyury results in skeletal defects and urorectal malformations resembling caudal regression syndrome. *Dev Biol,* 372**,** 55-67.

PICHIERRI, P., NICOLAI, S., CIGNOLO, L., BIGNAMI, M. & FRANCHITTO, A. 2012. The RAD9-RAD1-HUS1 (9.1.1) complex interacts with WRN and is crucial to regulate its response to replication fork stalling. *Oncogene,* 31**,** 2809-23.

POLO, S. E. & JACKSON, S. P. 2011. Dynamics of DNA damage response proteins at DNA breaks: a focus on protein modifications. *Genes & Development,* 25**,** 409-433.

RAUEN, M., BURTELOW, M. A., DUFAULT, V. M. & KARNITZ, L. M. 2000. The human checkpoint protein hRad17 interacts with the PCNA-like proteins hRad1, hHus1, and hRad9. *J Biol Chem,* 275**,** 29767-71.

REINHARDT, H., JIANG, H., HEMANN, M. & YAFFE, M. 2009. Exploiting synthetic lethal interactions for targeted cancer therapy. *Cell Cycle,* 8**,** 3112-3119.

ROMEO, F., FALBO, L., DI SANZO, M., MISAGGI, R., FANIELLO, M. C., VIGLIETTO, G., CUDA, G., COSTANZO, F. & QUARESIMA, B. 2011. BRCA1 is required for hMLH1 stabilization following doxorubicin-induced DNA damage. *Int J Biochem Cell Biol,* 43**,** 1754-63.

ROTHKAMM, K., KRUGER, I., THOMPSON, L. H. & LOBRICH, M. 2003. Pathways of DNA Double-Strand Break Repair during the Mammalian Cell Cycle. *Molecular and Cellular Biology,* 23**,** 5706-5715.

ROY, R., CHUN, J. & POWELL, S. N. 2012. BRCA1 and BRCA2: different roles in a common pathway of genome protection. *Nat Rev Cancer,* 12**,** 68-78.

SABBIONEDA, S. 2005. The 9-1-1 Checkpoint Clamp Physically Interacts with Pol and Is Partially Required for Spontaneous Pol -dependent Mutagenesis in Saccharomyces cerevisiae. *Journal of Biological Chemistry,* 280**,** 38657-38665.

SAKURAI, S., KITANO, K., YAMAGUCHI, H., HAMADA, K., OKADA, K., FUKUDA, K., UCHIDA, M., OHTSUKA, E., MORIOKA, H. & HAKOSHIMA, T. 2005. Structural basis for recruitment of human flap endonuclease 1 to PCNA. *EMBO J.,* 24**,** 683-693.

SAVAGE, J. 1976. Classification and relationships of induced chromosomal structual changes. *Journal of medical genetics,* 13**,** 103-122.

SHI, G., CHANG, D. Y., CHENG, C. C., GUAN, X., VENCLOVAS, C. & LU, A. L. 2006. Physical and functional interactions between MutY glycosylase homologue (MYH) and checkpoint proteins Rad9-Rad1-Hus1. *Biochem J,* 400**,** 53-62.

SHIGERU, S., KEN, K., HIROTO, Y., KEISUKE, H., KENGO, O., KOTARO, F., MAKIYO, U., EIKO, O., HIROSHI, M. & TOSHIO, H. 2005. Structural basis for recruitment of human flap endonuclease 1 to PCNA. *The EMBO Journal,* 24**,** 683-693.

SHIOTANI, B., NGUYEN, H. D., HAKANSSON, P., MARECHAL, A., TSE, A., TAHARA, H. & ZOU, L. 2013. Two distinct modes of ATR activation orchestrated by Rad17 and Nbs1. *Cell Rep,* 3**,** 1651-62.

SINGH, T. R., ALI, A. M., PARAMASIVAM, M., PRADHAN, A., WAHENGBAM, K., SEIDMAN, M. M. & MEETEI, A. R. 2013. ATR-dependent phosphorylation of FANCM at serine 1045 is essential for FANCM functions. *Cancer Res,* 73**,** 4300-10.

SMIRNOVA, E., TOUEILLE, M., MARKKANEN, E. & HUBSCHER, U. 2005. The human checkpoint sensor and alternative DNA clamp Rad9–Rad1–Hus1 modulates the activity of DNA ligase I, a component of the long-patch base excision repair machinery. *Biochem J,* 389**,** 13-17.

SOHN, S. Y. & CHO, Y. 2009. Crystal Structure of the Human Rad9–Hus1–Rad1 Clamp. *Journal of Molecular Biology,* 390**,** 490-502.

SONG, W., PASCAL, J. M., ELLENBERGER, T. & TOMKINSON, A. E. 2009. The DNA binding domain of human DNA ligase I interacts with both nicked DNA and the DNA sliding clamps, PCNA and hRad9-hRad1-hHus1. *DNA Repair,* 8**,** 912-919.

SORENSEN, C. S., HANSEN, L. T., DZIEGIELEWSKI, J., SYLJUASEN, R. G., LUNDIN, C., BARTEK, J. & HELLEDAY, T. 2005. The cell-cycle checkpoint kinase Chk1 is required for mammalian homologous recombination repair. *Nat Cell Biol,* 7**,** 195-201.

SPARROW, D. B., CHAPMAN, G., SMITH, A. J., MATTAR, M. Z., MAJOR, J. A., O'REILLY, V. C., SAGA, Y., ZACKAI, E. H., DORMANS, J. P., ALMAN, B. A., MCGREGOR, L., KAGEYAMA, R., KUSUMI, K. & DUNWOODIE, S. L. 2012. A mechanism for gene-environment interaction in the etiology of congenital scoliosis. *Cell,* 149**,** 295-306.

STOTT, D., KISPERT, A. & HERRMANN, B. G. 1993. Rescue of the tail defect of Brachyury mice. *Genes Dev,* 7.

SUNG, P., KREJCI, L., VAN KOMEN, S. & SEHORN, M. G. 2003. Rad51 recombinase and recombination mediators. *J Biol Chem,* 278**,** 42729-32.

SYMINGTON, L. S. 2002. Role of RAD52 Epistasis Group Genes in Homologous Recombination and Double-Strand Break Repair. *Microbiology and Molecular Biology Reviews,* 66**,** 630-670.

TAKAI, H., TOMINAGA, K., MOTOYAMA, N., MINAMISHIMA, Y. A., NAGAHAMA, H., TSUKIYAMA, T., IKEDA, K., NAKAYAMA, K., NAKANISHI, M. & NAKAYAMA, K. 2000. Aberrant cell cycle checkpoint function and early embryonic death in Chk1-/- mice. *Genes & Development,* 14**,** 1439-1447.

TODARO, G. & GREEN, H. 1963. Quantitative studies of the growth of mouse embryo cells in culture and their development into established lines. *Journal of Cell Biology,* 17**,** 299-313.

TOUEILLE, M., EL-ANDALOUSSI, N., FROUIN, I., FREIRE, R., FUNK, D., SHEVELEV, I., FRIEDRICH-HEINEKEN, E., VILLANI, G., HOTTIGER, M. O. & HUUBSCHE, U. 2004. The human Rad9/Rad1/Hus1 damage sensor clamp interacts with DNA polymerase and increases its DNA substrate utilisation efficiency: implications for DNA repair. *Nucleic Acids Research,* 32**,** 3316-3324.

VASILEVA, A., HOPKINS, K. M., WANG, X., WEISBACH, M. M., FRIEDMAN, R. A., WOLGEMUTH, D. J. & LIEBERMAN, H. B. 2013. The DNA damage checkpoint protein RAD9A is essential for male meiosis in the mouse. *J Cell Sci,* 126**,** 3927-38.

VENCLOVAS, C. & THELEN, M. P. 2000. Structure-based predictions of Rad1, Rad9, Hus1 and Rad17 participation in sliding clamp and clamp-loading complexes. *Nucleic Acids Research,* 28**,** 2481-2493.

VLANGOS, C. N., O'CONNOR, B. C., MORLEY, M. J., KRAUSE, A. S., OSAWA, G. A. & KEEGAN, C. E. 2009. Caudal regression in adrenocortical dysplasia (acd) mice is caused by telomere dysfunction with subsequent p53-dependent apoptosis. *Dev Biol,* 334**,** 418-28.

WANG, W. 2004. The human Rad9-Rad1-Hus1 checkpoint complex stimulates flap endonuclease 1. *Proceedings of the National Academy of Sciences,* 101**,** 16762-16767.

WANG, X., HU, B., WEISS, R. S. & WANG, Y. 2005. The effect of Hus1 on ionizing radiation sensitivity is associated with homologous recombination repair but is independent of nonhomologous end-joining. *Oncogene,* 25**,** 1980-1983.

WARBRICK, E., LANE, D. P., GLOVER, D. M. & COX, L. S. 1997. Homologous regions of Fen1 and p21Cip1 compete for binding to the same site on PCNA: a potential mechanism to co-ordinate DNA replication and repair. *Oncogene,* 14**,** 2313-2321.

WATANABE, K., TATEISHI, S., KAWASUJI, M., TSURIMOTO, T., INOUE, H. & YAMAIZUMI, M. 2004. Rad18 guides polg to replication stalling sites through physical interaction and PCNA monoubiquitination. *The EMBO Journal,* 23**,** 3886-3896.

WATKINS-CHOW, D. E., COOKE, J., PIDSLEY, R., EDWARDS, A., SLOTKIN, R., LEEDS, K. E., MULLEN, R., BAXTER, L. L., CAMPBELL, T. G., SALZER, M. C., BIONDINI, L., GIBNEY, G., PHAN DINH TUY, F., CHELLY, J., MORRIS, H. D., RIEGLER, J., LYTHGOE, M. F., ARKELL, R. M., LORENI, F., FLINT, J., PAVAN, W. J. & KEAYS, D. A. 2013. Mutation of the diamond-blackfan anemia gene Rps7 in mouse results in morphological and neuroanatomical phenotypes. *PLoS Genet,* 9**,** e1003094.

WEISS, R., KOSTRUB, C., ENOCH, T. & LEDER, P. 1999. Mouse Hus1, a homolog of the Schizosaccharomyces pombe hus1+ cell cycle checkpoint gene. *Genomics,* 59**,** 32-39.

WEISS, R. S., ENOCH, T. & LEDER, P. 2000. Inactivation of mouse Hus1 results in genomic instability and impaired responses to genotoxic stress. *Genes Dev,* 14**,** 1886-1898.

WEISS, R. S., LEDER, P. & VAZIRI, C. 2003. Critical Role for Mouse Hus1 in an S-Phase DNA Damage Cell Cycle Checkpoint. *Molecular and Cellular Biology,* 23**,** 791-803.

WEISS, R. S., MATSUOKA, S., ELLEDGE, S. J. & LEDER, P. 2002. Hus1 Acts Upstream of Chk1 in a Mammalian DNA Damage Response Pathway. *Curr Biol,* 12**,** 73-7.

WILLIS, J., PATEL, Y., LENTZ, B. L. & YAN, S. 2013. APE2 is required for ATR-Chk1 checkpoint activation in response to oxidative stress. *Proc Natl Acad Sci U S A,* 110**,** 10592-10597.

WU, X., SHELL, S. M., LIU, Y. & ZOU, Y. 2007. ATR-dependent checkpoint modulates XPA nuclear import in response to UV irradiation. *Oncogene,* 26**,** 757-64.

XING, G., KIROUAC, K., SHIN, Y. J., BELL, S. D. & LING, H. 2009. Structural insight into recruitment of translesion DNA polymerase Dpo4 to sliding clamp PCNA. *Mol Microbiol,* 71**,** 678-91.

XU, M., BAI, L., GONG, Y., XIE, W., HANG, H. & JIANG, T. 2009. Structure and functional implications of the human rad9-hus1-rad1 cell cycle checkpoint complex. *J Biol Chem,* 284**,** 20457-61.

XU, X., GUARDIANI, C., YAN, C. & IVANOV, I. 2013. Opening pathways of the DNA clamps proliferating cell nuclear antigen and Rad9-Rad1-Hus1. *Nucleic Acids Res,* 41**,** 10020-31.

YAZINSKI, S. A., WESTCOTT, P. M., ONG, K., PINKAS, J., PETERS, R. M. & WEISS, R. S. 2009. Dual inactivation of Hus1 and p53 in the mouse mammary gland results in accumulation of damaged cells and impaired tissue regeneration. *Proc Natl Acad Sci U S A,* 106**,** 21282-7.

YOSHIDA, K., KONDOH, G., MATSUDA, Y., HABU, T., NISHIMUNE, Y. & MORITA, T. 1998. The Mouse RecA-like Gene Dmc1 Is Required for Homologous Chromosome Synapsis during Meiosis. *Mol Cell,* 1**,** 707-718.

YOSHIOKA, K., YOSHIOKA, Y. & HSIEH, P. 2006. ATR kinase activation mediated by MutSalpha and MutLalpha in response to cytotoxic O6-methylguanine adducts. *Mol Cell,* 22**,** 501-10.

ZHANG, Y., YUAN, F., PRESNELL, S. R., TIAN, K., GAO, Y., TOMKINSON, A. E., GU, L. & LI, G. M. 2005. Reconstitution of 5'-directed human mismatch repair in a purified system. *Cell,* 122**,** 693-705.

ZHOU, B. & ELLEDGE, S. 2000. The DNA damage response: putting checkpoints in perspective. *Nature,* 408**,** 433-439.

ZHU, M. & WEISS, R. S. 2007. Increased Common Fragile Site Expression, Cell Proliferation Defects, and Apoptosis following Conditional Inactivation of Mouse Hus1 in Primary Cultured Cells. *Mol Biol Cell,* 18**,** 1044-1055.

ZIV, Y., BIELOPOLSKI, D., GALANTY, Y., LUKAS, C., TAYA, Y., SCHULTZ, D. C., LUKAS, J., BEKKER-JENSEN, S., BARTEK, J. & SHILOH, Y. 2006. Chromatin relaxation in response to DNA double-strand breaks is modulated by a novel ATM- and KAP-1 dependent pathway. *Nat Cell Biol,* 8**,** 870-6.